

**MAGNETIC FINGERPRINTING OF THE BEDLOAD SEDIMENTS
FROM THE ESTUARIES OF TIRACOL, CHAPORA, SAL, TALPONA
& GALGIBAG RIVERS - WEST COAST OF INDIA**

A Dissertation report for

GEO-651 Dissertation

Credits 16

Submitted in the partial fulfilment of

Masters of Science in Applied Geology

By

PRASHILA PRAKASH PEDNEKAR

Seat No: 22P0450014

ABC Id: 649502045447

PR No: 201900946

Under the supervision of

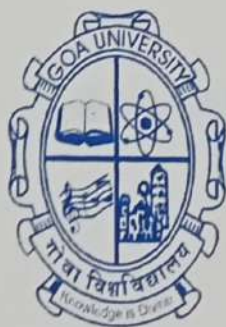
DR. FIROZ KADAR BADESAB

Senior Scientist – Geological Oceanographic Division

CSIR-NIO, Panjim Goa

School of Earth, Ocean and Atmospheric Science

Applied Geology



GOA UNIVERSITY
गोय विद्यापीठ

Goa University

Date: April 2024

Examined by



Seal of the school

DECLARATION BY STUDENT

I hereby declare that the data presented in this Dissertation report entitled, "MAGNETIC FINGERPRINTING OF THE BEDLOAD SEDIMENTS FROM THE ESTUARIES OF TIRACOL, CHAPORA, SAL, TALPONA & GALGIBAG RIVERS - WEST COAST OF INDIA" is based on the results of investigations carried out by me in the Applied Geology at the School of Earth Ocean and Atmospheric science, Goa University under the Supervision of Dr. Firoz Kadar Badesab Senior scientist Geological Oceanographic Division CSIR NIO Dona paula Panjim Goa and the same has not been submitted elsewhere for the award of a degree or diploma by me. Further, I understand that Goa University or its authorities will be not be responsible for the correctness of observations/experimental or other findings given the dissertation.

I hereby authorize the University/college authorities to upload this dissertation on the dissertation repository or anywhere else as the UGC regulations demand and make it available to any one as needed.



PRASHILA PEDNEKAR

Roll no / Seat no: 22P0450014

Applied Geology

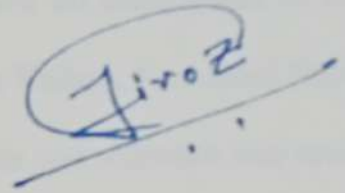
School of Earth Ocean and Atmospheric Science

Date: 02/05/2024

Place: Goa University

CERTIFICATE

This is to certify that the dissertation report "Magnetic fingerprinting of the bedload sediments from the estuaries of Terekhol, Chapora, Sal, Talpona and Galgibag Rivers – west coast of India" is a bonafide work carried out by Ms. Prashila Prakash Pednekar under my supervision in partial fulfilment of the requirements for the award of the degree of Masters of Science in Applied Geology at School of Earth Ocean and Atmospheric Sciences, Goa University.



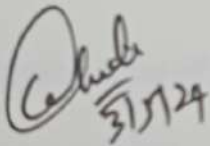
Dr Firoz Kadar Badesab

Senior Scientist

Geological Oceanographic Division

CSIR – NIO, Dona paula

Panjim Goa



Senior Professor Sanjeev C. Ghadi

Dean, School of Earth Ocean and Atmospheric Sciences

Date:

Place: Goa University



**MAGNETIC FINGERPRINTING OF THE BEDLOAD SEDIMENTS
FROM THE ESTUARIES OF TIRACOL, CHAPORA, SAL, TALPONA
& GALGIBAG RIVERS - WEST COAST OF INDIA**

A Dissertation report for

GEO-651 Dissertation

Credits 16

Submitted in the partial fulfilment of

Masters of Science in Applied Geology

By

PRASHILA PRAKASH PEDNEKAR

Seat No: 22P0450014

ABC Id: 649502045447

PR No: 201900946

Under the supervision of

DR. FIROZ KADAR BADESAB

Senior Scientist – Geological Oceanographic Division

CSIR-NIO, Panjim Goa

School of Earth, Ocean and Atmospheric Science

Applied Geology



GOA UNIVERSITY
गोय विद्यापीठ

Goa University

Date: April 2024

Examined by

Seal of the school

DECLARATION BY STUDENT

I hereby declare that the data presented in this Dissertation report entitled, “**MAGNETIC FINGERPRINTING OF THE BEDLOAD SEDIMENTS FROM THE ESTUARIES OF TIRACOL, CHAPORA, SAL, TALPONA & GALGIBAG RIVERS - WEST COAST OF INDIA**” is based on the results of investigations carried out by me in the Applied Geology at the School of Earth Ocean and Atmospheric science, Goa University under the Supervision of Dr. Firoz Kadar Badesab Senior scientist Geological Oceanographic Division CSIR NIO Dona paula Panjim Goa and the same has not been submitted elsewhere for the award of a degree or diploma by me. Further, I understand that Goa University or its authorities will be not be responsible for the correctness of observations/experimental or other findings given the dissertation.

I hereby authorize the University/college authorities to upload this dissertation on the dissertation repository or anywhere else as the UGC regulations demand and make it available to any one as needed.

PRASHILA PEDNEKAR

Roll no / Seat no: 22P0450014

Applied Geology

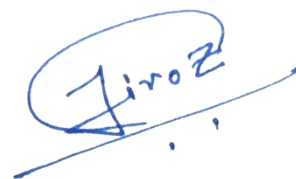
School of Earth Ocean and Atmospheric Science

Date:

Place: Goa University

CERTIFICATE

This is to certify that the dissertation report “Magnetic fingerprinting of the bedload sediments from the estuaries of Terekhol, Chapora, Sal, Talpona and Galgibag Rivers – west coast of India” is a bonafide work carried out by Ms. Prashila Prakash Pednekar under my supervision in partial fulfilment of the requirements for the award of the degree of Masters of Science in Applied Geology at School of Earth Ocean and Atmospheric Sciences, Goa University.



Dr Firoz Kadar Badesab

Senior Scientist

Geological Oceanographic Division

CSIR – NIO, Dona paula

Panjim Goa

Senior Professor Sanjeev C. Ghadi

School Stamp

Dean, School of Earth Ocean and Atmospheric Sciences

Date:

Place: Goa University

ACKNOWLEDGEMENT

Every achievement needs the assistance of several people. This report did not represent a unique instance. Many people mentored and encouraged the efforts and hard work that went into finishing the dissertation and report. I want to start by sincerely thanking my advisor, Dr. Firoz Badesab, Senior Scientist, Geology Oceanography Division, National Institute of Oceanography, Goa. Throughout the course of my dissertation, his unwavering support, great interest, deserving direction, and insightful suggestions have all contributed to my successful completion of the project. I also like to thank Mr. Nitin Kadam, Kamasani Shiva kumar and Mr. Omkar Sagvekar whose help in explaining the tools and software was really helpful to me in my work

I also thank Dr. Niyati Kalangutkar, the program director, and Dr. Anthony Arthur A. Viegas, head of the department of earth science at Goa University, for letting me complete my dissertation at CSIR-NIO. Along with thanking Dr. Poornima Sawant for serving as my co-guide, I also want to convey my sincere appreciation to the instructors and staff of Goa University's Department of Earth Science for their encouragement and support.

I am appreciative of my understanding parents and Maternal family, for always being there for me in everything; without you, none It would be feasible to accomplish this. A debt of gratitude is also owed to my friend Mr. Dawood Shaikh, I appreciate your assistance anytime I need it. Lastly, I convey my genuine Thank you to everyone who has offered to assist, either directly or indirectly, in order to make this research fruitful.

To sum up, I want to express my gratitude to God for allowing me despite all the challenges. Every day, your guidance has been felt by me. will continue to have faith in you for my future.

CONTENTS

CHAPTER NO.	TITLE	PAGE NO.
CHAPTER 1	<u>INTRODUCTION</u>	
	Abstract	1
	1.1 Introduction	2
	1.2 Iron cycling	4
	1.3 Earth's magnetic field	5
	1.4 Environmental magnetism	6
	1.4.1 Diamagnetism	7
	1.4.2 Paramagnetism	7
	1.4.3 Ferromagnetism	7
	1.5 Magnetic domain	9
	1.6 Magnetic susceptibility	12
	1.7 Magnetic remanence	13
	1.7.1. Anhyseretic remanent magnetization (arm)	13
	1.7.2 Isothermal remanent magnetism	13
	1.7.3 Saturated isothermal remanent magnetism	14
	1.8 Magnetic minerals in the environment	15
	1.9 Aquatic sediment system	16
	1.9.1 Sediment transport	16
	1.9.2 suspended load	16
	1.9.3 Bed load	16
	1.9.4 Wash load	17
	1.9.5 Cross shore transport	17
	1.10. Previous work	18

CHAPTER 2	<u>UNDERSTANDING STUDY AREA</u>	
	2.1. Objectives of the study	24
	2.2 Study area and collection of sediment samples	25
	2.3 Regional geology and environmental setting	29
CHAPTER 3	<u>METHODOLOGY</u>	
	3.1 sediment sampling from study area	34
	3.2 sample analysis	36
	3.2.1 Processing of samples for magnetic analyses	36
	3.2.2 Magnetic susceptibility measurement	36
	3.2.3 AF demagnetization and ARM	37
	3.2.4 Isothermal remanent magnetisation (IRM)	38
	3.2.5 AGICO dual speed spinner magnetometer JR-6A	39
	3.2.6 Hysteresis loop measurements and χ -t curves	40
	3.2.7 Magnetic mineral extraction and sem analysis	40
CHAPTER 4	<u>ANALYSIS AND CONCLUSION</u>	
	4.1 Magnetic mineral susceptibility maps along all five studied rives from source to sink.	44
	4.2 Rock magnetic properties of bedload sediments	48
	4.3 Scatter plots comparing the magnetic parameters of all five rivers	56
	4.4 Susceptibility-thermomagnetic heating curves for selected samples of rivers.	58

CHAPTER 5	4.5 Electron microscopy	68
	4.6 Hystersis loops for selective river sediments samples	74
	4.7 Day plot	88
	<u>CONCLUSION</u>	92
	References	94
	Appendix I : Rock magnetic data used in study	99

LIST OF TABLES

TABLE NO.	TITLE	PAGE NO.
1	Table 1: Details of rock magnetic parameters and inter-parametric ratios, their units and interpretation (after Thompson and Oldfield, 1986; Oldfield, 1991; Walden et al., 1999)	11
2	Common magnetic minerals in the environment (after Evans and Heller, 2003)	15

LIST OF FIGURES

FIGURE NO.	DESCRIPTION	PAGE NO.
1	Schematic representation of the distribution of magnetization vectors in crystals, showing the resultant spontaneous magnetization (a)Ferromagnetic (b)Anti-ferromagnetic (c)Ferrimagnetic (d)Canted Anti ferromagnetic (after McElhinny, 1973)	8
2	Magnetic Domain's (After Evans and Heller, 2003)	9
3	Magnetic hysteresis. The initial susceptibility (K) is given by the slope of the M-It curve in low fields. He is known as the coercive force, whereas the field necessary to reduce Mrs to zero is called the coercivity of remanence, Hcr.	10
4	Map showing the location of Terekhol, Chapora, Sal, Talpona and Galgibagh Rivers on the west coast of India.	28
5	Geological map of Goa (A.G Dessai et. al 2011)	32
6	Various location sites for bulk sediment sample collections	34
7	Bulk Sediment collection from grab sampler and collected bulk sediment samples	35
8	prepared sediment samples for magnetic susceptibility measurement	36
9	Magnetic Susceptibility MS2B and MS2C instrument	37
10	AF Demagnetizer and ARM attachment	38
11	Pulse magnetiser instrument used to apply forward and backward field	39
12	AGICO Dual Speed Spinner Magnetometer JR-6A	40

13	sample processing for magnetic mineral separation	41
14	Scanning Electron Microscope	42
15	Copper stubs used to place the magnetic particles and extracted magnetic minerals	42
16	magnetic susceptibility maps of five studied rivers in goa	46
17	The above plots for Tiracol river showing variation in (a) magnetic mass susceptibility (χ_{lf}) represents the abundance of ferrimagnetic minerals (magnetite), (b) Magnetic mineral grain distribution, (c) Concentration of magnetic minerals, (d) Concentration of fine ferrimagnets, (e) magnetic grain size indicator (ARM/SIRM), (f) magnetic mineralogy indicators (S-ratio)	48
18	The above plots for Chapora river showing variation in (a) magnetic mass susceptibility (χ_{lf}) represents the abundance of ferrimagnetic minerals (magnetite), (b) Magnetic mineral grain distribution, (c) Concentration of magnetic minerals, (d) Concentration of fine ferrimagnets, (e) magnetic grain size indicator (ARM/SIRM), (f) magnetic mineralogy indicators (S-ratio)	49
19	The above plots for Sal river showing variation in (a) magnetic mass susceptibility (χ_{lf}) represents the abundance of ferrimagnetic minerals (magnetite), (b) Magnetic mineral grain distribution, (c) Concentration of magnetic minerals, (d) Concentration of fine ferrimagnets, (e) magnetic grain size indicator (ARM/SIRM), (f) magnetic mineralogy indicators (S-ratio)	50

20	The above plots for Talpona river showing variation in (a) magnetic mass susceptibility (χ_{lf}) represents the abundance of ferrimagnetic minerals (magnetite), (b) Magnetic mineral grain distribution, (c) Concentration of magnetic minerals, (d) Concentration of fine ferrimagnets, (e) magnetic grain size indicator (ARM/SIRM), (f) magnetic mineralogy indicators (S-ratio)	51
21	The above plots for Galgibag river showing variation in (a) magnetic mass susceptibility (χ_{lf}) represents the abundance of ferrimagnetic minerals (magnetite), (b) Magnetic mineral grain distribution, (c) Concentration of magnetic minerals, (d) Concentration of fine ferrimagnets, (e) magnetic grain size indicator (ARM/SIRM), (f) magnetic mineralogy indicators (S-ratio)	52
22	Scatter plots comparing the different magnetic parameters in correlation of five studied rivers.	56
23	Temperature dependent χ -T curves (a-t) of representative selected sediment samples from different goan river systems	58 - 66
24	scanning electron microscope images	68 - 72
25	The hysteresis loops for selected representative samples from the five river estuaries, Goa, west coast of India.	74 - 83
26	Day plot representing magnetic domain size for various analysed sediment of five river systems.	88

CHAPTER 1

INTRODUCTION

Abstract

The present study sets out to elucidate how magnetic minerals derived from wide array of source regions respond to source to sink processes in complex estuarine systems along goa westcoast. Characterizing magnetic minerals in the Goa estuarine zone is made easier by the region's varied geology, climate, and oceanography. The environmental factors that impact magnetic materials during transportation often leave an imprint on the mineral from the point of origin to the sink. Total of 140 samples collected from five estuarine systems from goa west coast were analyzed for magnetic measurements including dual frequency magnetic susceptibility, anhysteretic remanent magnetization (ARM), isothermal remanent magnetization (IRM), grain size analysis, and total organic carbon (TOC). Magnetic susceptibility of all rivers showed discrete zones of enrichment and depletion of magnetic mineral distribution throughout, relatively high S-ratio of sediments suggest the presence of ferrimagnetic minerals throughout whereas low S-ratio indicative of dominance of antiferromagnetic minerals. Cyclic variations in magnetic grain size diagnostic proxy (Fd% and ARM/SIRM) revealed the changes in the distribution of fine and coarse grained magnetic particles linked with weathering and erosion of catchment rocks. Temperature dependence of magnetic susceptibility (χ -t) curves confirmed the presence of magnetite, titanomagnetite and titanohematite particles. Scanning electron microscopy data indicated the presence of varying size, sharp edge magnetic particles at the river catchment and sub rounded to rounded particles at nearshore indicates the varying morphology due to transportation of grains from source to sink. Bivariant plots plotted against magnetic susceptibility and other magnetic parametrs helped in discriminating over grain size and coercivity of minerals as a comparative study for five rivers.

1.1 Introduction

An interdisciplinary field known as "environmental magnetism" links environmental factors including sediment transport and temperature change to the evolution of magnetic mineral features across geological time (Thompson et al., 1980; Thompson et al 1986; Verosub et al, 1995; Maher et al, 1999). Fluvial processes transport substantial amounts of magnetic minerals from catchment rocks, deteriorated top and subsurface soils from the hinterland, riverbanks, agricultural input, and human sources to the estuary. (Kissel et al., 2016; Nguyen et al., 2016; Rey et al., 2005; Badesab et al., 2023; Evans & Heller, 2003; Franke et al., 2009; Kayvantash et al., 2017). Based on the underlying hydro- and sediment dynamics as well as the composition (density, particle size), the magnetic minerals that originate from different sources become mixed, sorted, enriched, and dispersed throughout the estuary (Badesab et al.,2023; Liu et al., 2016; Sikora & Kjerfve, 1985; Slingerland & Smith, 1986; Tomkins et al., 2003). Fine magnetic particles stay under suspended load while heavier magnetic minerals settle at the base as a result of gravitational sorting when they interact with various hydrodynamic processes. Important information about the mechanisms governing the accumulation, fractionation, and dispersal of magnetic particles during their transport from source to sink can be gained from studying magnetite settling patterns, concentration, and grain size distributions in various estuarine system sub-environments (Badesab et al.,2023; Gallaway et al., 2012; Hatfield et al., 2010; Kulgemeyer et al., 2017; Nguyen et al., 2016; Wang et al., 2020)

Magnetic minerals are ubiquitous in nature and provides vital insights into the dynamics of magnetic particles in sedimentary systems (Hatfield, 2014; Kulgemeyer et al., 2017). Aside from the material's initial deposition, modifications like authigenesis and diagenesis can also have an impact on magnetic minerals. A tried-and-true technique, rock magnetism mainly makes use of the magnetic characteristics of sediments that are particular to minerals and grain size. Studying estuarine and coastal systems has become more and more dependent on

magnetic approaches for example to decipher the origin, and dynamics of heavy (magnetic) minerals (Gallaway et al., 2012; Hatfield et al., 2010; Kulgemeyer et al., 2017), identify the sediment accretion and erosion sites (Franke et al., 2020; Hatfield et al., 2010; Kayvantash et al., 2017; Wang et al., 2011), track changes in sediment provenance, transport pathways, and depositional system (Booth et al., 2005; Hatfield, 2014; Maher et al., 2009; Prizomwala et al., 2013), map the heavy (magnetic) mineral deposits (Badesab et al., 2012; Troch et al., 2021), reconstruct the pollution history (Blaha et al., 2011), characterize the sedimentary environment and littoral drift system (Chaparro et al., 2017; Hatfield & Maher, 2008, 2009; Kulgemeyer et al., 2016), and investigate the magnetic mineral diagenesis (Ahn et al., 2021; Zhang et al., 2001).

1.2 Iron cycling

The Earth is a complicated system that has undergone continuous evolution for tens of thousands to millions of years. The seasonal pattern shift, tectonic activity, and the physical and chemical weathering of in-situ rocks on the continents are the criteria that will determine this transformation. Granular material is the source of sedimentation caused by terrigenous material; it is carried by glacial, aeolian, and river processes and is eroded off the continent. The fluvial system carries the majority of the continental debris to the ocean, where it is dispersed by ocean circulation. On the continental shelf, the carried silt with varying grain sizes will settle as a result of density differentiation. The shallow submerged edge of the continent, known as the continental shelf, is a broad, level platform that stretches between 70 and 100 kilometers. The strength of the wave that generates energy determines how much sedimentation occurs on the continental shelf. The grain size distribution on the shelf will depend on how strong the waves are. Because near-shore waves have more energy than their offshore counterparts, they will erode the coastline, causing finer particles to be suspended and medium- to coarse-sized particles to be left behind. In water, the speeds at which particles of various sizes settle vary. Sand-sized particles, muddy sand, and sandy mud settle closer to the coast at a depth of around 50–70 meters as a consequence. At depths below the continental shelf, pelagic clay builds at a rate of around one millimeter per year, settling considerably more slowly. Because of the melting of glacial ice, there is evidence of the shoreline retreating and the sea level rising. Magnetic minerals are excellent indicators to determine the provenance of sedimentation. The magnetic minerals found in marine sediments come primarily from three sources: terrigenous (coming from the land), chemical, and biogenic (originating from living organisms) (Henshaw and Merrith, 1980). Almost 30% of all elements on Earth are made up of iron, which makes up a sizable amount of the planet's mass. There are two oxidation states for iron: Fe^{2+} (ferrous) and Fe^{3+} (ferric). The majority of magnetic minerals originate from

igneous rocks that have crystallized. Magnetic minerals can be created as a byproduct of altering other minerals or as unique minerals. High-temperature oxidation, hydrothermal activity, or serpentinization can all result in these changes (Dunlop and Ozdemir, 1997). The global cycle is heavily reliant on the diagenetic reactions of fluids and minerals containing iron (Perez-Guzman et al 2010, Raiswell and Canwell 2012, Andrew, 2015). At favorable temperatures, the dissolution of iron-bearing minerals will take place, this is based on the reduction potential, microbial activity, and hydrogen iron concentration (Andrew, 2015). The physical, chemical, and biological processes in the environment will be the main determinants of the iron mineral cycle. The iron cycle has an effect on a number of things, including temperature, ocean biology, and desert dust. Additionally, it can alter the in-situ iron oxides that are found in sediments and soils, whether or not microbes are present. (Jickells et al, 2005; Maher et al, 2010, Cornell and Schwertmann, 2003; Malki et al, 2006).

1.3 Earth's Magnetic Field

The Earth's magnetic field may be compared as a large bar magnet that passes across the poles. The mechanism known as "geodynamo" is what creates Earth's magnetic field. The idea behind the Earth's magnetic field's workings serves as the foundation for the geodynamo. A geodynamo needs certain properties in order to work, including a suitable rotation of the globe and a fluid inside that can conduct electricity and energy sources for the fluid to be connected to. Two crucial sources are necessary for the Earth's magnetosphere to remain active and ignite activity through geodynamo activity. The first is thermal convection in the outermost layer of the magnetosphere, and the second is compositional convective movements that are prominently caused by the expanding innermost sphere (Kutzner et al 2000, Stevenson, 2003). Density differentiation and latent heat cause iron to crystallize on the

inner surfaces which leads heavy elements sinking while light elements accumulating in the outer core.

Due to the earth's magnetic field's ability to deflect solar radiation, the planet's magnetism is essential to life as we know it. Prior to crystallization, the magnetic field also affects how the magnetic grain aligns itself. This offers a doorway into determining the earth's magnetic reversal that has happened on each occasion.

1.4 Environmental Magnetism

Environmental magnetism is an interdisciplinary field that studies the magnetism found in the environment by connecting geology, biology, chemistry, and physics. According to Evans and Heller (2003), the magnetic mineral will bear the marks of numerous environmental processes. To name a few uses, the magnetic characteristics of minerals are employed as stand-ins for research on paleoclimate, palaeoceanography, provenance, and archaeology. Methods for measuring these attributes are provided by rock magnetism. Nearly all substances have some magnetic properties, which makes employing rock magnetic techniques advantageous. Additionally, the techniques are rapid and non-destructive. The magnetic dipole moment is the total magnetic moment of all the electron orbitals and spins in an atom. Based on the vector magnetic moment, several categories of magnetic behavior have been established.

The magnetic dipole moment is the resultant of all the orbital and spin magnetic moments of the electrons of an atom. Based on the alignment of the magnetic moments, several categories of magnetic behaviour been identified:

1.4.1 Diamagnetism

It's a property that occurs if the atom contains only paired electrons. A material will exhibit a diamagnetism if an external magnetic field is introduced to the material of only paired electrons, the electron spin will align with the magnetic flux causing a repulsion. Therefore, the diamagnet repels both the poles of the magnet. When a strong magnetic field is induced to a diamagnetic material, due to the electromagnetic induction change and by Faraday law an EMF is induced in the electron current loops that tend to oppose the external field. the magnetic flux passing through the diamagnet material is less compared to the flux outside of the material. Some of the materials showing diamagnetic properties are zinc, water, gold, bismuth, and mercury.

1.4.2 Paramagnetism

When a material has some unpaired electrons in its atomic orbitals, it is termed a paramagnet. The unpaired electron, due to its spin has a magnetic dipole moment and behaves as a tiny magnet. When an external magnet is introduced to a paramagnetic material the unpaired electrons will orient themselves to the external field which causes a net attraction Paramagnetic materials retain their magnetization even when there is no external magnetic field present., this is due to thermal vibration which causes disorder in spin orientation. Some examples of a paramagnet are oxygen, titanium, aluminum, and iron oxide.

1.4.3 Ferromagnetism

Ferromagnetism is a collective term for a group of related magnetic phenomena observed in substances with unpaired electrons in atoms that are closely and regularly spaced and where,

as a consequence strong interaction between unpaired electron spins occur. Due to the interaction of forces between unpaired electrons and adjacent atoms, their spins become aligned even in the absence of an externally applied field. Different forms of ferromagnetic behaviour result from the arrangement of atoms in the crystal lattice and four conditions can be defined; In the case of ferromagnetic metals and their alloys, parallel coupling of all unpaired electrons may take place resulting in the development of strong magnetization. This phenomenon is called **ferromagnetism**. If these alternate layers or sub-lattices become magnetized in opposite directions (anti parallel), the phenomenon is called **anti-ferromagnetism**. If the magnetic moments of these sub-lattices are unequal, then there is a net spontaneous magnetisation. This behaviour is called **ferrimagnetism**. Sometimes the sub-lattices in an anti-ferromagnetic arrangement may not be perfectly anti-parallel, and a small residual spontaneous magnetization exists. This behaviour is called **canted anti-ferromagnetism**.

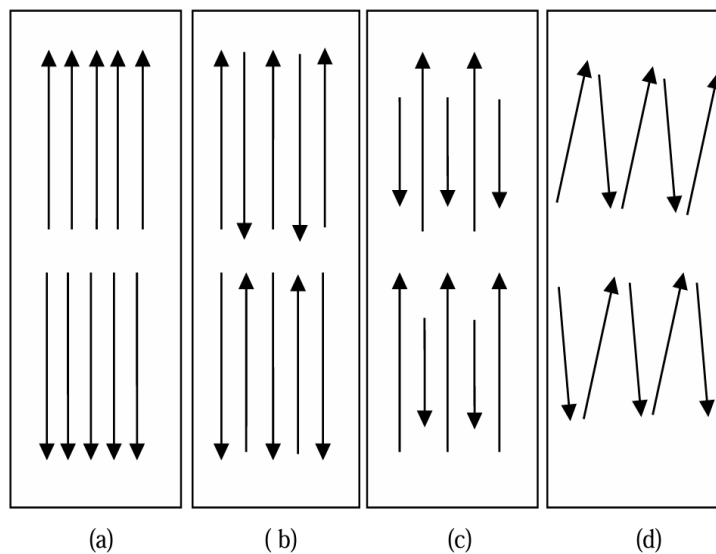


Figure 1: Schematic representation of the distribution of magnetization vectors in crystals, showing the resultant spontaneous magnetization (a)Ferromagnetic (b)Anti-ferromagnetic (c)Ferrimagnetic (d)Canted Anti ferromagnetic (after McElhinny, 1973)

1.5 Magnetic Domain

A domain is a region of sequential magnetic moments in a crystal. Consider a magnetized ferrimagnet. Inside, it is divided into small regions with uniform magnetization, the magnetic vector moment within each region is different from its neighbouring regions. These regions are called magnetic domains (Evans and Heller, 2003)

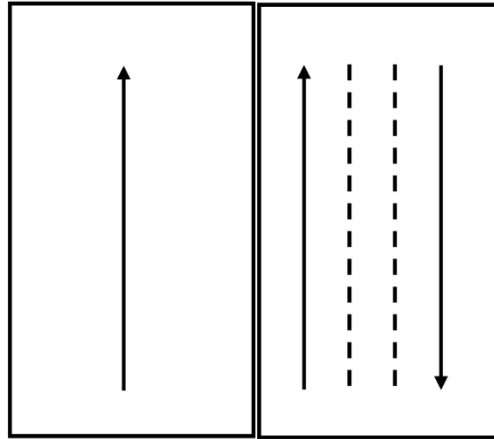


Figure 2: Magnetic Domain's (After Evans and Heller, 2003)

Single Domain (SD): If the grains comprise of only one domain or if they uniformly magnetized, they are characterized as single domain particles smaller grains $<0.2\mu\text{m}$ due to the dependence of volume, one region that is, a domain is formed, and they are termed as single domain grains. A given material has its maximum coercivity with its SD range.

Multi-Domain (MD): Grains comprising of many domains are called multi-domain particles. Ferrimagnetic grains above $\sim 110\mu\text{m}$ are referred to as multi domain because they are separated by domain wall, inside the domain wall regions of vector magnetic moment exist, to have more than one domain to minimize its internal energy. The domains are separated from one another by a domain wall.

Pseudo-Single Domain (PSD): Grains which behave in part like MD grains, and in part like SD grains and contain only a few domains are called pseudo-single-domain particles.

Super Paramagnetic (SP): The term super paramagnetic is the ultrafine ($<0.03\mu\text{m}$) ferromagnetic. Superparamagnetic behaviour dependent on the temperature. SP grains have a much higher susceptibility value than that for simple paramagnetism. Grains that are superparamagnetically at room temperature, if cooled, will then behave as the usual ferromagnetic or ferrimagnetic properties of SSD grains.

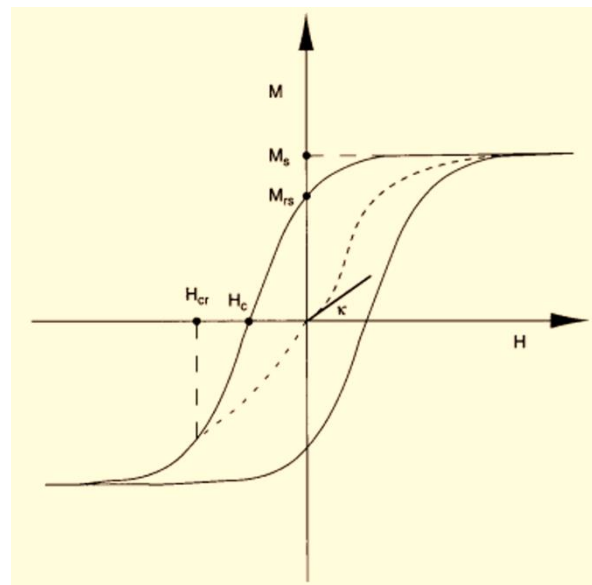


Figure 3: Magnetic hysteresis. The initial susceptibility (K) is given by the slope of the M - H curve in low fields. H_c is known as the coercive force, whereas the field necessary to reduce M_{rs} to zero is called the coercivity of remanence, H_{cr} .

Atomic dipole alignment with an externally applied magnetic field leads to phenomena like magnetic hysteresis in ferromagnetism - specifically in materials like iron. Following this process, partial retention of said alignment remains post-removal, resulting in what is commonly referred to as magnetization. In contrast, diamagnetic or paramagnetic interactions show no residual effects when eliminating exposure to non-endogenous fields. Through

exposure to strong magnetic fields initially applied for this purpose--one should be aware that any subsequent decreases in these fields (H), with regard to samples featuring induced magnetization (M), will not cause M levels to drop all the way back down to zero. This circumstance characterizes what we call "magnetic hysteresis", leading results for permanent magnetization/"magnetic remanence" outcomes instead. Moving forward with decreases in H towards more negative values results eventually in M hitting its lowest level possible before reversing course altogether and then saturating negatively once again upon further passes through this 'cycle'.

1.5 Coercivity The magnetic field that can required to demagnetise the samples, that is to strip the remanence of the sample it is given by Hc. For example, hematite grains, Bc is >100-300 millitesla. Whereas for magnetite it is only several tens of millitesla.

Sr No	Parameter	Units	Interpretation
1	χ_{lf}	10 ⁻⁶ m ³ K-G ⁻¹	Concentration of magnetic minerals
2	ARM	10 ⁻⁵ Am ² K-G ⁻¹	Concentration of fine ferrimagnets
3	SIRM	10 ⁻⁵ Am ² K-G ⁻¹	Concentration of magnetic minerals
4	S-ratio(300mT/SIRM)	dimensionless	proportions of ferromagnetic and canted antiferromagnetic minerals
5	SIRM/ χ_{lf}	10 ¹ Am ⁻¹	Grain size indicator. Higher values indicate significant SSD

Table 1: Details of rock magnetic parameters and inter-parametric ratios, their units and interpretation (after Thompson and Oldfield, 1986; Oldfield, 1991; Walden et al., 1999)

1.6. Magnetic susceptibility

Magnetic susceptibility is a measure of the magnetizability of a material (Thompson and Oldfield, 1986). It gives us an idea about the iron-bearing minerals found in rocks and sediments. These measurements enable us to calculate the concentration of the magnetic minerals present in a sample and to classify them. Magnetic susceptibility measurements are fast, non-destructive and can be made on all materials. Thus, they are very convenient. The volume susceptibility (κ) is defined as magnetization acquired per unit field.

$$\kappa = M/H$$

where M is the magnetization per unit volume and H is the applied uniform field.

Mass specific susceptibility is given by $\chi = \kappa/\rho$

It has the unit m³/K-G. Paramagnetic substances have strongly temperature dependent susceptibilities as given by Curie's law

$$\kappa = C/T$$

where T is the absolute temperature and C is the Curie's constant.

Measurements of susceptibility can be made under different conditions to give a range of information about the type, size, quantity and orientation of minerals in a sample.

Low field susceptibility: Low frequency measurements are carried out in a calm environment to neglect the unwanted interference/noise in the surroundings. This noise can affect the measurements. the sample is measured at room temperature in a single AC or DC low magnetic field, typically 0.1 mT. This gives an idea about the total concentration of ferrimagnetic minerals, or the total concentration of paramagnetic and canted antiferromagnetic minerals if the ferrimagnetic minerals are very low in concentrations.

High field susceptibility: High field susceptibility measurements are done to identify weaker magnetic mineral. High field susceptibility measurements are made at a high Dc field, typically 800 mT. This gives information about the paramagnetic and canted antiferromagnetic mineral concentrations.

Frequency-dependent susceptibility: Frequency-dependent susceptibility is calculated from the difference in susceptibilities measured at two or more AC frequencies in constant low magnetic fields produced at room temperatures. It is useful in detecting ultrafine ferromagnetic minerals lying in the superparamagnetic grain size region.

1.7. Magnetic remanence

The study of magnetic remanence is a central part of rock magnetism, both as natural remanent magnetization (NRM) in rocks obtained from the field, and remanence induced in the laboratory. NRM of a sample is the vector sum of all the different possible components of magnetization acquired by a sample over its history. The various types of remanence induced in the laboratory are:

1.7.1. Anhyseretic Remanent Magnetization (ARM)

ARM is produced by the combined actions of a large alternating field and a smaller, steady DC field. ARM is imparted by slowly reducing the alternating field from a peak value to zero, at the same time applying a steady DC field. The samples are normally demagnetized before inducing an ARM to the sample.

1.7.2 Isothermal Remanent Magnetism

Under fast and immediate applications of powerful magnetic fields that range from nanoseconds to milliseconds in duration, samples undergo Isothermal Remnant Magnetization (IRM). The result is that their magnetizations become realigned with that of aforementioned

external fields. IRM is acquired because of deliberate exposure of a sample to a steady field at a given temperature. The magnitude of the acquired remanence is governed by the intensity of the field applied (Evans and Heller, 2003). The maximum remanence which can be imparted to the sample by the action of a magnetic field is known as its saturation isothermal remanent magnetization (SIRM). The field that is necessary to reduce the SIRM to zero is the coercivity or remanence (H_{cr}). Hematite has a much larger coercivity as compared to that of magnetite as a result, it is much more strenuous to saturate samples containing hematite during IRM acquisition. The IRM increases with increasing applied field until the response is saturated and the sample acquires a room temperature saturation IRM (SIRM)

1.7.3 Saturated Isothermal Remanent Magnetism

The induced magnetization (M) increases with increasing applied field. At a critical field (appx. 300 mT for magnetite), the electronic spin are fully aligned and M no longer responds to increasing applied fields. The resulting magnetization is the saturation magnetization (M_s). Saturation magnetization is independent of grain size.

1.8 magnetic minerals in the environment

Magnetic minerals may be created, altered, transported, and deposited by the action of a variety of natural and man-made processes (Walden et al., 1999). Ferromagnetic minerals consist of a small portion of the total mineral assemblages of igneous and metamorphic rocks, and their formation provides the major primary source of magnetic minerals to environmental systems. Sedimentary rocks may contain magnetic minerals as detrital particles within them. Silicates which are the major rock forming minerals, are diamagnetic or paramagnetic. The most common magnetic minerals are iron oxides and iron-titanium oxides and they are ferromagnetic and anti-ferromagnetic. Magnetite, hematite and maghemite are the dominant iron oxides. All three are ferrimagnetic. Some significant iron sulphides are pyrrhotite, greigite and pyrite. Goethite is a significant iron oxyhydroxide.

Sr. No	Mineral	Formula	Curie Temperature (°C)
1.	Magnetite	Fe ₃ O ₄	580
2.	Hematite	α-Fe ₂ O ₃	675
3.	Maghemite	γ-Fe ₂ O ₃	590-675
4.	Goethite	α-FeOOH	120
5.	Pyrrhotite	Fe ₇ S ₈	320
6.	Greigite	Fe ₃ S ₄	~330

Table 2: Common magnetic minerals in the environment (after Evans and Heller, 2003)

1.9. Aquatic sediment system

1.9.1 Sediment Transport

As soon as the material is weathered away from its parent rock, water movements transport the sediments when they are exposed to strong enough forces or shear stresses. Current or wave orbital velocities or the combination of both can cause these movements. Transportation rate is mainly determined by particle size. Besides, the necessary flow speed for transporting the load is variable. The material carried by the river constitutes its stream load. The stream load includes dissolved or solution load, suspended load, and bed load. The stream's dissolved load is mainly due to groundwater outflow.

1.9.2 Suspended Load

Finer materials, including clays, silts, and sands, typically make up the suspended load. The turbulent eddies suspend this material above the channel bed and transport it downstream in the main flow. Tiny clay particles with diameters of less than 0.0063 mm make up the wash load, which is the finest fraction of the suspended load. Even when water movement is barely perceptible, this material can remain in suspension at very low flow velocities. Sediment from a washing load can travel several kilometers in just a few hours.

1.9.3 Bed Load

The bed of the channel sees movement of bed load. The sediment transport component that moves along the bottom of a waterway can roll, slide, or bounce. The sediment intermittently contacts the streambed and moves non-uniformly and discontinuously, indicating it is not truly suspended. When the force of the water flow is strong enough to overcome the weight and cohesion of the sediment, bedload is formed.

1.9.4 Wash Load

The wash load is a part of the suspended load. Wash load comprised of the finest suspended sediment. The wash load can be differentiated from the suspended load as it will not settle to the bottom of a waterway during a low or no flow period. Instead, Wash load will remain in permanent suspension as the particles are small enough to bounce off water molecules and stay afloat. During flow periods, the wash load and suspended load are still indistinguishable. Due to the wash load, there is turbidity in lakes and slow-moving rivers. When there is increase in the flow rate (increasing the suspended load and overall sediment transport), turbidity also increases. Though turbidity cannot be used to estimate sediment transport, it can approximate suspended sediment concentrations at a specific location.

1.9.5 Cross Shore Transport

The movement of beach and nearshore sand perpendicular to the shore caused by the combined action of tides, wind, and waves, as well as the shore-perpendicular currents produced by them, is referred to as cross-shore transport. These forces cause nearly continual movement of sand, either in suspension in the water column or as flows at the seafloor's surface. This happens in a complicated, three-dimensional pattern that changes fast with time. At any one time, some of the sand of interest will be onshore, while the rest will be migrating offshore.

1.10. Previous work

In estuarine, coastal, and shelf sedimentary environments, magnetic minerals are widely distributed and suggestive of the sediment composition. With several advantages, magnetic approaches have been developed as a stand-in for the analysis of heavy metal contamination, biomagnetism, marine sediments, tectonics and geomagnetic studies, urban dusts, and fluvial (coastal) sediments. These methods can be applied on a large scale and are non-destructive, inexpensive, sensitive, and quick (Chaparro et al., 2008; Dong et al., 2014; Shishkov and Kolev, 2014). In contrast, older geochemical methods are more complicated, take longer, and are only applicable to point samples (Zhang et al., 2011; Chaparro et al., 2017). D. Yang et al.'s 2019 study in mangrove sediments: a case study on the Chinese province of Fujian came to a conclusion The presence of detrital magnetic particles and potential post-depositional activities was associated with a high degree of variability in the magnetic concentration-dependent metrics that were assessed. Thus, the combination of magnetic parameter measurement and anthropogenic metal concentration measurement offered compelling evidence for their application in assessing the level of heavy metal contamination in mangrove forest fragments.

B. S. Praseetha et al (2022) conducted study along Beypore Estuary, Northern Kerala, using standard environmental magnetism technique The low field magnetic susceptibility (χ), Frequency dependent susceptibility (χ_{fd}), Anhysteretic Remanent Magnetization (χ_{ARM}), Isothermal Remanent Magnetization (IRM) of different field strength was analyzed following the standard procedure by employing the Barrington Susceptibility Meter (Model MS2B), Molspin AF demagnetizer and Magnetometer. Which made the conclusion that the distribution of the magnetic characteristics, namely χ_{lf} , $\chi_{fd}\%$, ARM, HIRM, χ_{ARM} , S-ratio, and SIRM, differs from upper to lower estuary. The existence of ferrimagnetic minerals, such as magnetite, in the estuary is confirmed by magnetic characteristics including S-ratios, χ_{lf} , ARM, SIRM, and IRM.

Magnetic characteristics have been shown to be beneficial in differentiating amongst watershed magnetic mineral types (Oldfield et al., 1979). A model for such work is provided by Dearing et al. [2001], who conducted a systematic examination of the source-lake relationship. In addition to several hundred soil samples from the catchment, these authors examined sediments from river bed loads, two floodplain cores, lake sediments from the middle plain of Petit Lac d'Annecy, France. Magnetic mineral concentrations in lake sediments frequently exhibit individual peaks. Though other mechanisms may potentially be involved, such peaks are frequently associated with sediments carried and deposited by density flows. Overall, the magnetic record of lake sediments can be greatly influenced by both diagenesis and individual events (such as floods, landslides, volcanic eruptions, etc.) and thus these archives remain an important source of information concerning terrestrial environmental change.

The goal of Kadam et al.'s (2022) study along the Indian continental shelf (the Bay of Bengal) is to clarify how complex shelf systems with a wide range of source regions' magnetic minerals react to shelfal sedimentary processes. He came to the conclusion that the sediment core off the P-S shelf (Pennar and Swarnamukhi Rivers) showed a regular pattern of down-core fluctuation in magnetite content, particle size, and mineralogy, which offered important insights into the processes connected to source-to-sink exchange. The beginning of DcB (Deccan Basalt) derived material in the shelf sediments off P-S was indicated by a significant change in the mineralogy diagnostic proxy (S-ratio).

Magnetic susceptibility has been determined estuarine, and marine environments India for sediments from the riverine, near Mulki, west coast of India by A.R. Karbassi and R. Shanka concluded that the estuary is where magnetic susceptibility starts to decline from the heads of both rivers. The magnetic susceptibility of well-sorted sediments is lower than that of poorly sorted sediments. The presence of both primary (detrital) and secondary (enhanced) minerals may be indicated by the bimodal distribution of magnetic minerals. Magnetic susceptibility and

magnetite weight percentage have a positive association, which is amplified for fine fractions. Due to the conveying agency's decreased velocity and energy, fine fractions (rich in magnetic minerals) are deposited at meander loops in the Mulki River, where magnetic materials appear to be concentrated.

Surface sediments and suspended particles' magnetic characteristics along the Yangtze's turbidity maximal zone's significant spatial variability are displayed by estuaries (C.Dong et al.2014). wherein he found out particle size fluctuations, such as those induced by currents and waves. There is a bimodal distribution of magnetic minerals, with coarser ones in the 63 μm size fraction and finer ones in the 16 μm size fraction. The North Channel's surface sediments are the coarsest due to stronger currents, and there are higher χ and SIRM values linked with it than the other two channels. Shallower water depth sediments in each channel have greater sand fractions because of active wave effects, and their χ and SIRM values are higher than those of deeper site sediments. The lower χ and SIRM values of suspended particles in relation to surface sediments can also be explained by the lowers and fractions in the former mixture. This indicates the function of selective hydrodynamic sorting along the primary sediment transport pathway, and the movement of coarser magnetic grains leads to the enrichment of inert ferrimagnetic grains in the direction of the increasing trend of $\chi_{\text{ARM}}/\text{SIRM}$ in suspended particles towards these. Moreover, the exposed buried sediments resulting from channel erosion exhibit unique magnetic characteristics.

R. Alagarsamy et.al 2008 collected Surface sediments from the east and west coasts of India and were analysed using magnetic parameters which concluded that in shelf sediments from the east and west coast of India, the magnetic parameter χ_{ARM} displays more significant relationships with the heavy metals in the east coast sediments than the west. An effective normalizer for comparing the level of pollution at various locations is χ_{ARM} . The significant

correlation seen between χ_{ARM} and heavy metal concentrations can be attributed to the function of iron oxides and particle size in regulating metal concentrations.

There is a stronger correlation between the concentration of Fe, Cr, Cu, and Ni in the east coast of India than in the west, as indicated by the magnetic parameters χ , χ_{ARM} , IRM20 mT, and SIRM. The magnetic approach can be used as a quick, easy, and non-destructive method to measure the level of heavy metal contamination in the shelf region because of the linear relationship between parameters related to magnetic mineral concentration and the concentrations of Fe, Cr, Cu, and Ni.

A study carried out by Badesab et al. 2017 along the north coast of Maharashtra found a general trend of down-pit decrease in magnetic susceptibility is observed in all the nine sand pits (sampling site). Sites that are abundant in heavy (magnetic) minerals are a result of severe sand erosion along the shore have been linked to higher magnetic susceptibility. These studies shed light on the dynamics of heavy (magnetic) mineral enrichment and transport.

The study by L. L. Fernandes et al. 2018 analysed that water quality of the estuaries in the six rivers with varying tidal ranges along the Goa coast was greatly impacted by seasonal changes in their coastal geomorphology. Because of the increased freshwater intake in the mesotidal rivers and the creation of sand bars in the microtidal rivers during the rainy sea season, the water column stratified close to the estuary mouths. In contrast, a well-mixed water column was the outcome of the sand bars' waning and the saline waters' incursion during the dry era. In contrast to chlorophyll fluorescence, which showed a clear seasonal trend, nutrient concentrations showed a high concentration during the wet season and a low concentration during the dry season. Within the system, the microtidal estuaries performed a critical role in regenerating both bottom-up and land-derived nutrients. Here, the sandbars regulated the river's

hydrodynamic behavior, which in turn influenced the river's hydrochemistry and supported the system's nutrient needs.

Badesab et al. (2023) did careful evaluation of the rock magnetic, mineralogical, and sedimentological data of the catchment rocks, soils, riverbank soils, estuarine, and nearshore surface sediments of the Mandovi estuary, which provided new data and interpretations on the dynamics (mixing, dispersal, fractionation, settling) of the magnetic particles and the underlying constraints during their transit from source-to-sink. sediment magnetic mineralogy-based proxy (S-ratio), which is sensitive and can be utilized for tracking riverbank erosion in fluvial and estuarine systems.

CHAPTER 2

UNDERSTANDING STUDY AREA

AIM

A dedicated magnetomineralogical based study elucidating the control of source-to-sink processes on the dynamics (sorting, dispersal, settling) of magnetic particles in the different estuarine system of Goa is so far lacking.

2.1. OBJECTIVES OF THE STUDY

- To develop the magnetic mineral distribution map for the different estuarine system of Goa.
- Elucidate the factors governing the mixing, sorting, dispersal & settling of magnetic particles in different parts of estuarine system.
- Identify the potential provenance of the estuarine sediments using sediment magnetism based proxies.

2.2 Study area and collection of sediment samples

Study Area

The main source of particulate matter entering coastal oceans is rivers. Currently, rivers use the suspended load and bed load (Gaillardet et al. 2003; Walling 2006) to carry around 95% of all sediment to the ocean. Rivers around the Indian coast discharge about 1.2×10^{12} kg of sediment annually (Chandramohan et al. 2001). The majority of India's rivers rise in hilly or mountainous areas and flow through plains, valleys, and plateaus before emptying into the ocean. There are nine minor rivers (catchment area below 2,000 km² ; Rao 1979) draining the Goa region, namely the Terekhol, Chapora, Baga, Mandovi, Zuari, Sal, Talpona, Saleri, and Galgibagh. According to Ahmad (1972), these rivers and estuaries are drowned river valleys. They are primarily straight with acute bends.

There are five rivers considered for the present study. The Terekhol and Chapora rivers originate in Maharashtra state, while the Sal River originates as a small stream in the hilly region of Verna village in south Goa and opens up into the Arabian Sea near the Betul beach. It has a very low shoreline with gentle submarine slope and a narrow mouth, which hinders the transport of domestic wastes into the sea. The Talpona River originates in the dense, mixed jungles of the Sahayadri Hills and drains into the Arabian Sea near the village of Talpona. Rocky outcrops and vertical cliffs are present along the shores from the Terekhol to the Zuari rivers, followed by a long stretch of sandy beach until Betul. At Betul, the shore is mostly of laterite cliff.while the Galgibagh river is located in the south of Goa in the Canacona region of famous Palolem Beach.

- **Terekhol River**

West India is home to the Terekhol or Tiracol River. 71 square kilometers make up this basin's area. The Tiracol is the name given to it in the lower portions, while the Banda River is its uppermost name. It creates a long-term border between the North Goa district of Goa state and the Sindhudurg district of Maharashtra state. The Terekhol empties into the Arabian Sea after rising near the Manohargad in the Western Ghats and flowing southwest. A total of 21 sediment samples were obtained on February 24, 2021, from the 28 kilometer long river.

- **Chapora River**

The Chapora River flows across northern Goa, India. spans an area of around 250 square kilometers. It divides the talukas of Pernem and Bardez in North Goa and runs westward into the Arabian Sea at Chapora. The river rises near Ramghat in Maharashtra, a neighboring state, runs into Goa, and then empties into the Arabian Sea. To the south is the estuary and the settlement of Morjim to the north is Vagator Beach, a popular tourist attraction. Thirty kilometers is its length. Approximately fifty samples of sediment were taken from these river sites on October 19, 2021.

- **Sal River River**

A minor river called Sal, or the Sal River, is situated in South Goa, India's Salcete Taluka district. The river begins in the vicinity of Margao, Kharea-bandh, flows through Benaullim, Navelim, Varca, Orlim, Carmona, Dramapur, Chinchinim, Assolna, Cavelossim-Mobor, and finally empties into the Arabian Sea at Betul. River Sal is said to be the Salcete Taluka in Goa's Mississippi. The 300 km³ Salcete taluka is closely related to the health of its sole river basin, the ecologically sensitive and unique River Sal basin. With a basin area of 301 km², River Sal is the third largest river in the State of Goa, measuring 35 km Its catchment area (700 million cubic meters annually) and runoff (one-third of the Zuari river) are comparable to those of the

Zuari and Mandovi rivers combined, yet it has gotten less than one-third of the attention. The Sal River has a unique feature of both geology and hydrology. It is the only river that flows from Margao to Betul in a north-south direction, ending at the Arabian Sea. About approximately 40 samples of sediment were taken from this river on May 16, 2022.

- **Talpona River**

The vast, mixed jungles of Ravan Dongor, located between Nane and Kuske on the Sahyadri Mountains, are the source of the Talpona River. It descends via Bhatpal, where it receives water from the river with the same name. It empties into the Arabian Sea close to Talpona hamlet. The river grows to a length of approximately 31 kilometers. Three further tributaries, Nadke, Gaondongrem, and Khalwade, are named after it. Its entire area is 233 square kilometers, and on May 15, 2022, about 16 sediment samples were taken from this river site.

- **Galgibagh River**

South Goa is home to Galgibaga Beach, also known as Galgibagh Beach. It is one of India's less well-known yet cleanest beaches, measuring around 4 km in length. Situated in the Canacona district to the south of Goa, it is 7 kilometers away from the well-known Palolem Beach. Its basin has an area of around 90 square kilometers, and as of May 15, 2022, 16 sediment samples had been taken from this river site.

Study area map

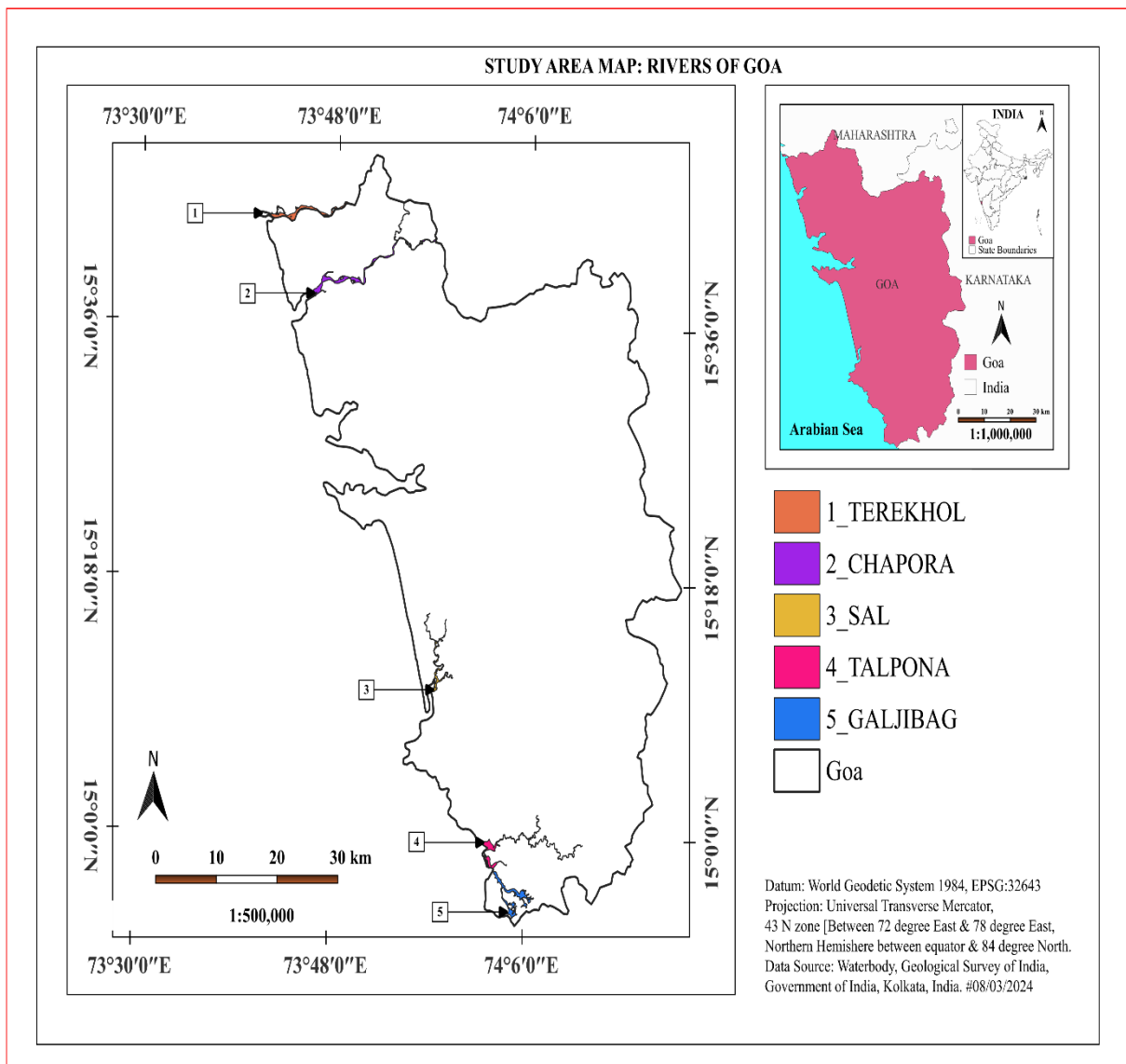


Fig 4: Map showing the location of Terekhol, Chapora, Sal, Talpona and Galgibagh Rivers on the west coast of India.

2.3 Regional geology and environmental setting

Goa's 105 km of coastline, which stretches from Polem in the south to Tiracol in the north, is distinguished by its distinctive coastal geomorphology. Goa is endowed with thirteen systems of estuarine rivers. Seldom seen marine, estuarine, and riverine environments can be found along the Goan coast. Goa's coastline edges are renowned for their alternately arranged emergent and submergent coasts. Rocks called meta-basalt and greywacke-argillite cover a sizable portion of the coast. There are numerous locations in Canacona, Anjuna, and Vagator where dyke intrusion into granite and gneiss is visible. Based on the environments in which they are found, the Goan islands can be divided into three groups: marine islands, estuarine islands, and riverine islands. The Arabian Sea is home to Marine Islands, while Estuaries are found close to river mouths and backwaters and Riverine Islands are mostly found in rivers. (Nadaf and colleagues, 2015)

Pre-Cambrian rocks known as the Dharwar rocks cover a significant portion of Goa and are made up of metavolcanics, conglomerates, banded ferruginous quartzites connected to phyllite, argillite, and limestone, and dolomite encroached by granites, ultrabasic, and basic rocks. On the coast, a layer of laterite thinning to the interior covers them, measuring around 30 to 40 meters. Sand and reddish-brown laterite soil make up the majority of the coast. Geologically, the state of Goa, which occupies an area of about 3700 sq. km. on the West coast of India, forms a part of the Indian Precambrian shield. In this region, there are greenschist supracrustal rocks which overlie a basement consisting of trondhjemitic (Peninsular) gneiss and are intruded by mafics, ultra-mafics and granites. The late Cretaceous Deccan Traps are found only at the northeastern part of the state. Laterite and alluvium and sand (on the coastal-estuarine plains) cover most of the geological formations.

The oldest known rock found in Goa is the Anmod Ghat Trondhjemitic Gneiss (>3.4 billion years, Dhoundial et al., 1987). the Goa Group can be divided into two lithostratigraphic

sequences namely the Barcem Group and the Ponda Group. The former comprises predominantly greenstones (metabasalts) and rests on a basement of TTG gneiss with quartz-pebble conglomerate at the base Gokul et al. (1985). Phonda group is further divided into formations namely vagheri formation, bicholim formation and savordem formation. Whereas barcem group consist of barcem formation.

In Goa, drainage and rainfall are mainly seasonal. The volume and composition (i.e., salinity) of water in these estuaries are determined by two separate seasons. According to Shetye et al. (2007) and Suprit and Shankar (2008), the maximum estimated runoff available for the Mandovi River is around $2,190 \times 10^6$ m³. The largest rainfall, approximately 300 cm/yr, happens during the southwest monsoon, which runs from June to September. In the dry season (October to May), there is very little rainfall and very little river discharge into the sea. The greatest wind speed, which happens during the wet season, ranges from 2.72 to 5.44 m/s. The wind comes from the southwest from June to September, and the northeast during the rest of the year. The sea breeze is the predominant wind from November to May. During the rainy season, waves along the west coast of India are mostly swells with periods ranging from 8 to 10 seconds (Kumar et al. 2000; Hameed et al. 2007). However, sea breeze is a crucial factor in regulating the features of waves during the dry season (Aparna et al. 2005). The tides exhibit two high and two low waters in a tidal day, making them semi-diurnal (i.e., exhibiting two high and two low waters in a tidal day). Goa is a coastal state located on India's west coast. Having more than 100 kilometers of shoreline along its whole length. The state can be divided into three different types of topography based on its physical makeup: low-lying coastal-estuarine plains to the west, an undulating region in the center, and the steep Western Ghats mountains on the state's eastern border.

All the rivers that flow within the state are estuarine, the tidal waters reaching several kilometres inland. Between the Sahyadris and the coastline, the relict landforms of the plains

and those of the midlands are dissected by these estuarine systems. The rivers have their source in the Western Ghat range, but they rapidly lose their force as they flow through the estuary plains and the midlands before emptying into the sea. Along with a few smaller coastal inlets, these estuaries include the Tiracol, Chapora, Mandovi, Zuari, Sal, Talpona, and Galgibag.

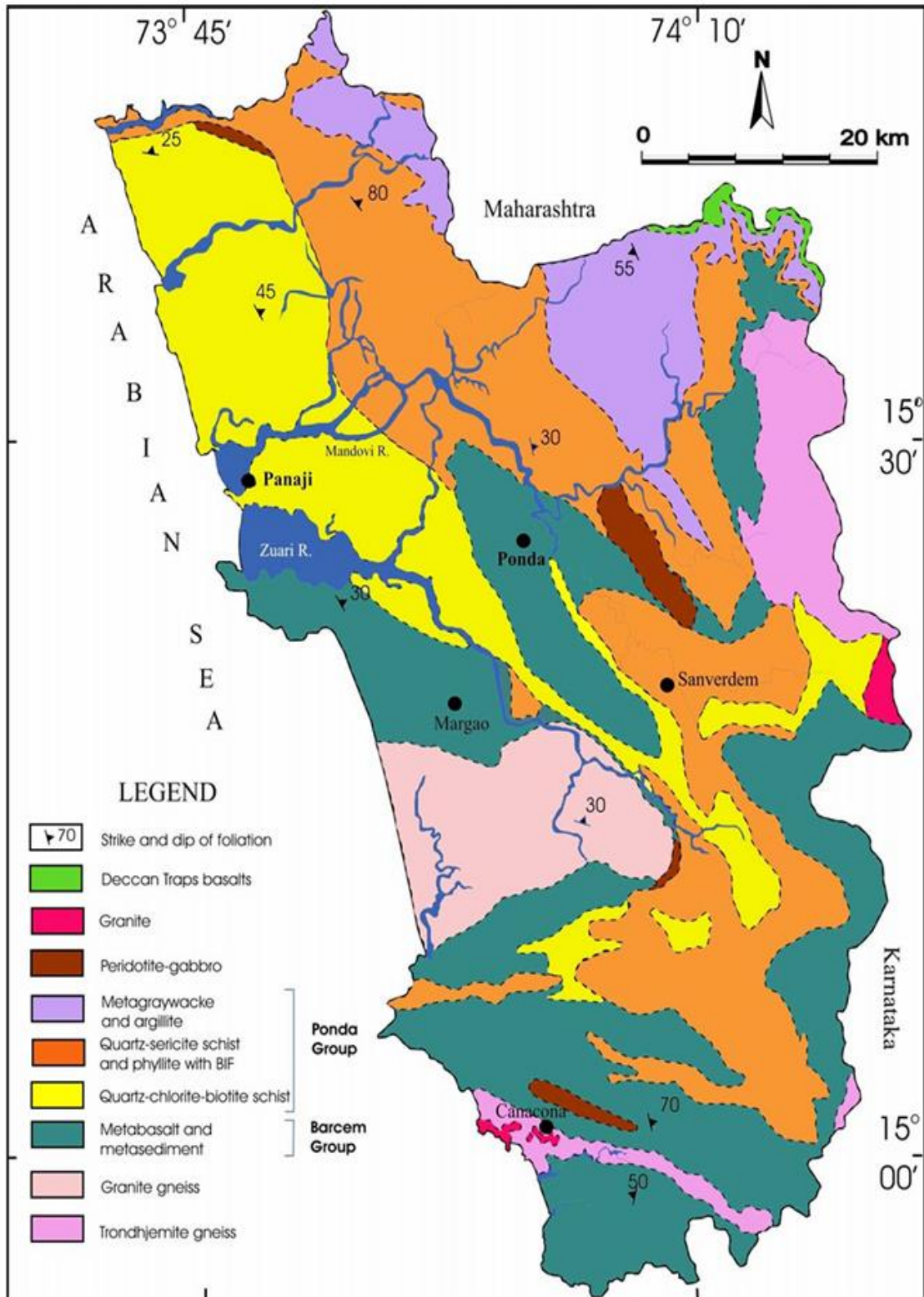


Fig 5: Geological map of Goa (A.G Dessai et. al 2011)

CHAPTER 3

METHODOLOGY

Methodology

3.1 Sediment Sampling from study area

There are around 143 pre-monsoonal wet bulk sediment samples were collected from five different west coast tropical river system on different date schedule. It includes 21 sediment sample from Terekhol (24-02-2021), 50 sediment samples from Chapora (19-01-2021), 40 sediment samples from Sal (16-05-2022), 16 sediment samples from Talpona and 16 sediment samples from Galgibagh river sites collected on same date (15-05-2021).



Fig 6: various location sites for bulk sediment sample collections



Fig 7: Bulk Sediment collection from grab sampler and collected bulk sediment samples.

3.2 Sample Analysis

3.2.1. Processing of Samples for Magnetic Analyses

During processing, all wet bulk sediment samples were cleaned in lab and kept for drying in oven, then after drying the samples were packed into the small individually labeled with river name and station no. plastic bottles of 10cm³. Further, these bottles were weighed before and after filling with sediment for the magnetic susceptibility measurement.



Fig 8: prepared sediment samples for magnetic susceptibility measurement

3.2.2. Magnetic susceptibility measurement:

Magnetic susceptibility measurements were performed using the Bartington MS2B dual frequency susceptibility instrument available at CSIR-National Institute of Oceanography, Goa, India. The meter expresses susceptibility in SI units. The instrument can measure the magnetic susceptibility of soil, rock and sediment samples. It measures susceptibility at two frequencies; a low frequency $\chi_{lf} = 0.47$ kHz and a high frequency $\chi_{hf} = 4.7$ kHz. This dual-frequency facility allows the detection of very fine ferrimagnetic minerals in rocks and soils (Walden et al., 1999). The MS2B meter has two ranges of measurement, 1.0 and 0.1. The 0.1 range takes ten times longer for a measurement, but has ten times the sensitivity as compared

to 1.0. The Bartington system accepts standard 10cm³ sample bottles. It is ideal for the sample bottles to be full to prevent errors. It is also advised to use standard sample bottles to minimize errors. The samples were analyzed by taking an average of three readings, this is done to negate the background noise (temperature, pressure etc). The instrument measures the samples in low frequency and high-frequency. The measurements were carried out in a magnetically quiet environment to minimize interference. A total of four background measurements were made before and after each sample measurement. The volume specific susceptibility was converted later to mass specific susceptibility.



Fig 9: Magnetic Susceptibility MS2B and MS2C instrument

3.2.3. AF Demagnetization and ARM

Anhyseretic remanent magnetization (ARM) is one of the standard measurements made in rock magnetic analysis. A sample is demagnetized by subjecting it to an alternating field which is gradually reduced from a peak initial value to a zero end value (Thompson and Oldfield, 1986). The steady DC field superimposing the alternating field imparts the ARM to the samples. The ARM was imparted to the samples using a peak AF field of 100 mT superimposed with a fixed DC bias field of 50 μ T. The AF demagnetizer and ARM attachment were both of

Molspin make. The instruments were switched on half an hour before taking measurements to allow them to stabilize. The imparted ARM was measured using an AGICO dual speed spinner magnetometer. The susceptibility of ARM was calculated by dividing the mass specific ARM by the DC bias field (Walden et al., 1999)



Figure 10: AF Demagnetizer and ARM attachment

3.2.4. Isothermal Remanent Magnetisation

Isothermal remanent magnetization (IRM) is imparted to the samples using a pulse magnetizer. The paleomagnetic laboratory at CSIR-NIO, Goa, is equipped with an MPM10 pulse magnetizer capable of applying a peak field of 3T. Pulse magnetizers operate on a capacitor system in which electrical charges are built up to the necessary level and the required magnetic field is then generated as a short duration pulse imparted to the samples. After applying the field, the remanent magnetization acquired by the samples are measured on a magnetometer.

IRM is induced to the samples in steps of increasing field strengths. Initially the samples are exposed to forward direction. Higher fields of strengths 700mT, 1T, and 2T were then imparted to the samples. The orientation of the samples in the pulse magnetizer was then reversed to apply the back fields. Fields of strengths -30mT, -100mT and -300mT were imparted to the samples in the backward direction. The induced remanence was then measured using an

AGICO dual speed spinner magnetometer. The remanence induced at a peak field of 1T was considered to be the saturation isothermal remanent magnetization (SIRM). S-ratio was calculated as the ratio between IRM at -300 mT and IRM at 1T (IRM 300mT/IRM1T) (Thompson and Oldfield, 1986).



Figure 11: Pulse magnetiser instrument used to apply forward and backward field

3.2.5. AGICO Dual Speed Spinner Magnetometer JR-6A

The magnetometer allows for the measurement of remanent magnetization acquired by the samples. The paleomagnetic laboratory at CSIR-NIO, Goa, is equipped with an AGICO JR-6A dual speed spinner magnetometer.

The instrument consists of a spinner/pickup unit and a microprocessor control unit. The instrument operates by rotating a rock specimen at a constant angular speed in the pick-up unit inside a pair of coils. Inside the coils an AC voltage is induced whose amplitude and phase depend on the magnitude and direction of the remanent magnetization vector. All functions are controlled by the microprocessor. The instrument was calibrated using the standard sample provided by the manufacturer and holder correction routine was performed using the standard 10cm³ cylindrical bottles. The remanent magnetization acquired by the samples were measured

on the spinner magnetometer. The measured data is displayed on the computer screen connected to the instrument and was used for further processing.



Figure 12: AGICO Dual Speed Spinner Magnetometer JR-6A

3.2.6. Hysteresis loop measurements and χ -T curves

For the experimentation of hysteresis loops and χ -T curves the selective samples were sent to CSIR- National Geophysical Research Institute (NGRI), Hyderabad.

3.2.7. Magnetic mineral extraction and SEM analysis

Magnetic mineral extraction facilitates the separation of magnetic minerals from bulk samples for identification and analysis of magnetic particles for grain size, shape / morphology, mineralogy and composition. For magnetic mineral extraction 8 samples were chosen TK-04, TK-19 (terekhol river), CP-01, CP-51 (chapura river), SL-27 (sal river), TO-01, TP-16 (talpona river), and GB-13 (galgibag river). these raw samples weighing 10g each were soaked in 300ml water for 18 hours for desalination, after which this water was rinsed and fresh water is added followed by A set of 10 magnets are loaded on the magnetic probe is dipped in beaker containing sediment plus water which facilitates attraction of magnetic minerals to the tip of the probe. The collected material is then removed from the probe on to a petri dish, Upon separation of magnetic minerals they were subjected to drying at 56⁰ C for six hours in oven.



figure 13: sample processing for magnetic mineral separation

Scanning electron microscope (SEM)

The SEM-EDS technique was used for the analysis of magnetic materials for morphology, mineralogy and composition. The Scanning Electron Microscope (SEM) uses a focused beam of high energy electrons to produce a high-resolution image of the sample. The magnetic minerals extracted from the bulk samples were used for SEM analysis. The extracted samples were loaded on the copper stub and was mounted firmly in the sample chamber. A scanning electron microscope (JEOL JSM-5800 LV) was used to capture images of the magnetic grains in secondary electron (SE) imaging mode. The SEM shoots a beam of highly concentrated electrons towards the sample from an electron gun located at the top of the device. The microscope comprises of a series of lenses inside a vacuum chamber. These lenses focus the electron beam towards the sample specimen. An electron detector picks up the secondary

electrons and records their imprint. This information is translated to a screen in the form of three-dimensional images.

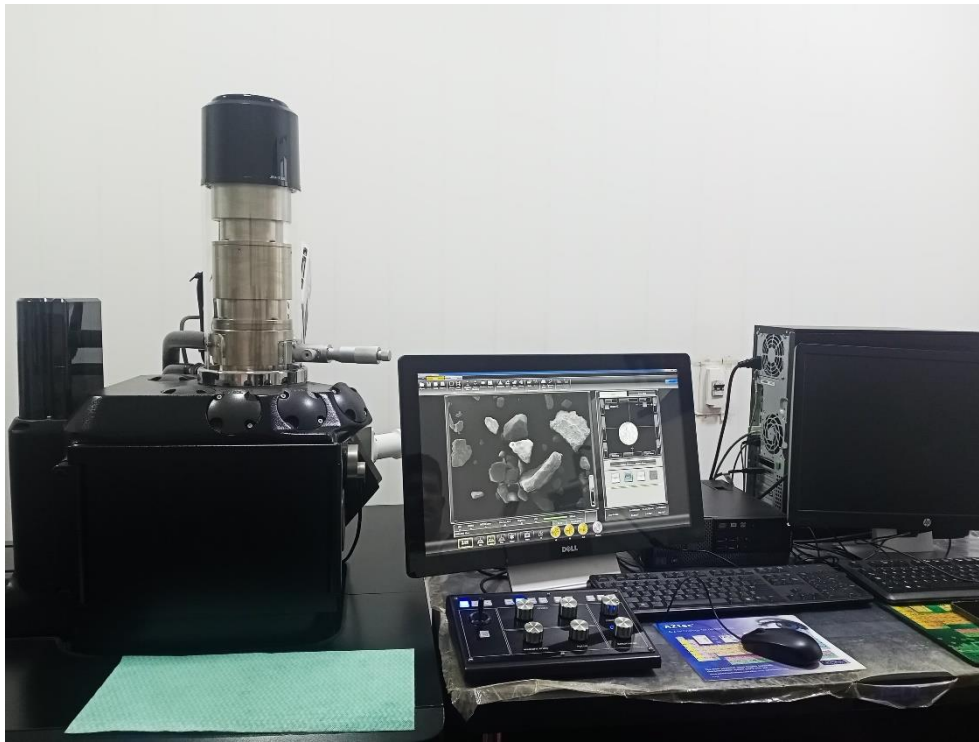


Figure 14: Scanning Electron Microscope

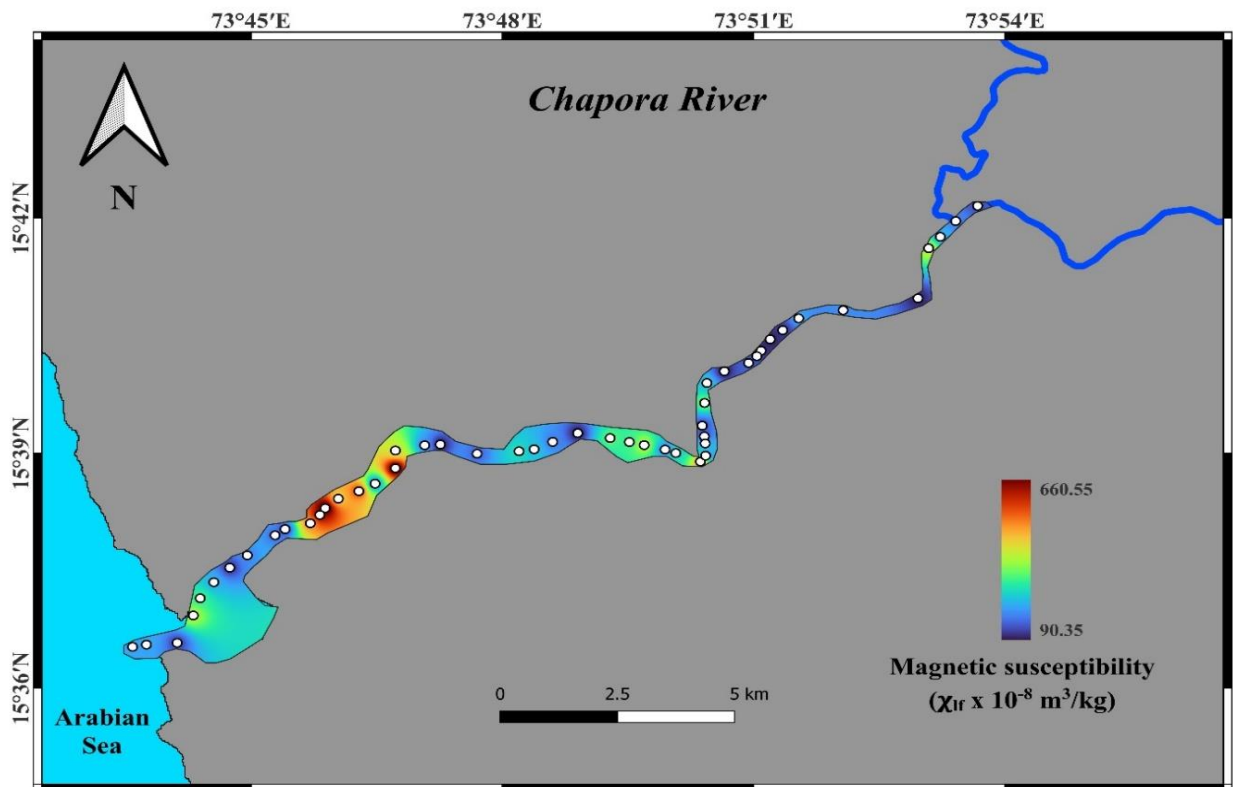
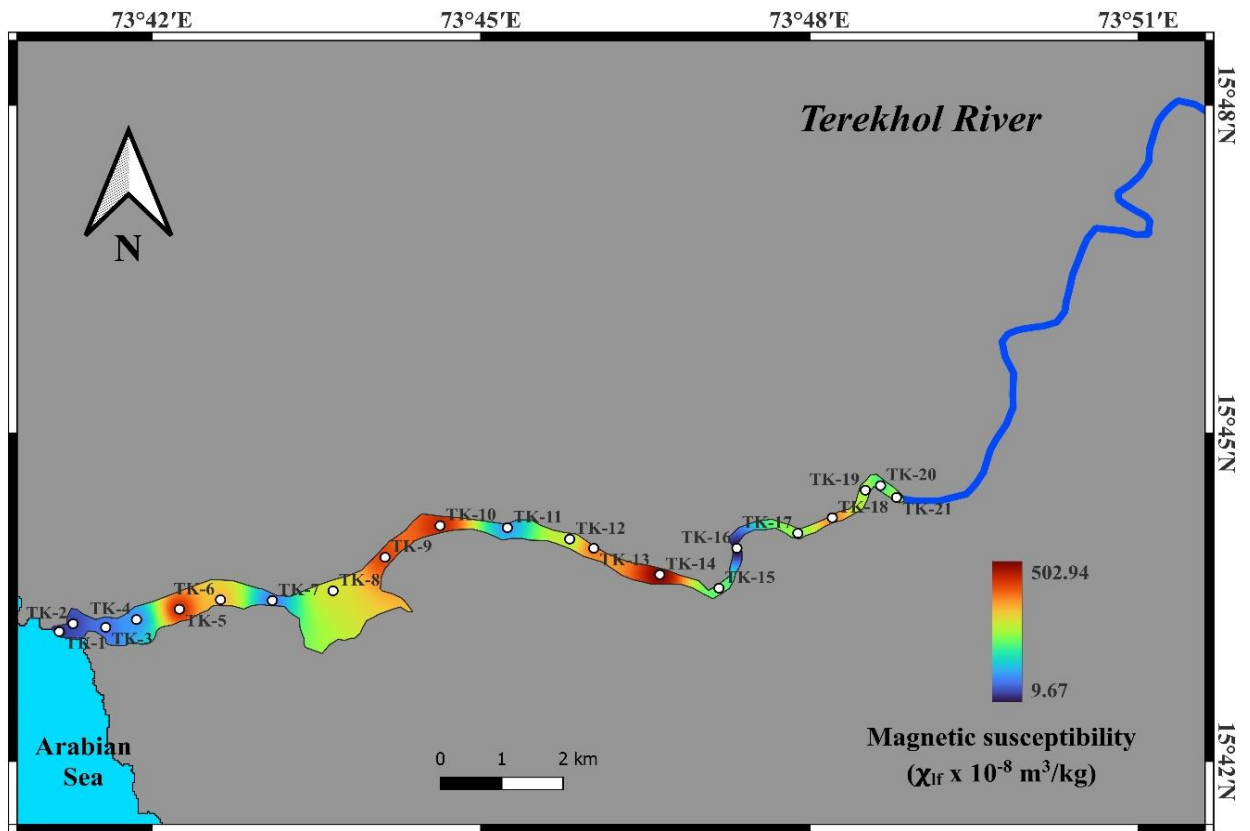


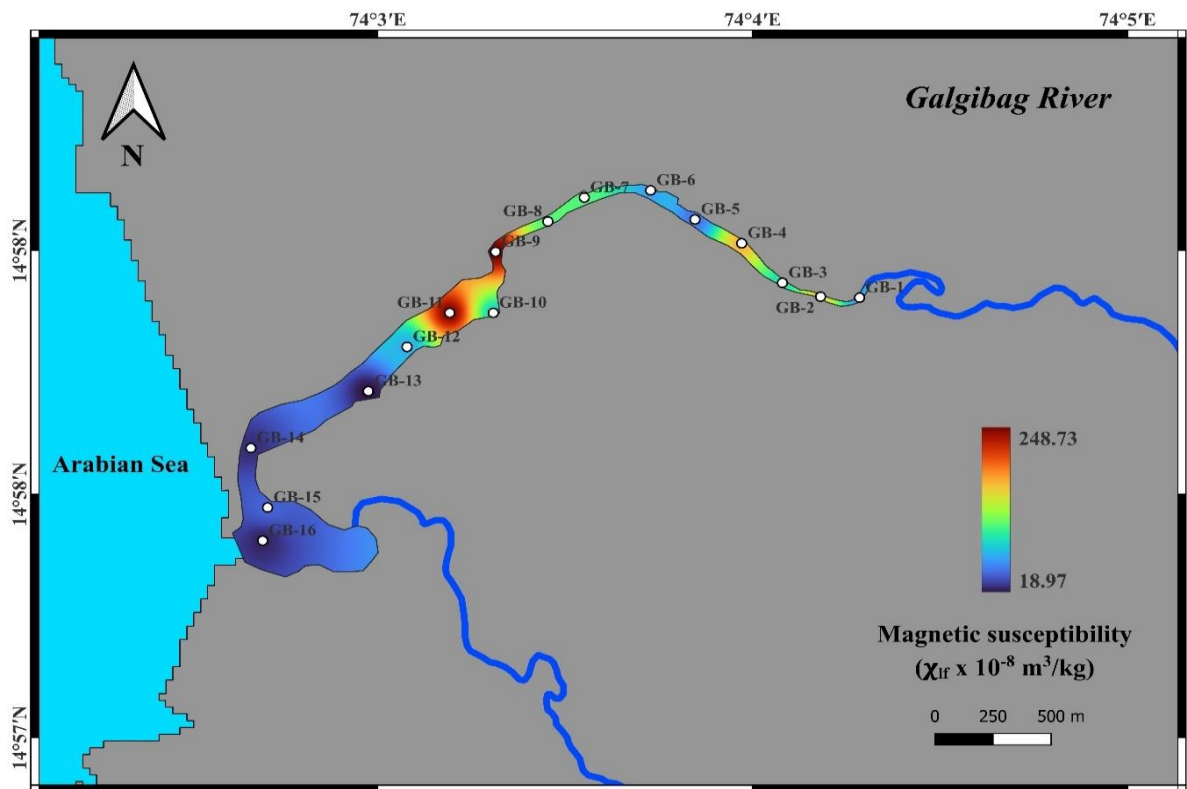
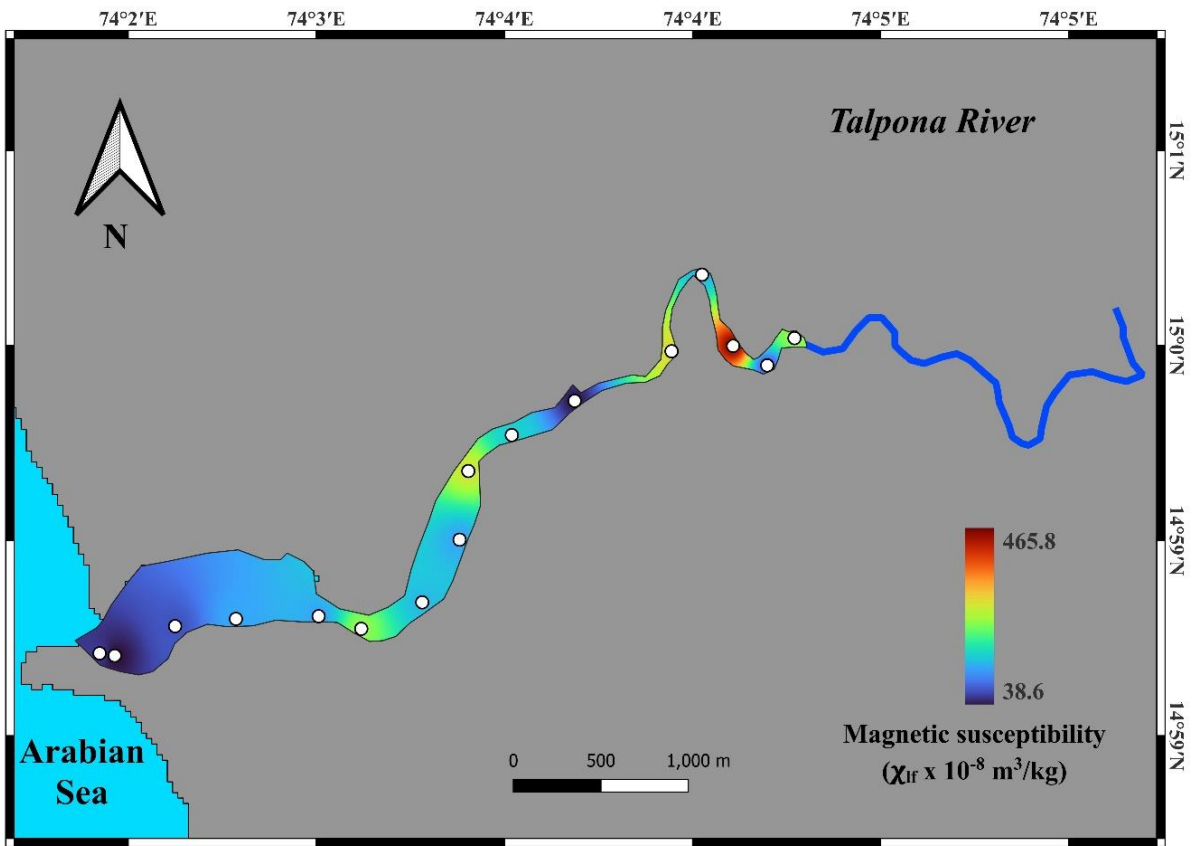
Figure 15: Copper stubs used to place the magnetic particles and extracted magnetic minerals

CHAPTER 4

ANALYSIS AND CONCLUSION

4.1. Magnetic mineral susceptibility maps along all five studied rives from source to sink.





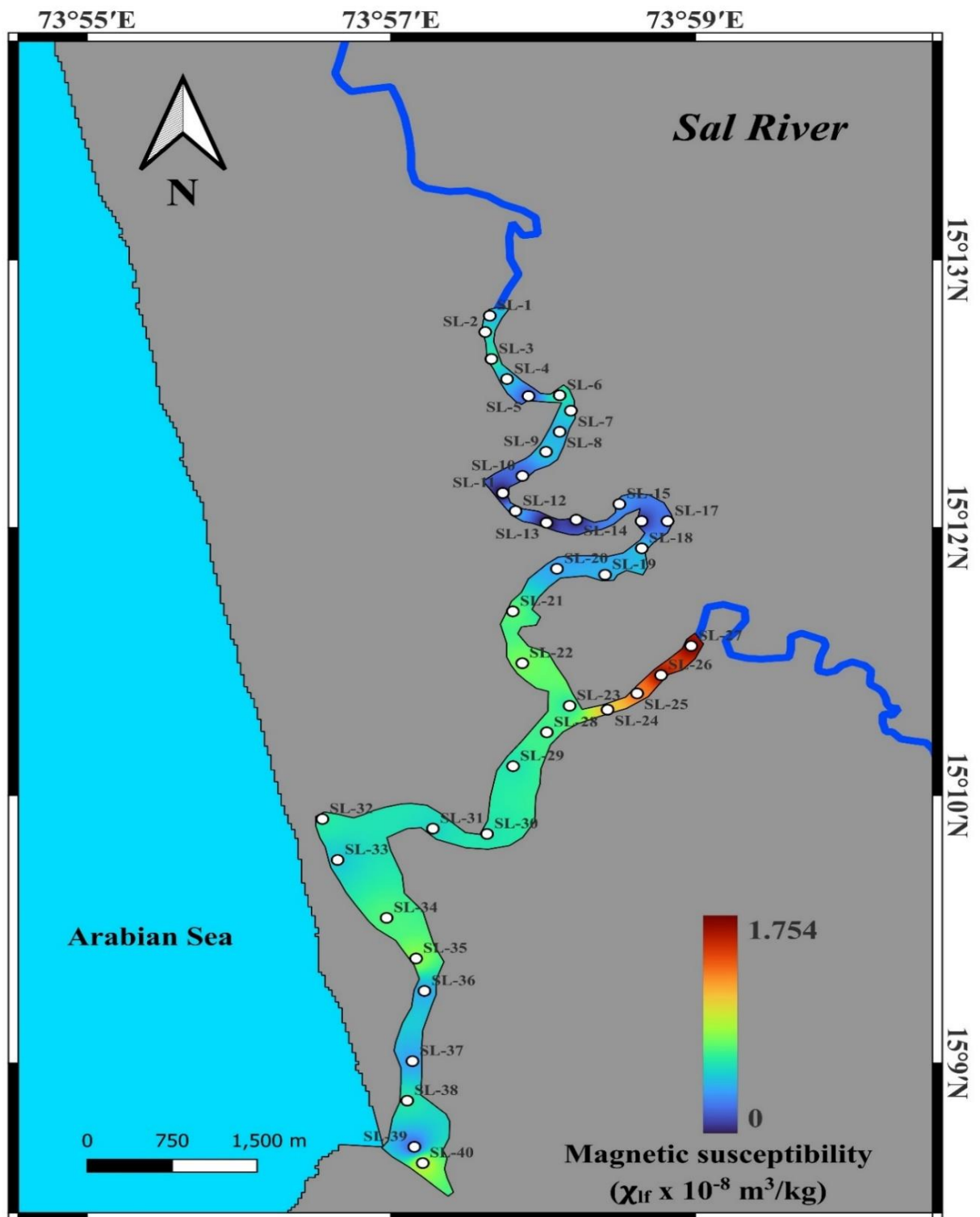


Fig 16: magnetic susceptibility maps of five studied rivers in goa.

Interpretation

The above maps made for 5 studied river of goa gives the information about Spatial distribution of magnetic minerals as indicated by concentration dependent magnetic susceptibility (χ_{lf}), over all the magnetic susceptibility in the studied samples vary over three orders of magnitude from 0.717 to $751.86 \times 10^{-8} \text{ m}^3 \text{ kg}^{-1}$ With highest values found for chapora river and lowest for sal river. Higher magnetic susceptibility values are exhibited by the coarser magnetic grain sizes, and lowest χ_{lf} values from indicate the presence of fine-grained magnetic particles at low concentrations.

Terekhol river throughout has shown variable values for χ_{lf} which indicates inappropriate distribution of magnetite concentration. Whereas chapora, sal and galgibag river samples shows low susceptibility values at river mouth and exceeding the values midway (before river meets coastline) which again specifies inadequate distribution and sorting of magnetite grains. Higher values of susceptibility is observed at initial sample collected site for talpona river which later manifested the apparent decrease in values at near shore zone.

4.2. Rock magnetic properties of bedload sediments

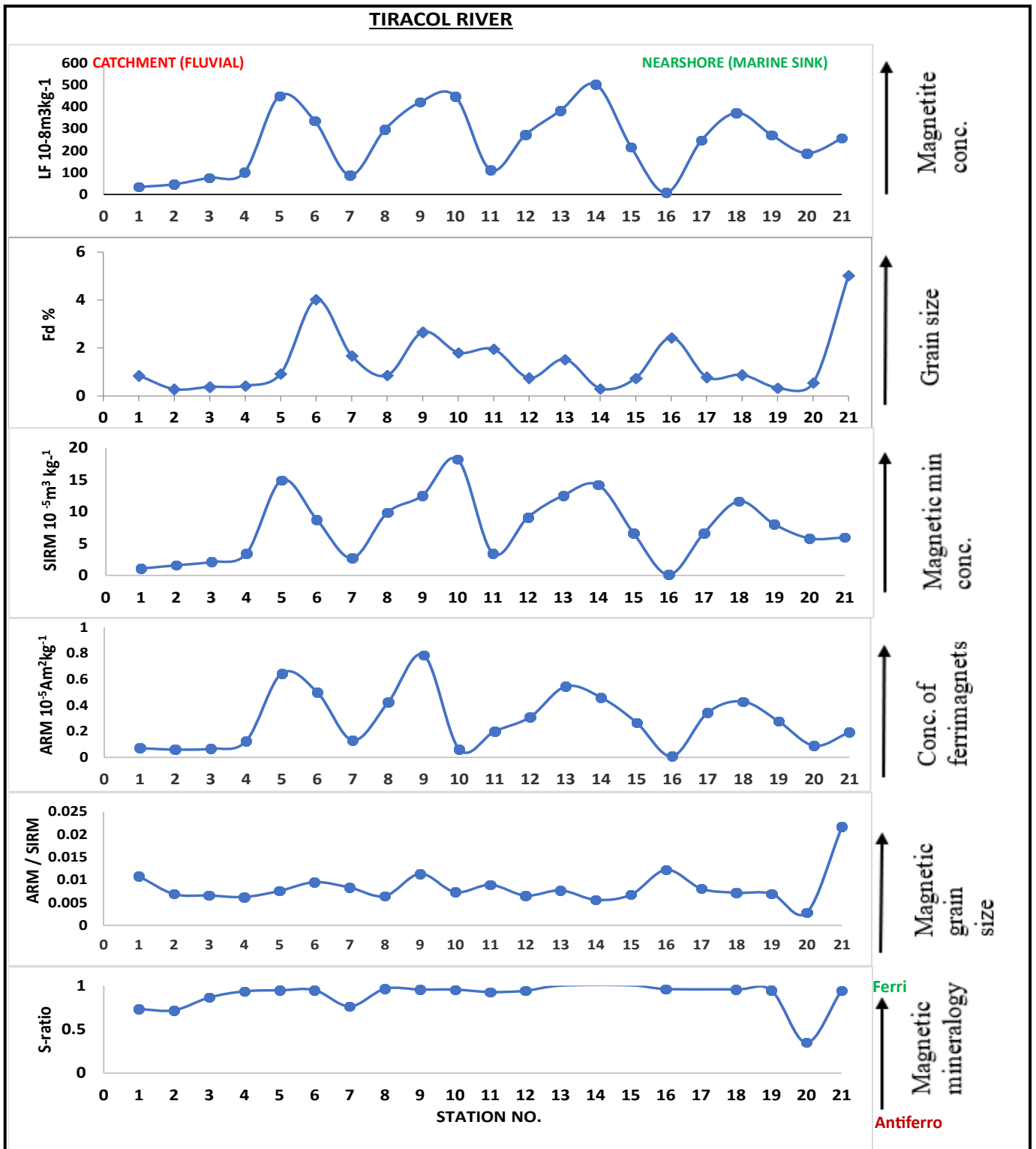


Figure 17: The above plots for Tiracol river showing variation in (a) magnetic mass susceptibility (χ_{lf}) represents the abundance of ferrimagnetic minerals (magnetite), (b) Magnetic mineral grain distribution, (c) Concentration of magnetic minerals, (d) Concentration of fine ferrimagnets, (e) magnetic grain size indicator (ARM/SIRM), (f) magnetic mineralogy indicators (S-ratio)

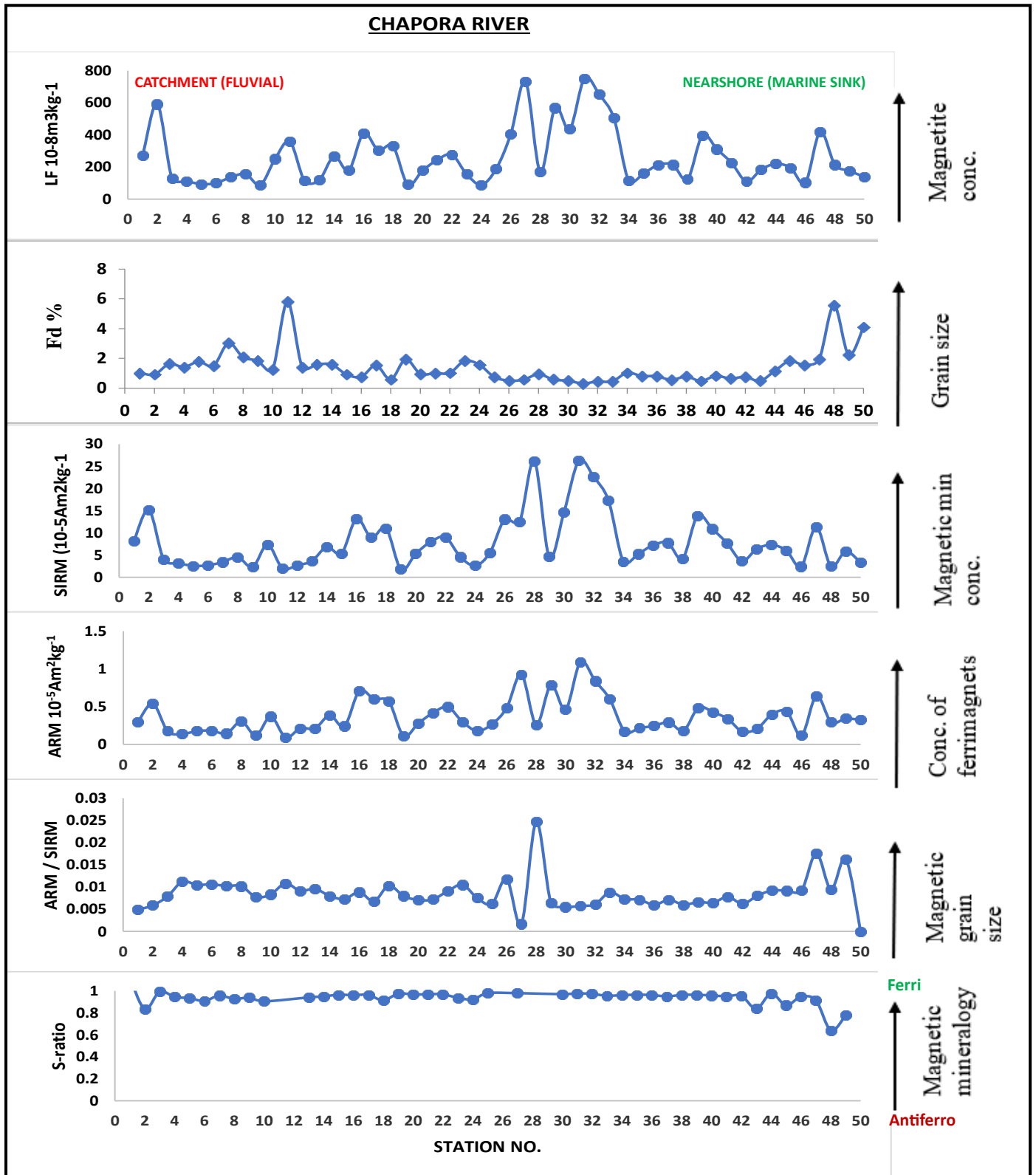


Figure 18: The above plots for Chapora river showing variation in (a) magnetic mass susceptibility (χ_{lf}) represents the abundance of ferrimagnetic minerals (magnetite), (b) Magnetic mineral grain distribution, (c) Concentration of magnetic minerals, (d) Concentration of fine ferrimagnets, (e) magnetic grain size indicator (ARM/SIRM), (f) magnetic mineralogy indicators (S-ratio)

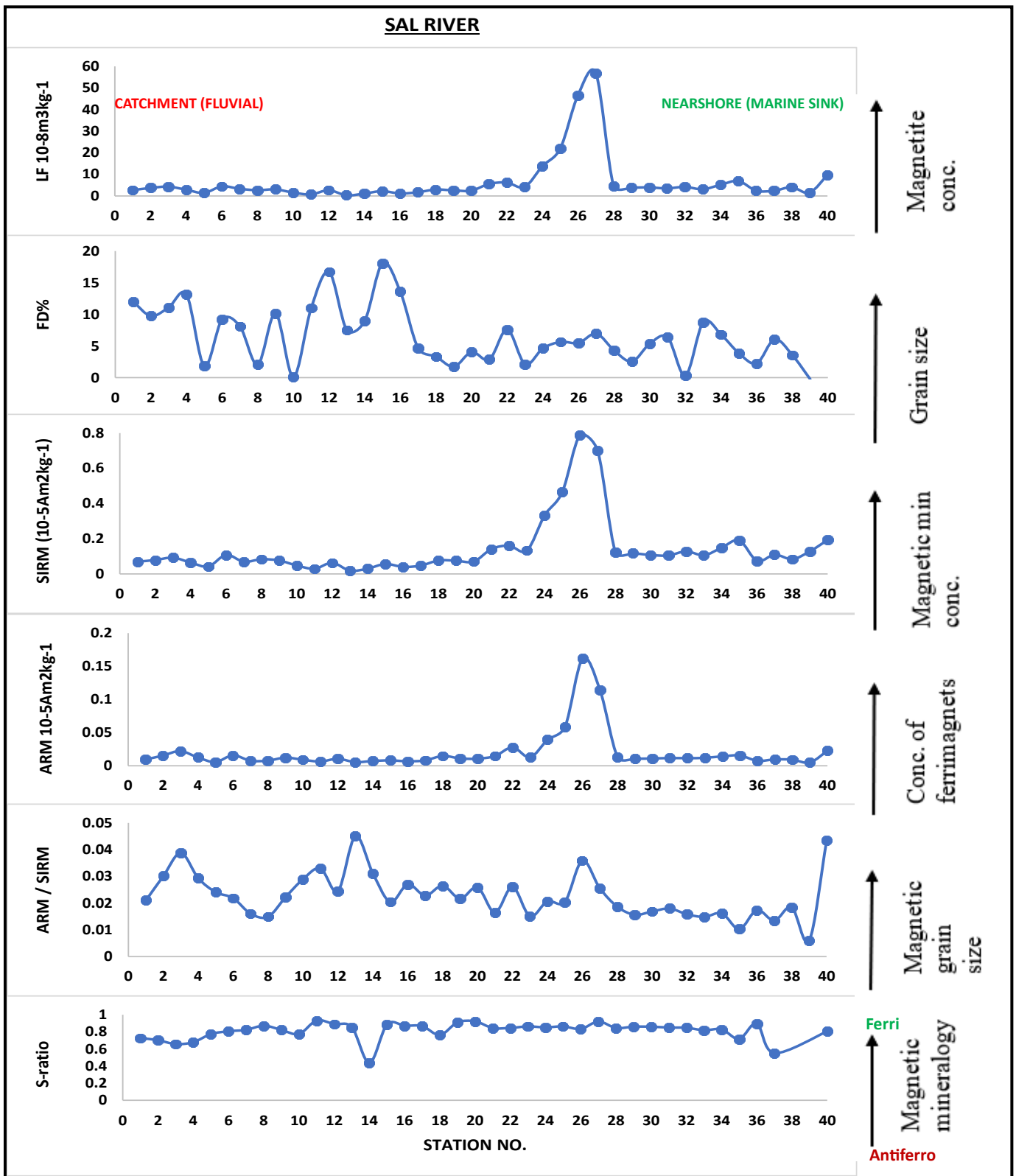


Figure 19: The above plots for Sal river showing variation in (a) magnetic mass susceptibility (χ_{lf}) represents the abundance of ferrimagnetic minerals (magnetite), (b) Magnetic mineral grain distribution, (c) Concentration of magnetic minerals, (d) Concentration of fine ferrimagnets, (e) magnetic grain size indicator (ARM/SIRM), (f) magnetic mineralogy indicators (S-ratio)

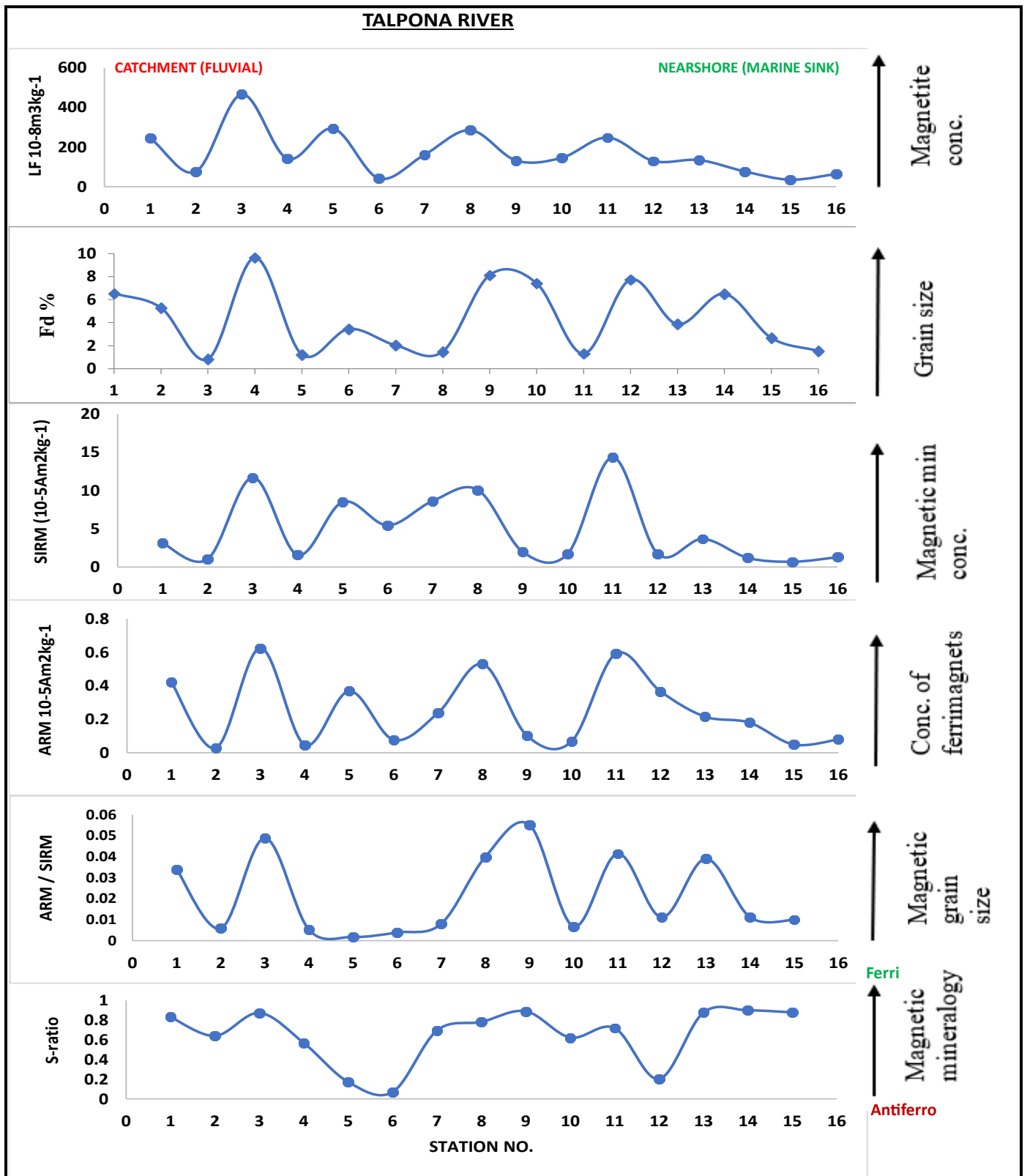


Figure 20: The above plots for Talpona river showing variation in (a) magnetic mass susceptibility (χ_{lf}) represents the abundance of ferrimagnetic minerals (magnetite), (b) Magnetic mineral grain distribution, (c) Concentration of magnetic minerals, (d) Concentration of fine ferrimagnets, (e) magnetic grain size indicator (ARM/SIRM), (f) magnetic mineralogy indicators (S-ratio)

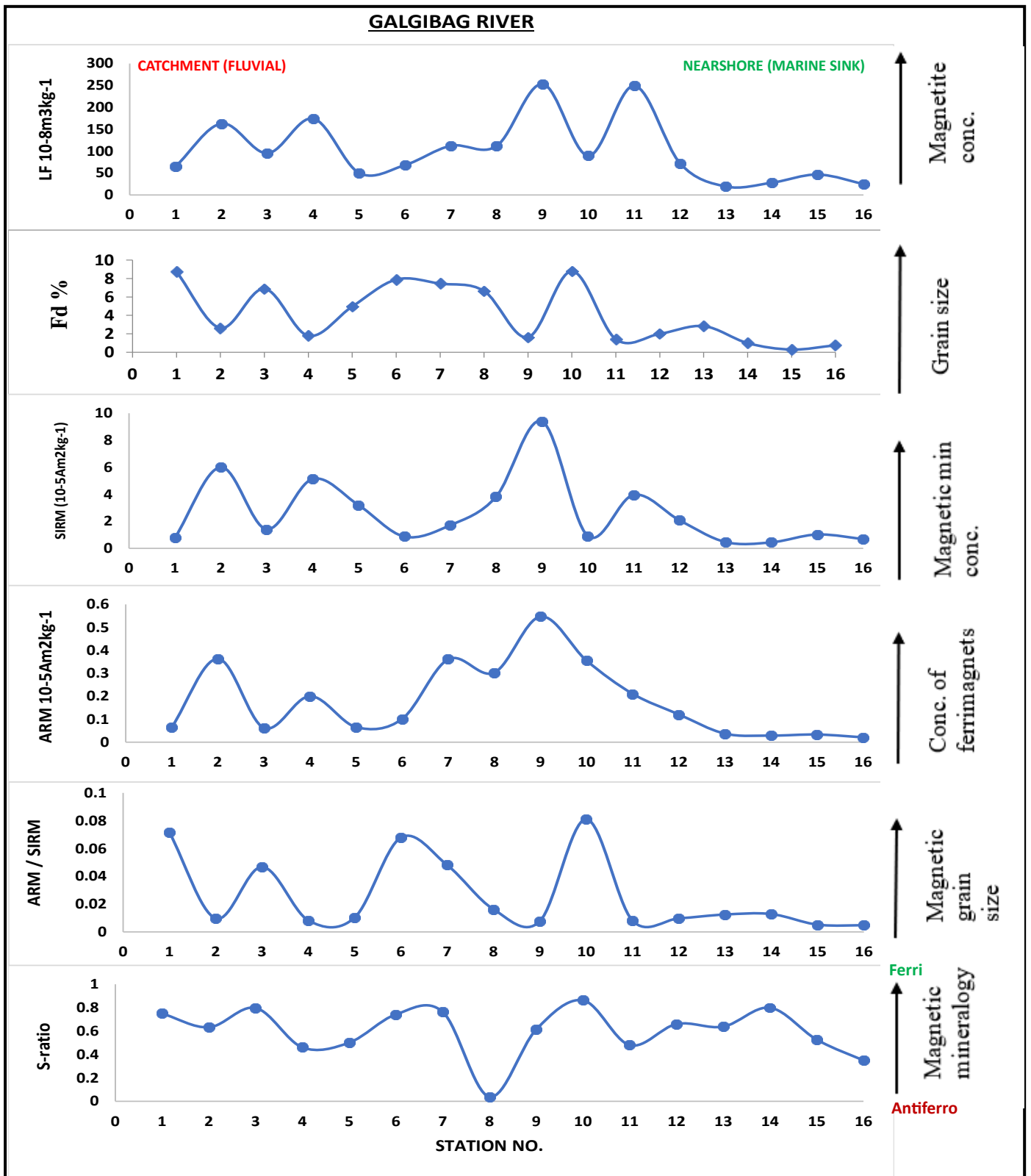


Figure 21: The above plots for Galgibag river showing variation in (a) magnetic mass susceptibility (χ_{lf}) represents the abundance of ferrimagnetic minerals (magnetite), (b) Magnetic mineral grain distribution, (c) Concentration of magnetic minerals, (d) Concentration of fine ferrimagnets, (e) magnetic grain size indicator (ARM/SIRM), (f) magnetic mineralogy indicators (S-ratio)

Spatial distribution of magnetic mineral and rock magnetic parameters

- Spatial distribution of magnetic minerals in different goan rivers from source-to-sink are presented in Fig 18,19,20,21,22. Based on the surficial magnetic susceptibility values, we have identified several regions of magnetite rich depositional sites throughout the estuary.
- Sediment magnetism data of surficial sediments from studied goan river showed high variability in terms of magnetite concentration (χ_{lf}), grain size (ARM/IRM), and mineralogy (S-ratio).

Tiracol River.

- As evident in magnetic susceptibility, ARM and SIRM profiles, we noticed several discrete zones enriched in magnetic mineral throughout the estuary.
- $F_d\%$ and ARM/SIRM data suggest that magnetic particles are relatively coarse grained except in sample from Station no 21.
- Majority of samples are dominated by ferrimagnetic minerals as confirmed through S-ratio.

Chapora River

- Concentration dependent parameters showed large fluctuations and higher concentration of magnetic mineral are observed in samples from stations 25 to 34.
- $F_D\%$ and ARM/SIRM profiles mimic each other and showed relatively lower values and near consistent trend suggesting the predominance of coarse-grained magnetic particles.
- Mineralogy diagnostic magnetic proxy (S-ratio) confirmed the dominance of ferrimagnetic minerals.

Sal River

- Compared to other goan river system, samples from Sal river sediments possesses low magnetite content.
- A uniform and low values of magnetic susceptibility, ARM, and SIRM values through the estuary (except station 24 to 28) indicate that these sediments possesses low magnetite content.
- Large fluctuation in FD% and ARM/SIRM values suggest that sediments are dominated by fine as well as coarse grained magnetic particles.
- Changes in S-ratio suggest the presence of ferri (low coercive) and antiferromagnetic (high coercive) minerals.

Talpona River

- A systematic trend of increase in magnetite content from upstream (Station no 16) to river mouth (Station no 1) suggest the gradual rise in magnetic mineral content.
- Wide range in S-ratio indicate the presence of ferri (low coercive) and antiferromagnetic (high coercive) minerals.

Galgibag River

- We did not observe any specific pattern in concentration, grain size, and magnetic mineralogy diagnostic parameters and rather these parameters exhibit large variations. This suggest that the sediments from Galgibag river are dominated by highly variable magnetic mineral content and grain sizes.

Preliminary Interpretation

A higher frequency-dependent susceptibility % translates into a stronger magnetic signal because of a higher fraction of SP particles, whereas higher frequency-dependent susceptibility values indicate a higher concentration of pedogenic iron oxide particles. Overall, large variability in magnetite content, grain size, and mineralogy in different goan rivers systems could be attributed to changes in catchment lithologies, riverine-estuarine hydrodynamics, river bed morphology, grain size, changes in distance between source-to-sink and depositional environment (erosive, accretion)

4.3. Scatter plots comparing the magnetic parameters of all five rivers.

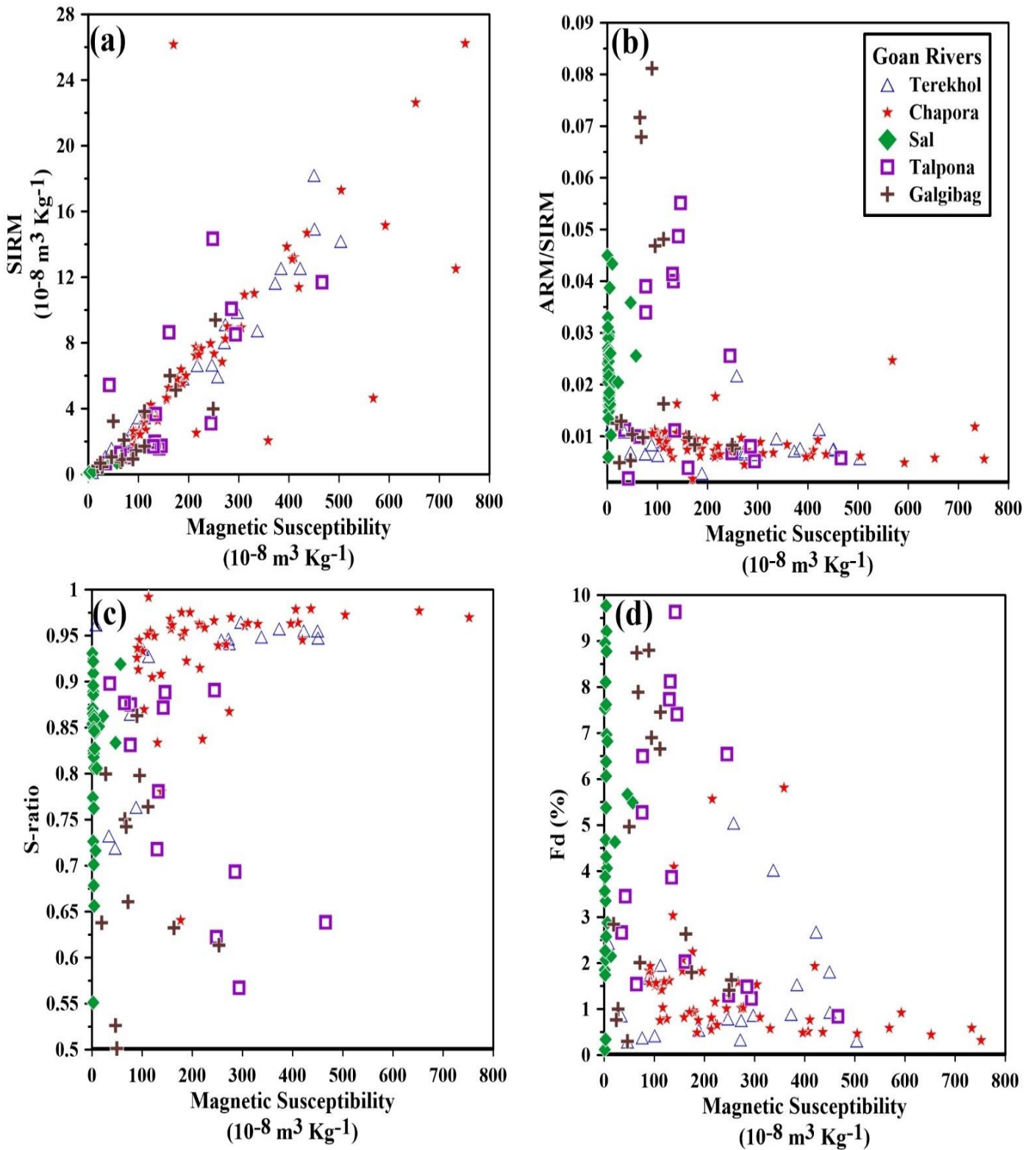


Fig 22: Scatter plots comparing the different magnetic parameters in correlation of five studied rivers.

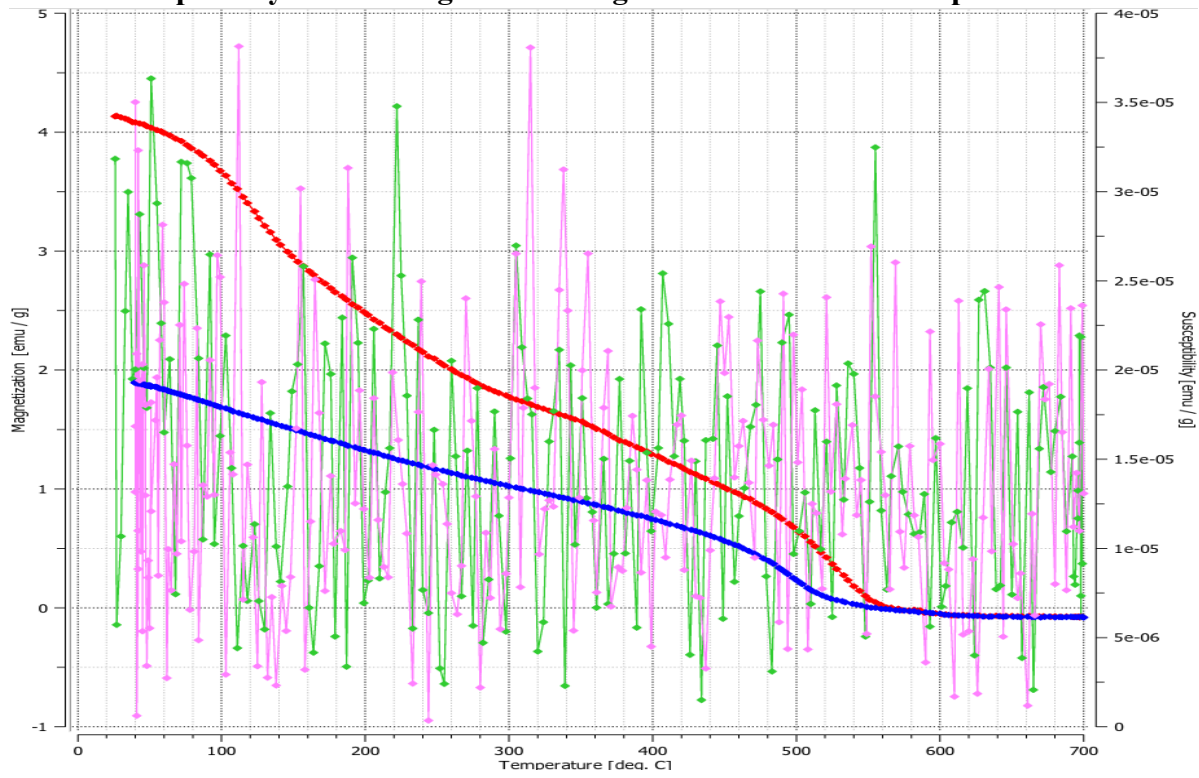
Bivariate plots between rock magnetic parameters of surficial sediments

A good covariation between magnetic susceptibility and SIRM values of majority of riverine sediment samples suggest that the sediment are dominated by ferrimagnetic minerals (Figure 23).

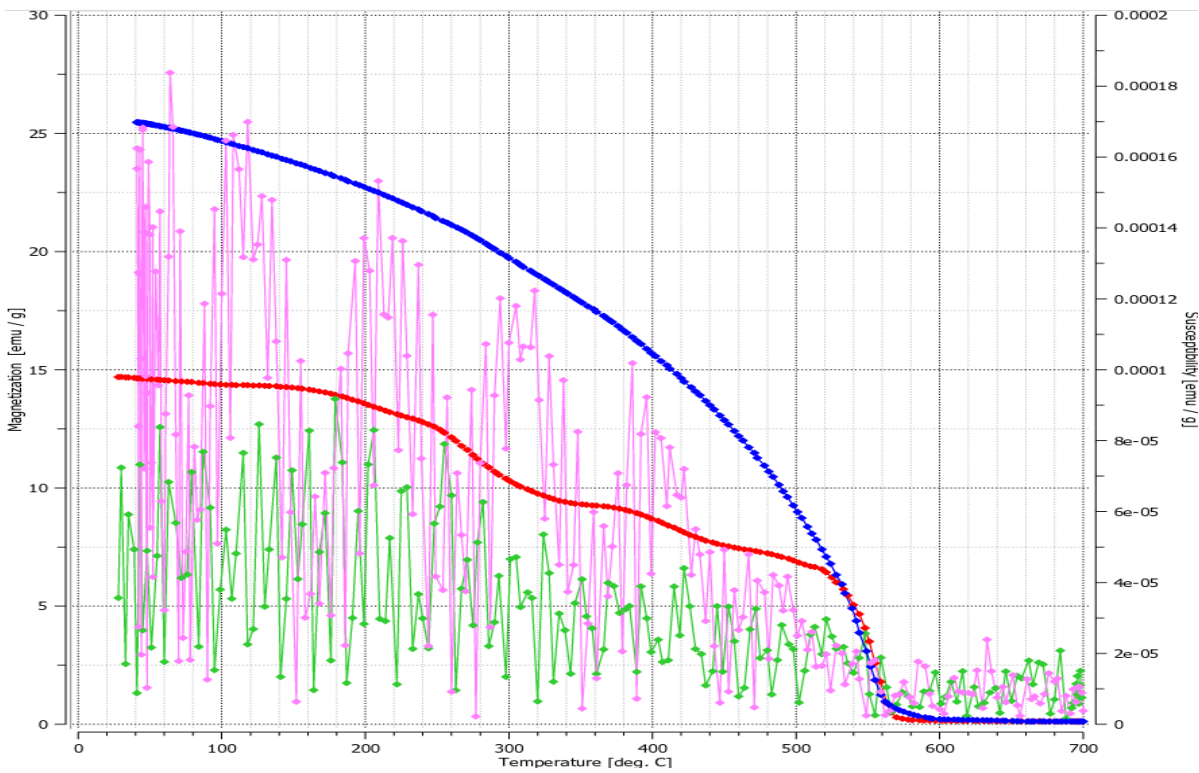
Bivariate plot between ARM/SIRM and magnetic susceptibility showed interesting trend. The samples exhibiting high susceptibility are dominated by coarse grained magnetic particles and vice versa. However, sal river samples showed different pattern exhibiting lowest susceptibility, but wide range in magnetic grain size (ARM/SIRM).

Talpona and Sal river sediment are mainly rich in high coercivity minerals compared to other rivers. This observation was clearly visible in cross plots between magnetic susceptibility Saturation and FD %.

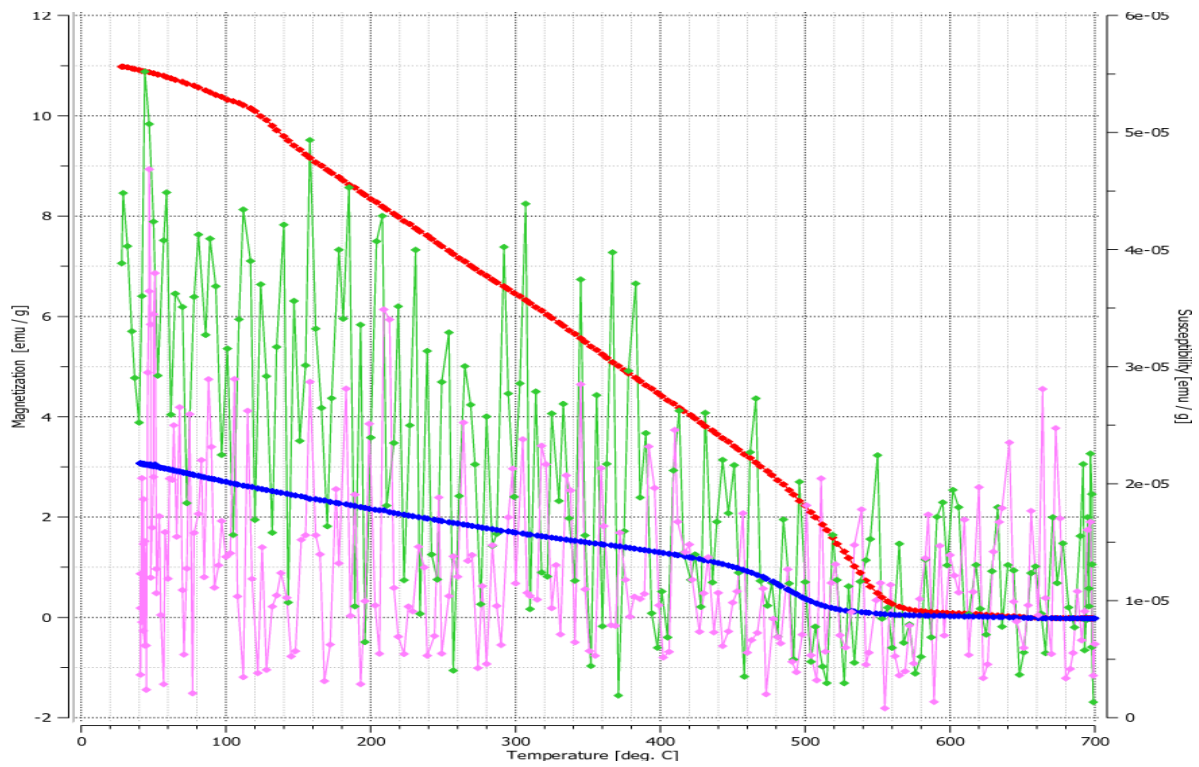
4.4. Susceptibility-thermomagnetic heating curves for selected samples of rivers.



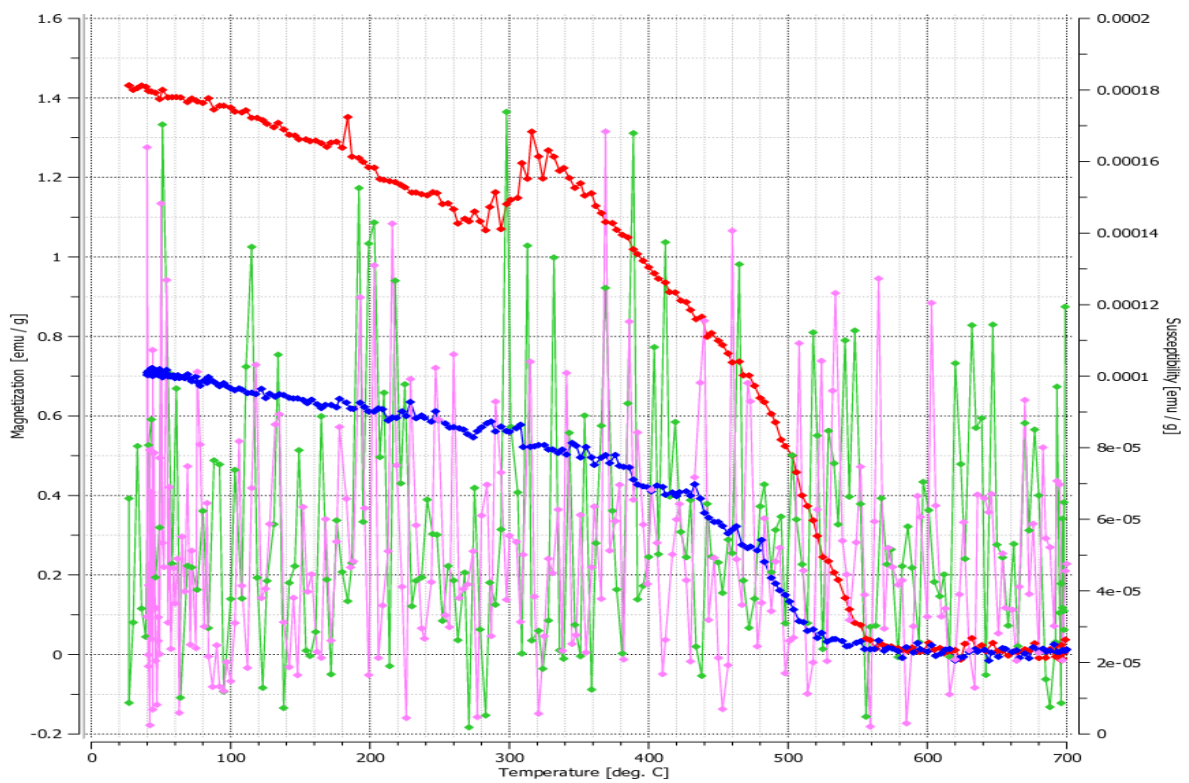
(a) TEREKHOL TK-01



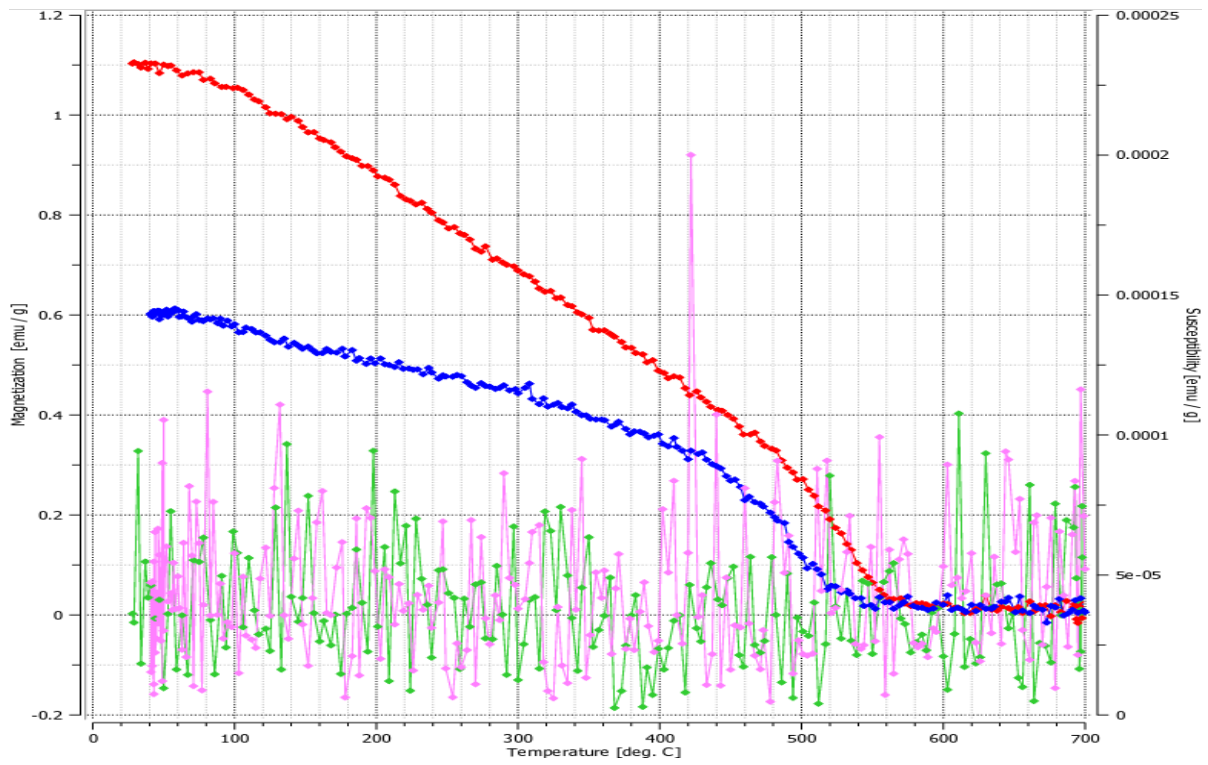
(b) TEREKHOL TK-06



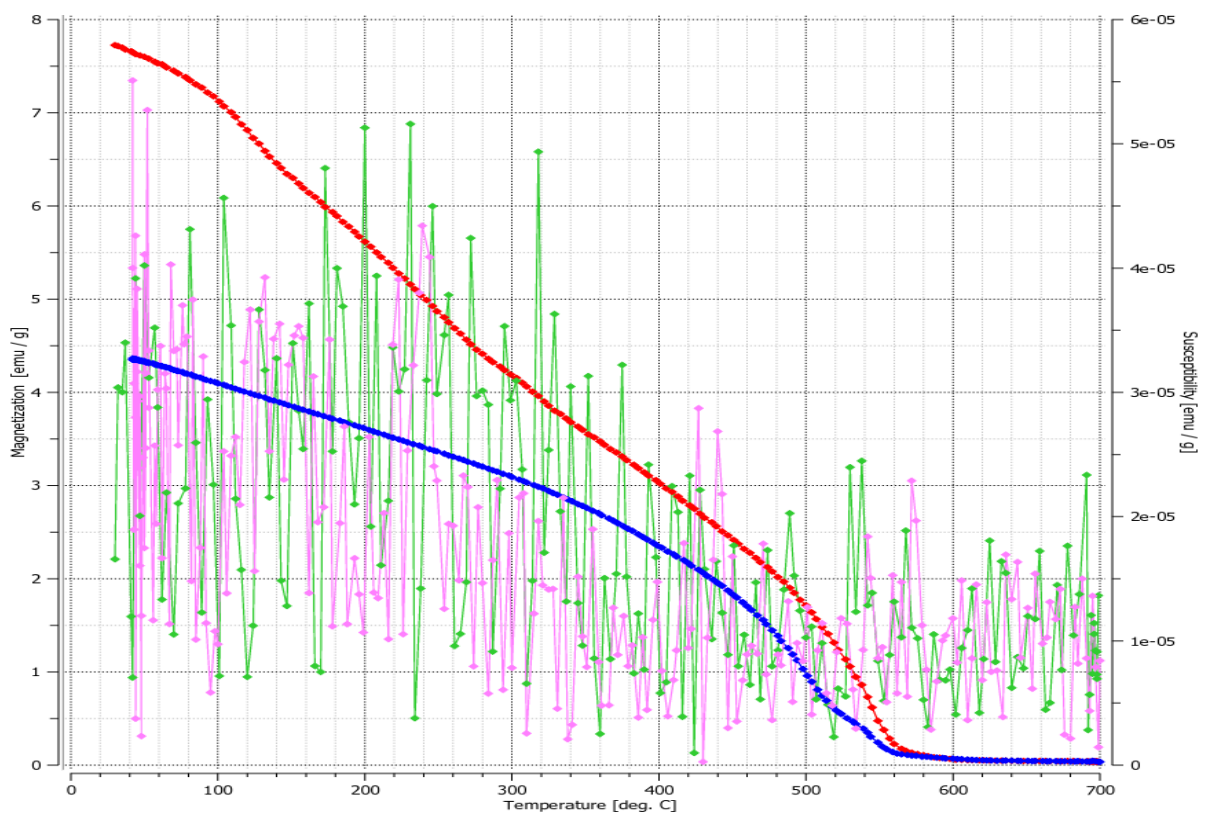
(C) TEREKHOL TK -11



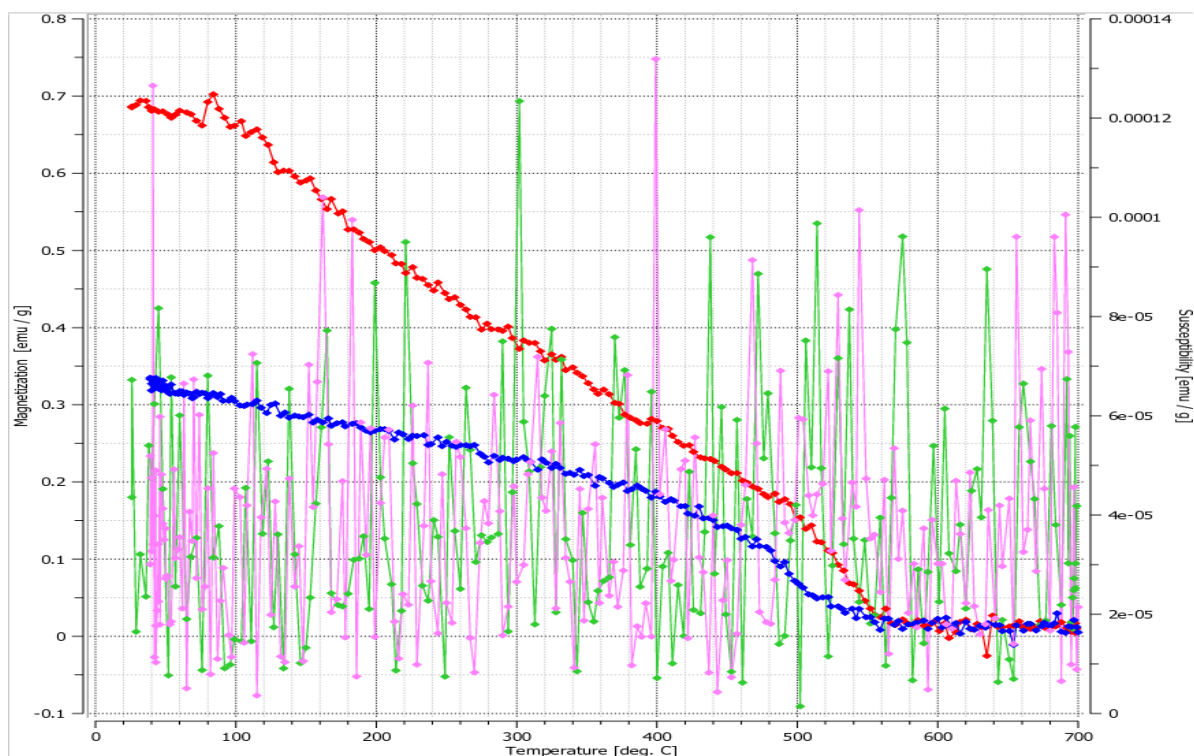
(d) TEREKHOL TK-19



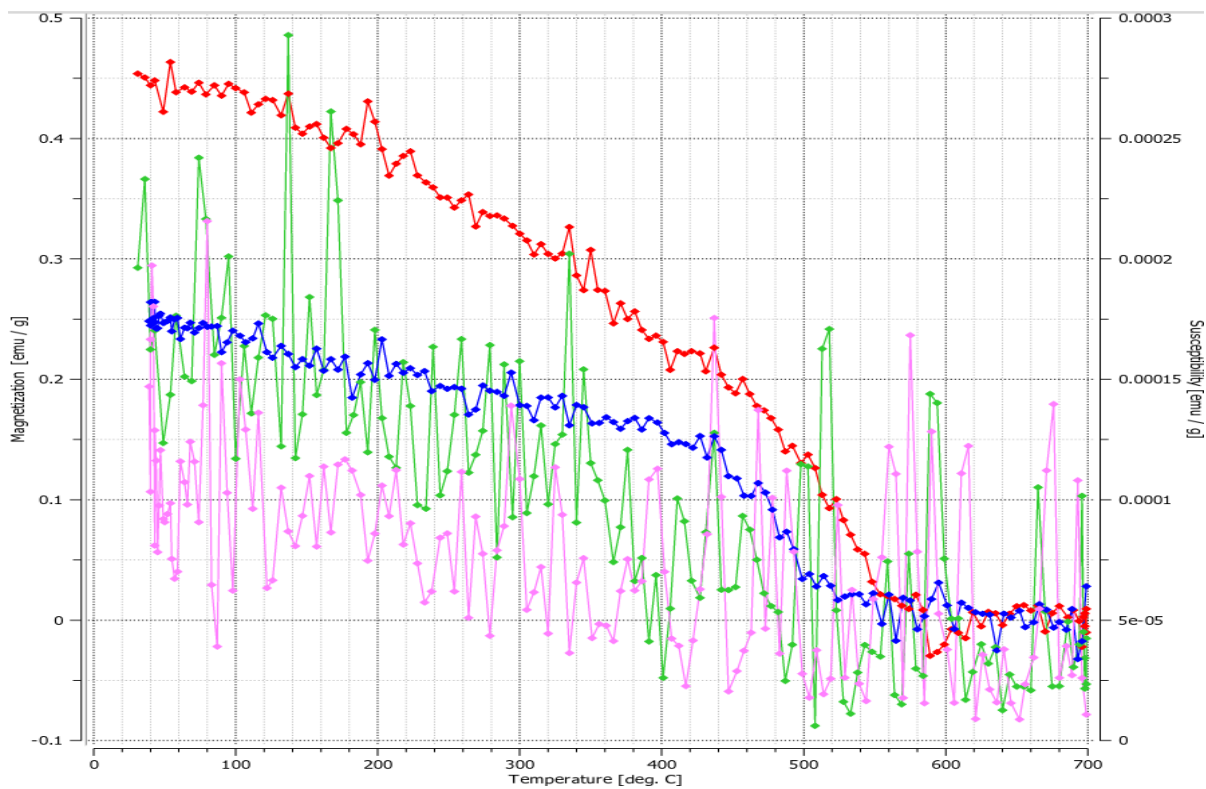
(e) CHAPORA-01



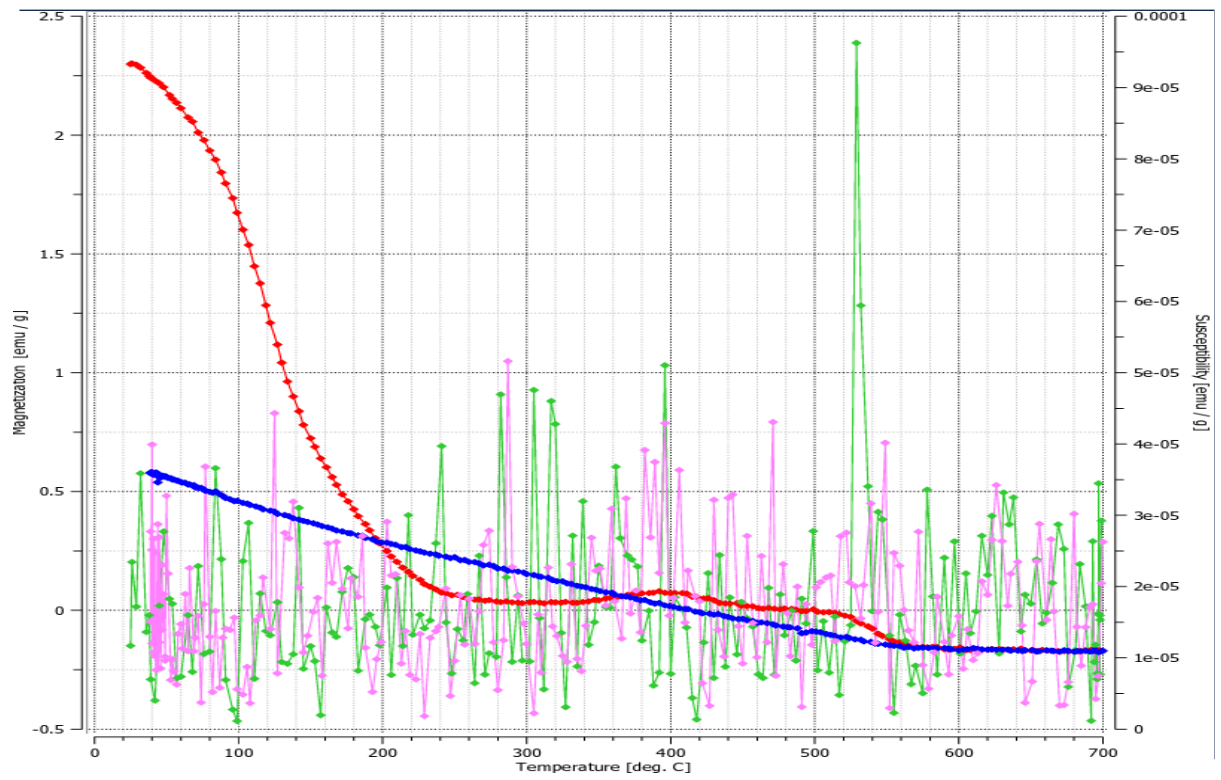
(f) CHAPORA-09



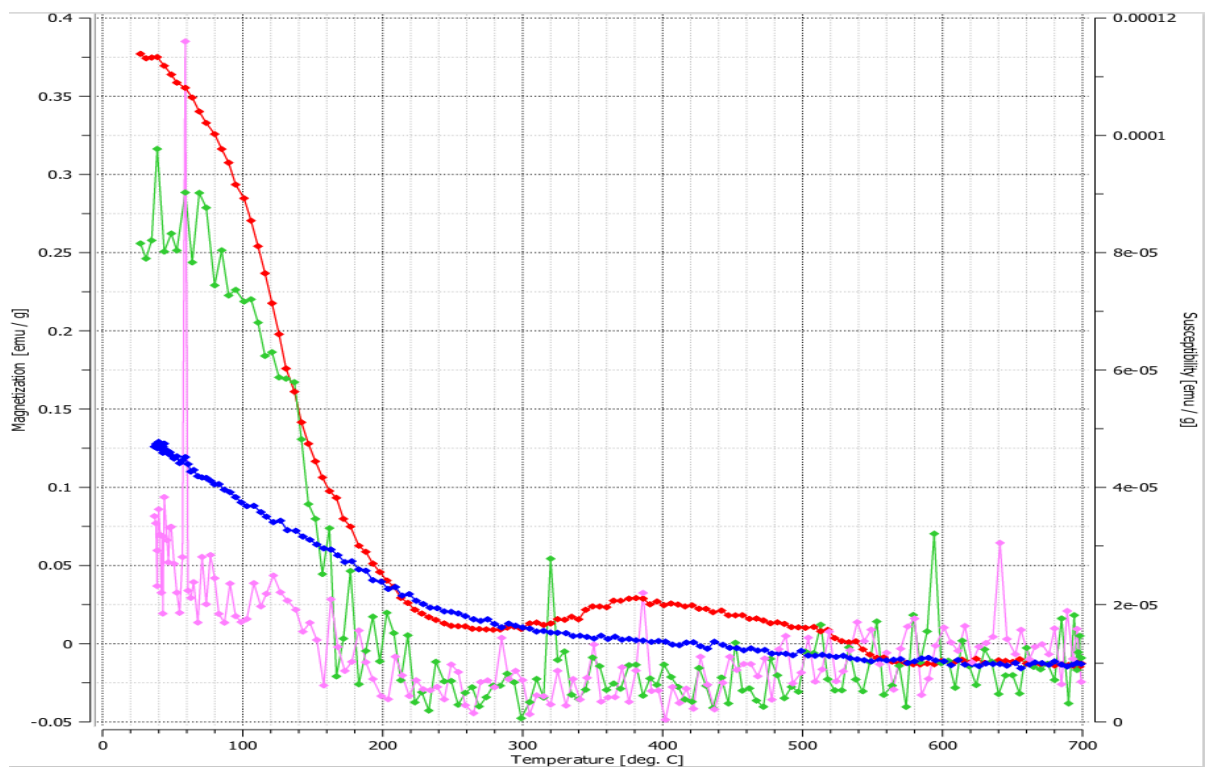
(g) CHAPORA- 37



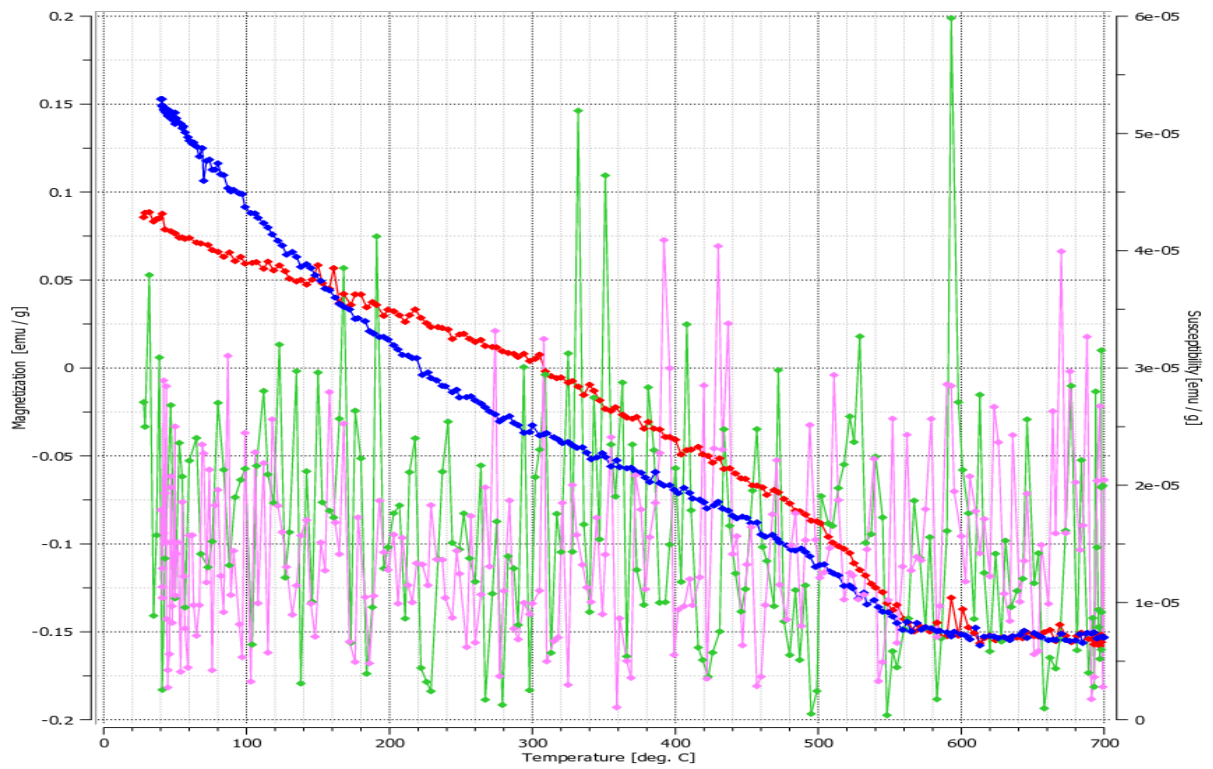
(i) CHAPORA- 66



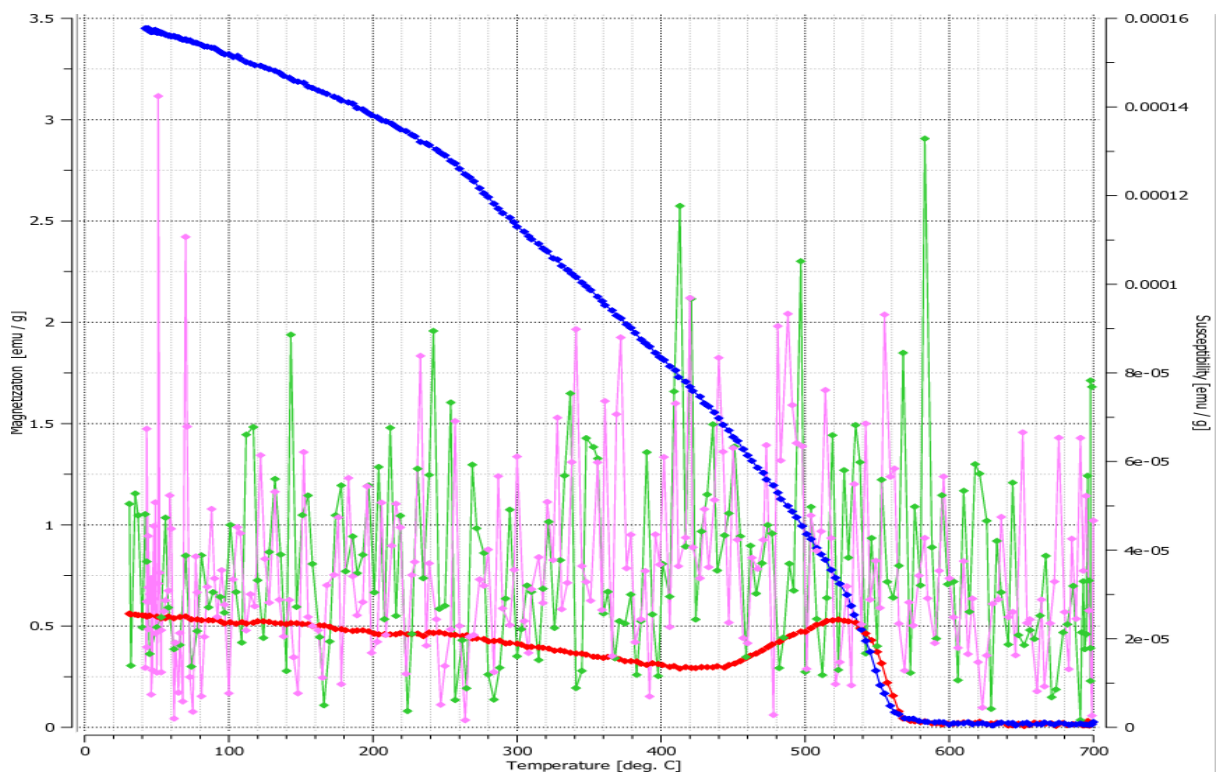
(j) SAL-01



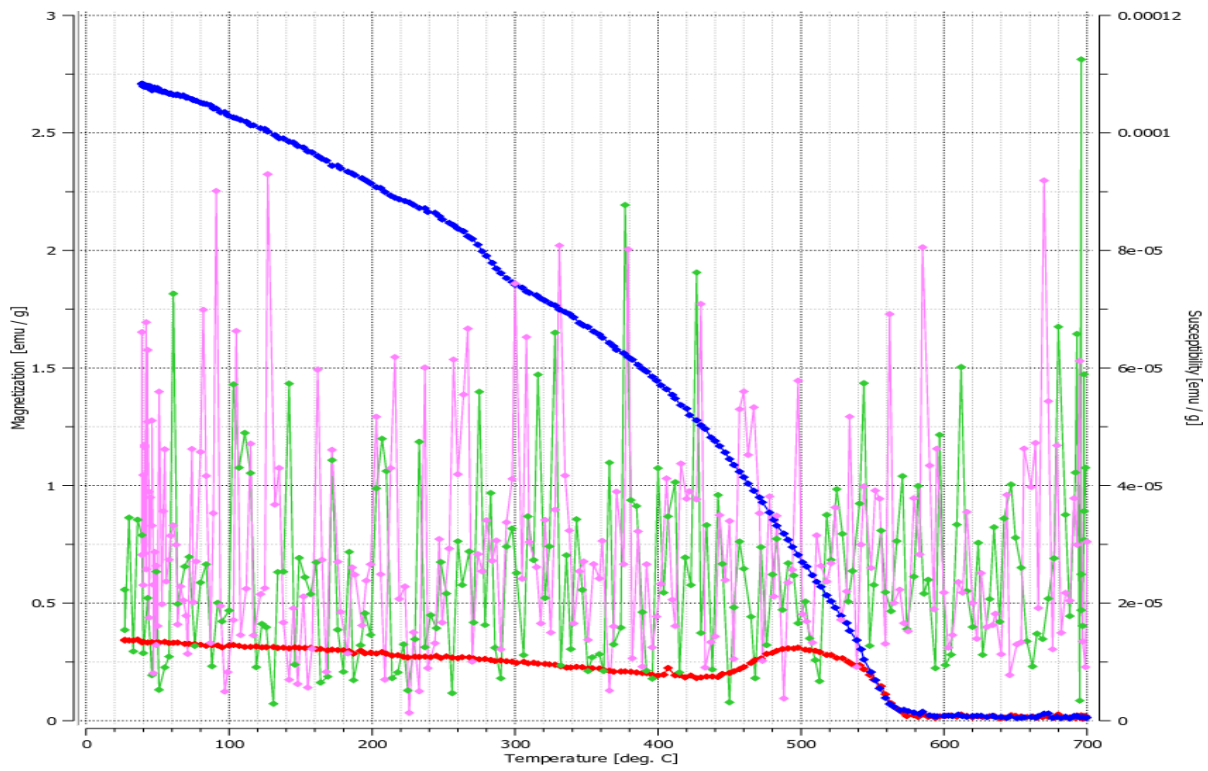
(k) SAL-10



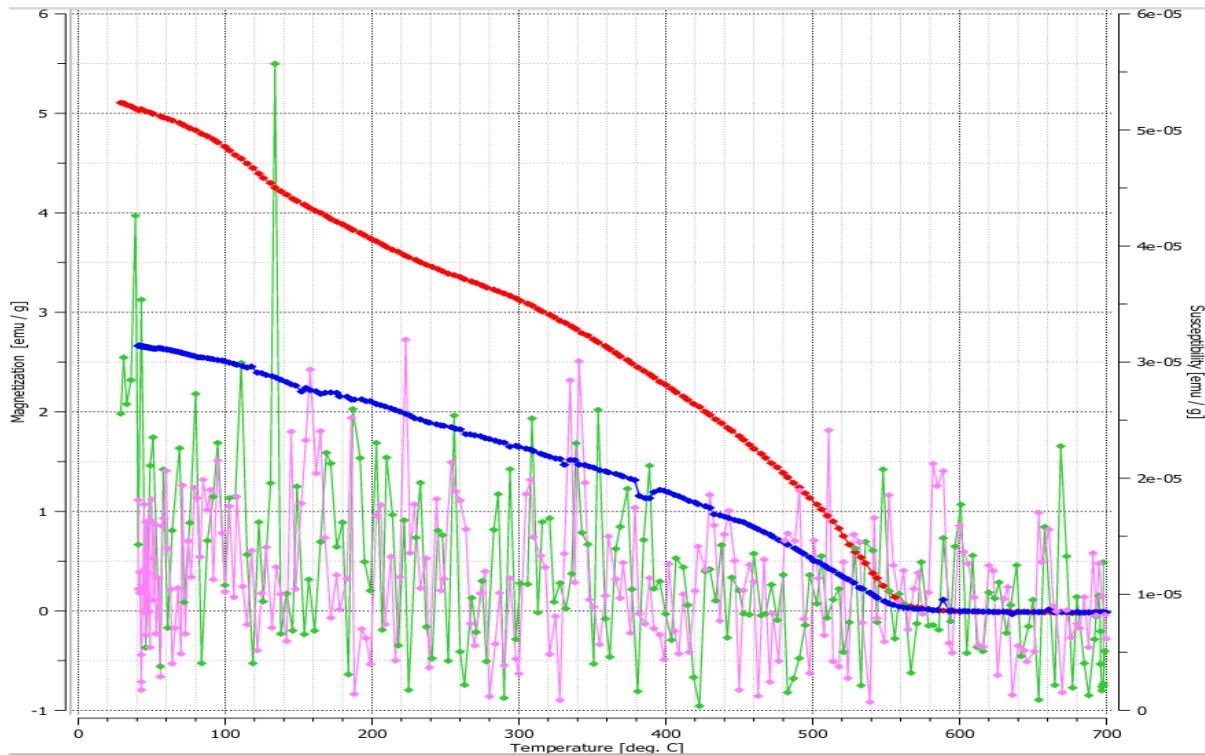
(l) SAL- 34



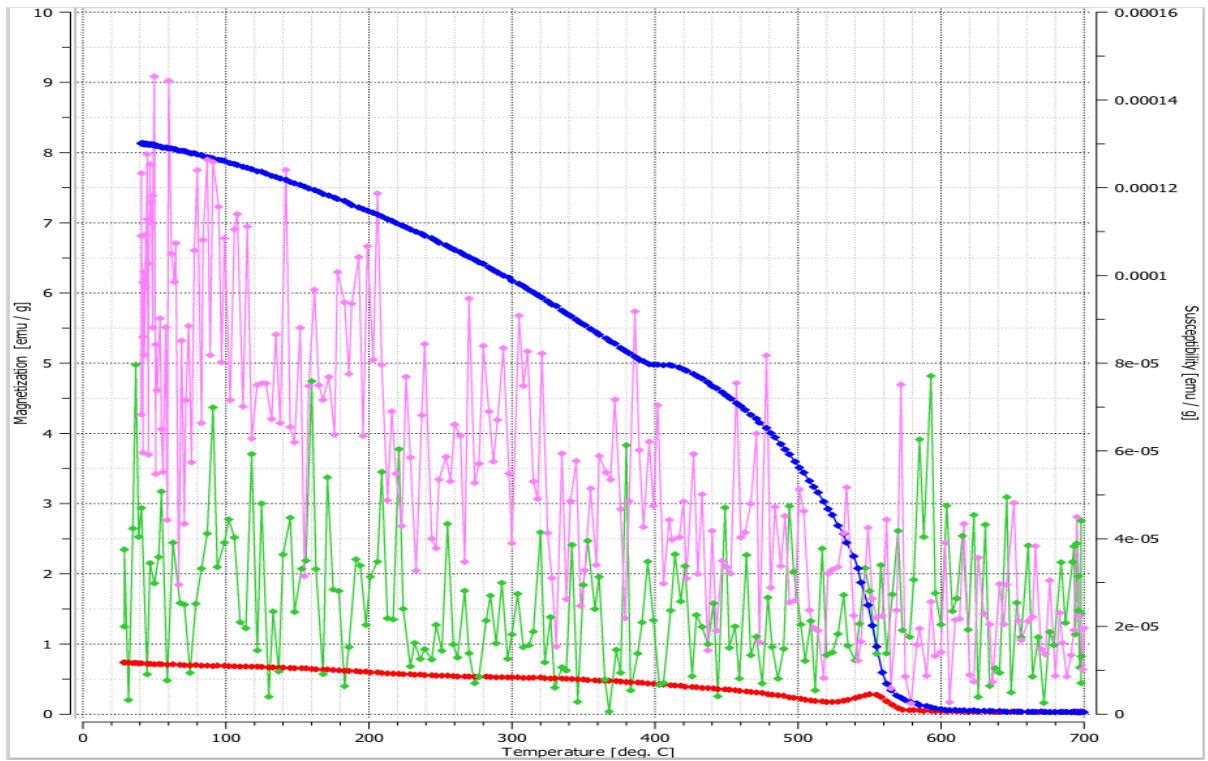
(m) SAL- 39



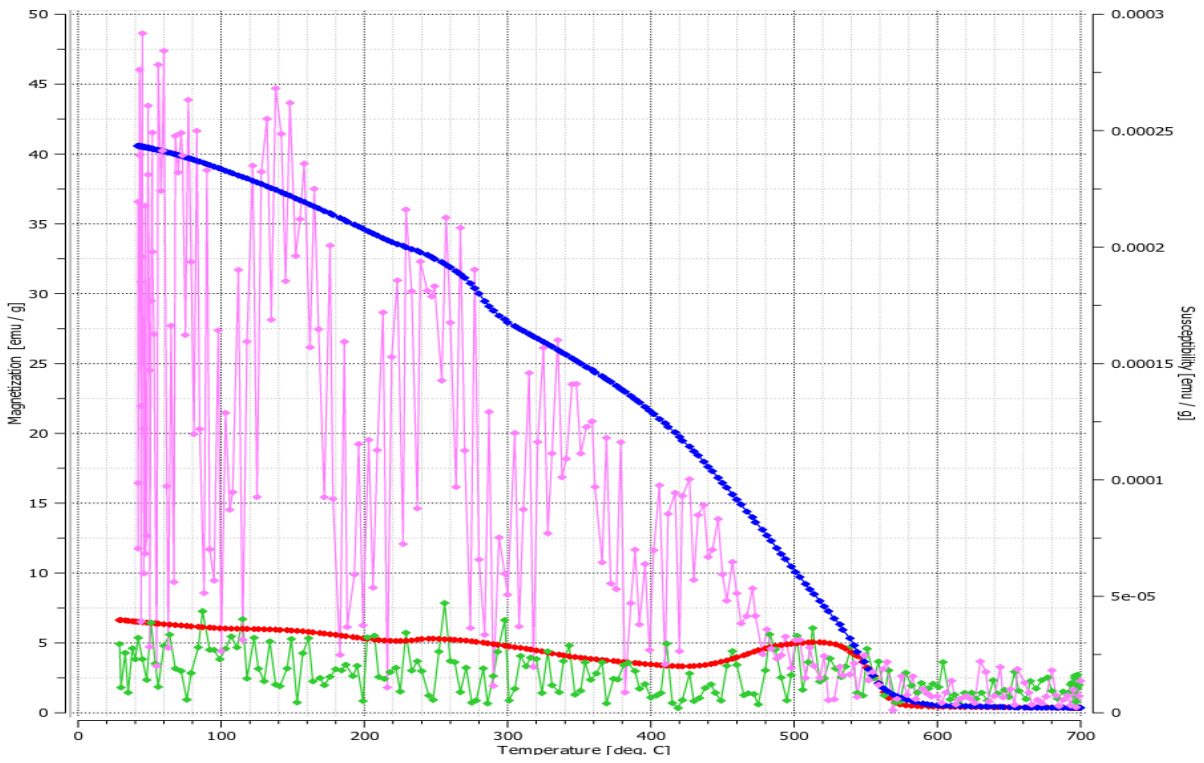
(n) TALPONA- 01



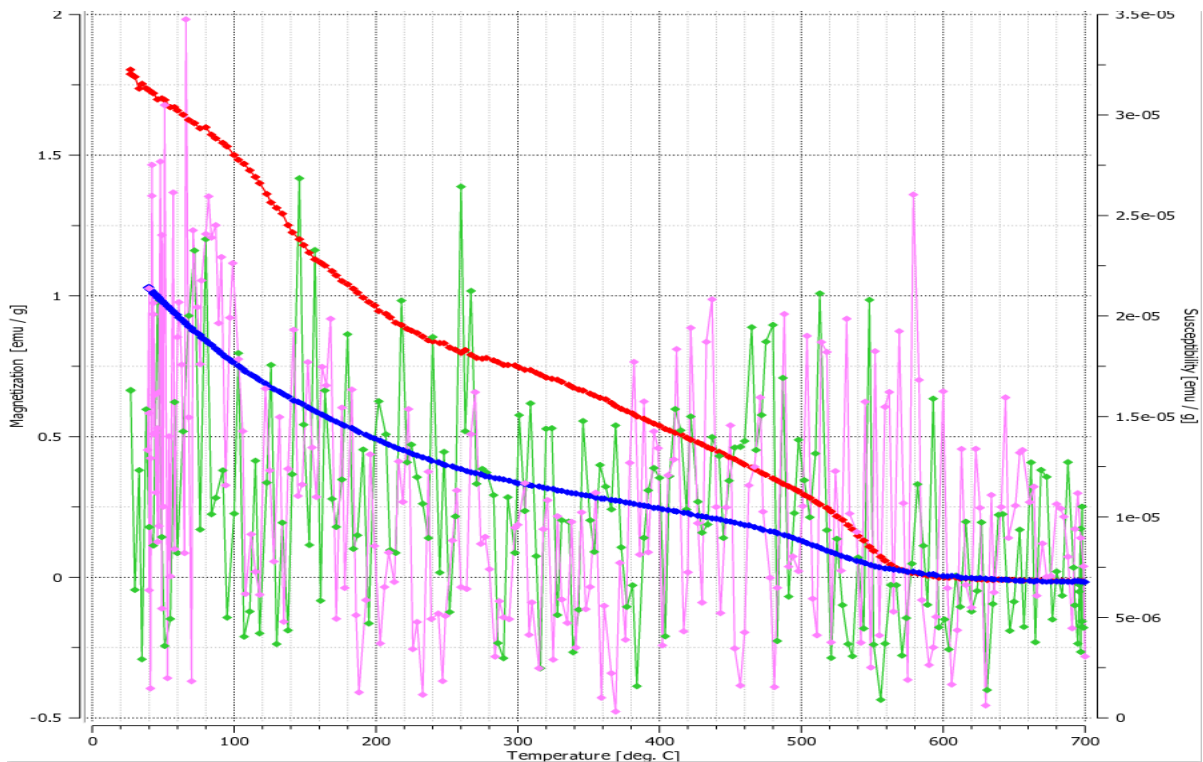
(o) TALPONA- 12



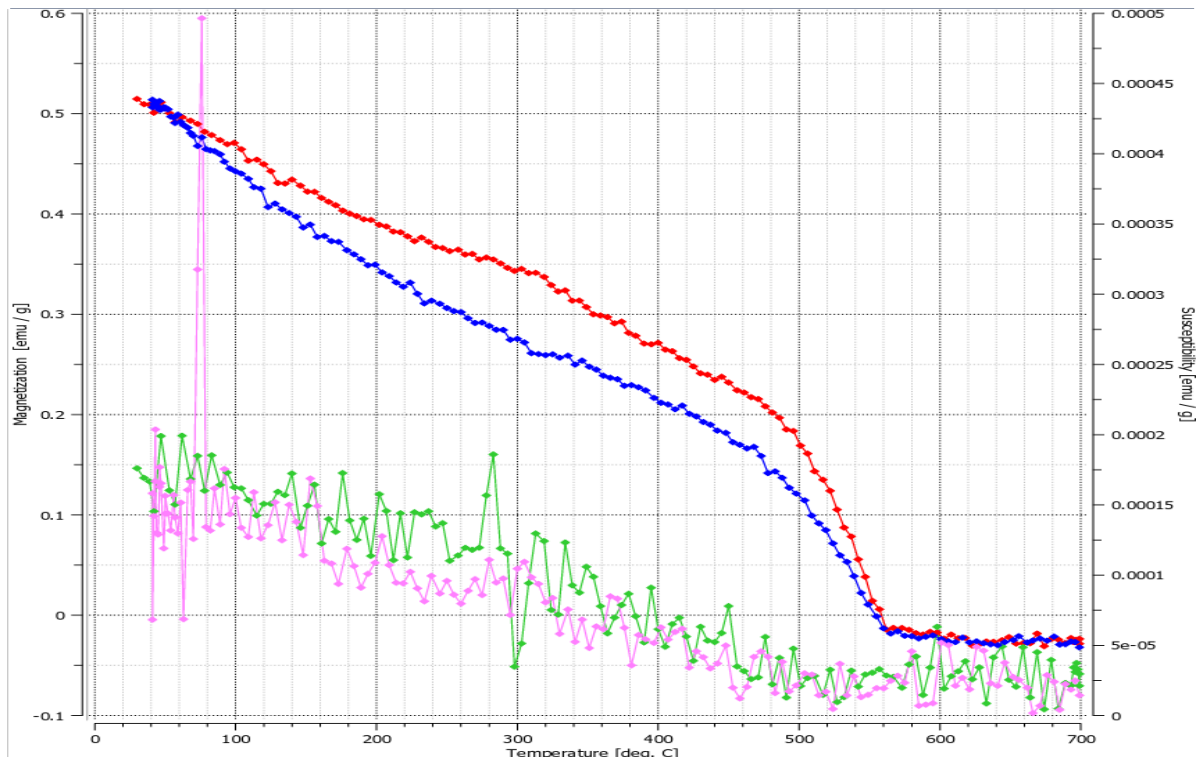
(q) GALGIBAG- 02



(r) GALGIBAG- 07



(s) GALGIBAG-13



(t) GALGIBAG-14

Fig 23: Temperature dependent χ -T curves (a-t) of representative selected sediment samples from different goan river systems

Temperature dependent magnetic properties

χ -T curves of representative selected sediment samples from different goan river systems are presented in Figure 23.

A distinct drop in χ values between 540 and 650°C in the most of the analyzed samples indicate that the magnetic mineralogy of the bulk sediment is mainly dominated by ferri-(magnetite, titanomagnetite) and antiferromagnetic (titanohematite) particles.

A minor χ rise between 352 and 452°C in few samples can be attributed to the dominance of titanomagnetite exhibiting a wide range of Ti-contents, transformation of maghemite into magnetite, or due to conversion of paramagnetic minerals and iron-containing silicates to magnetite during heating process, or transformation of iron-containing silicates to magnetite.

4.5. Electron Microscopy

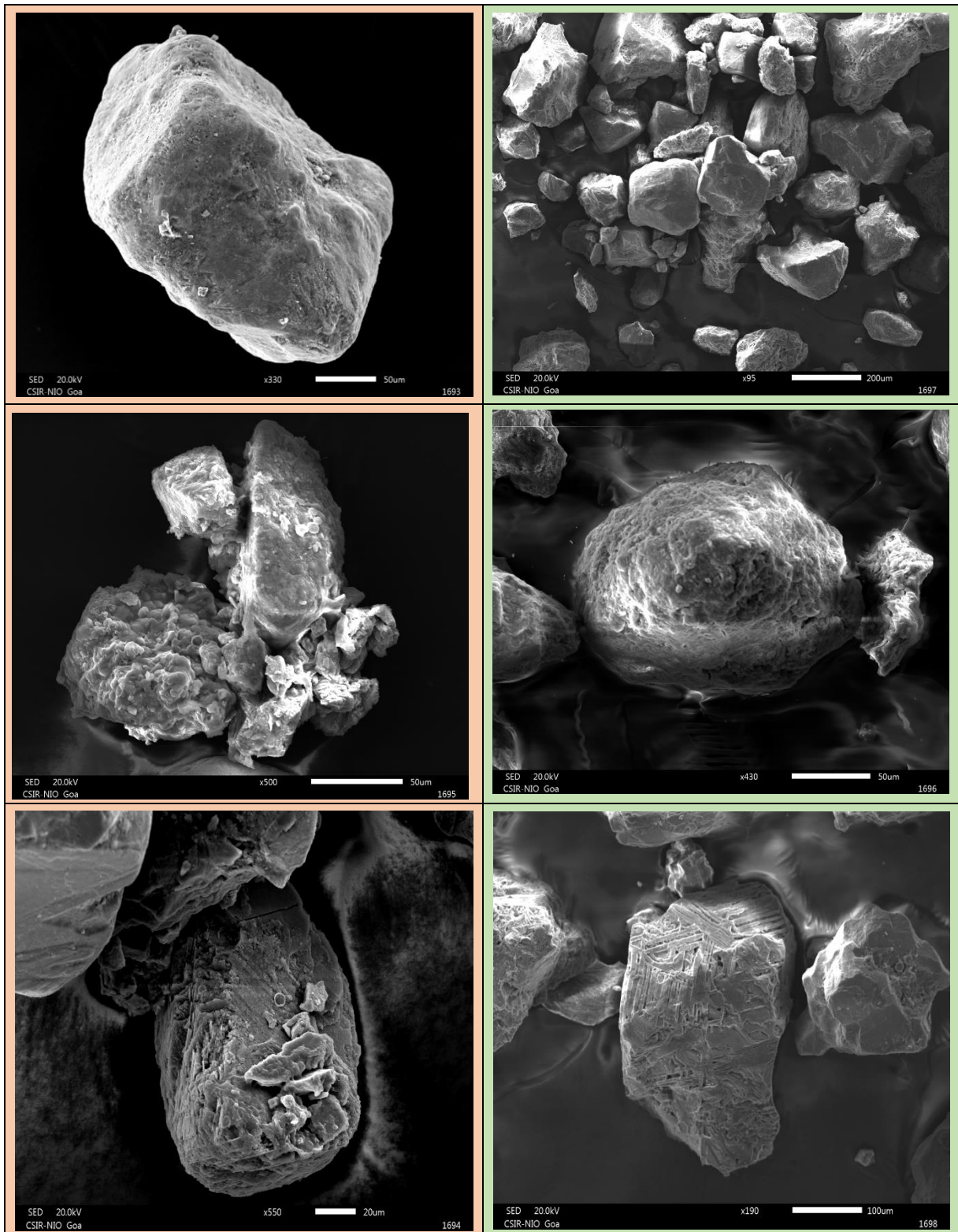
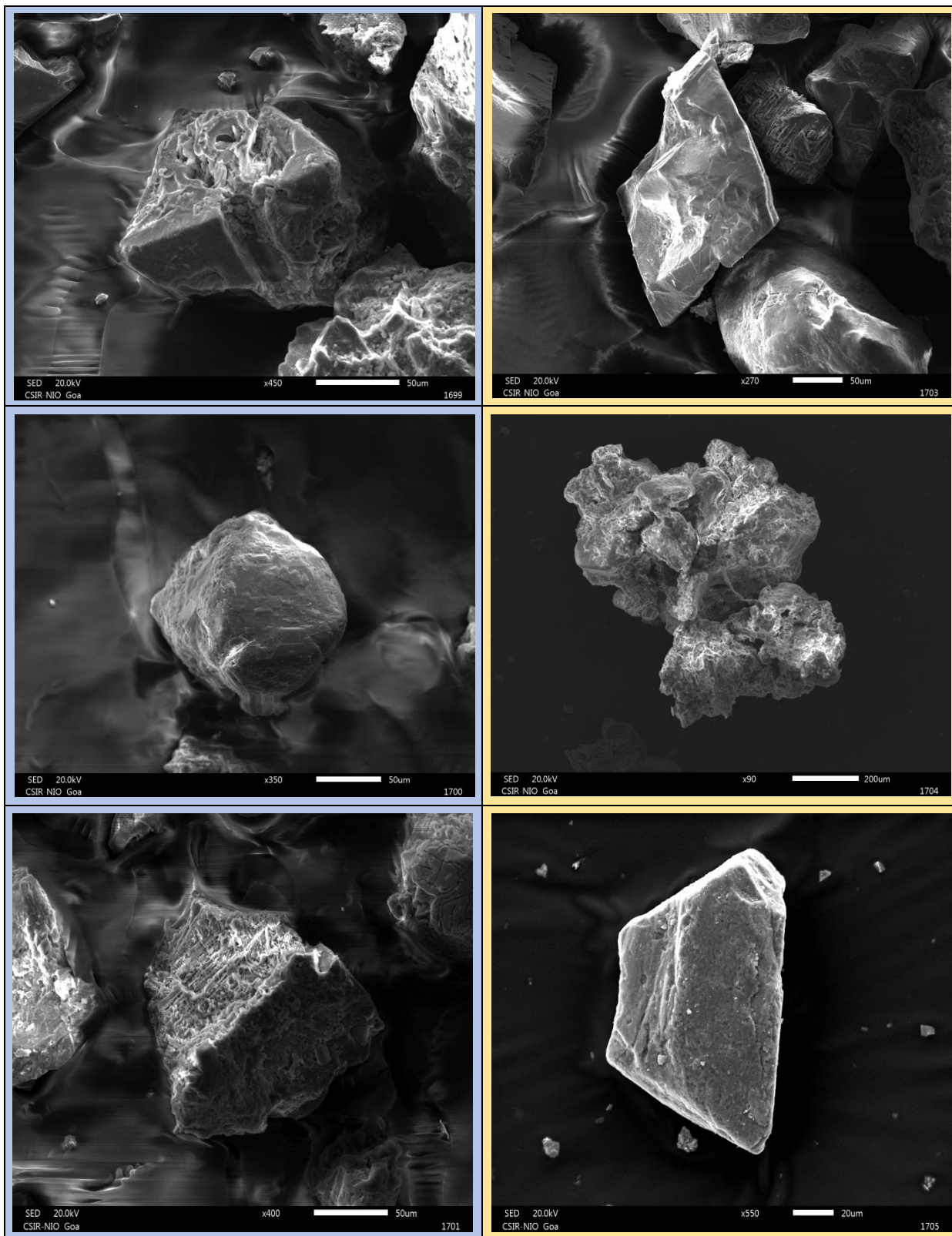
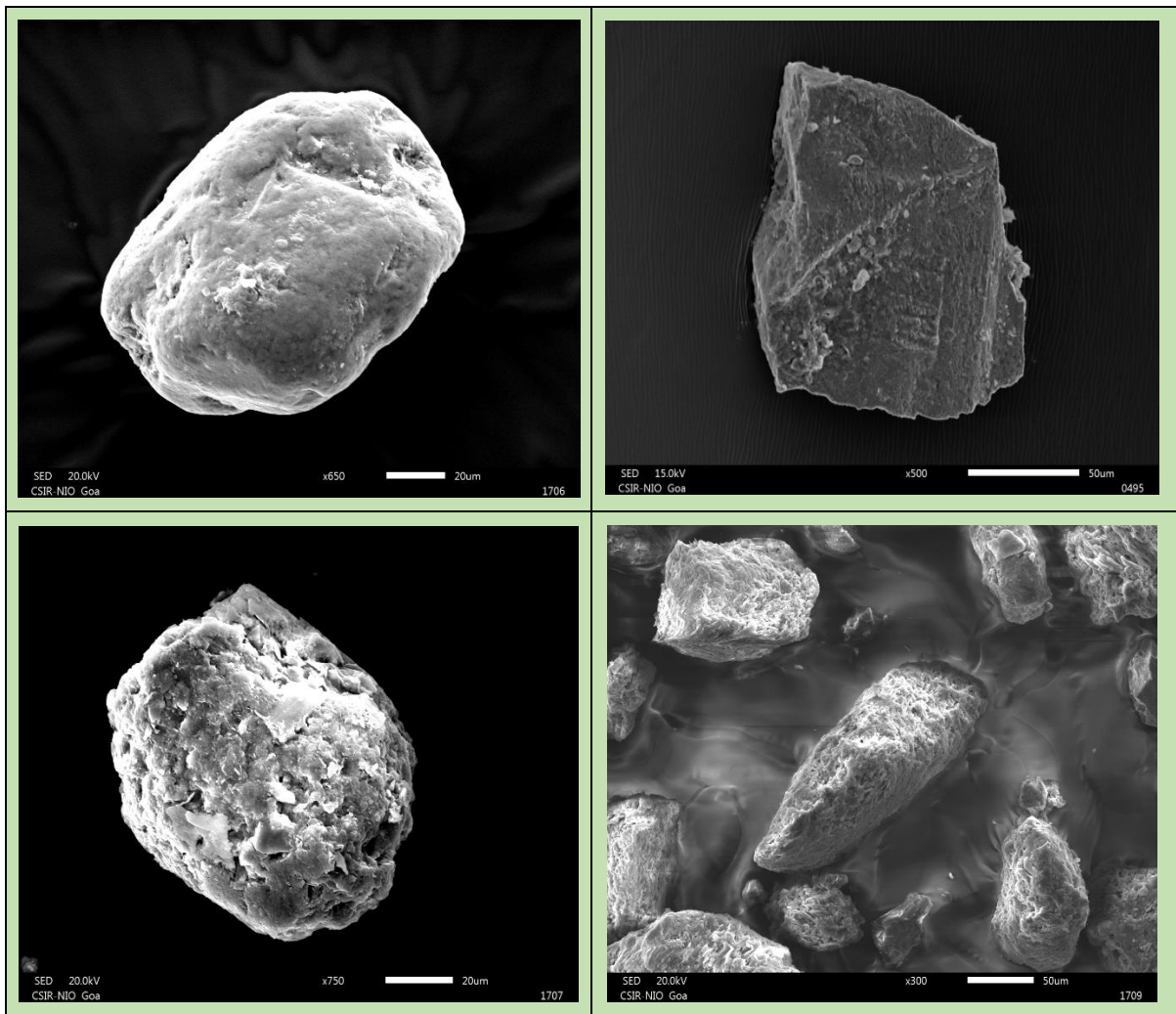


Fig 24: scanning electron microscope images

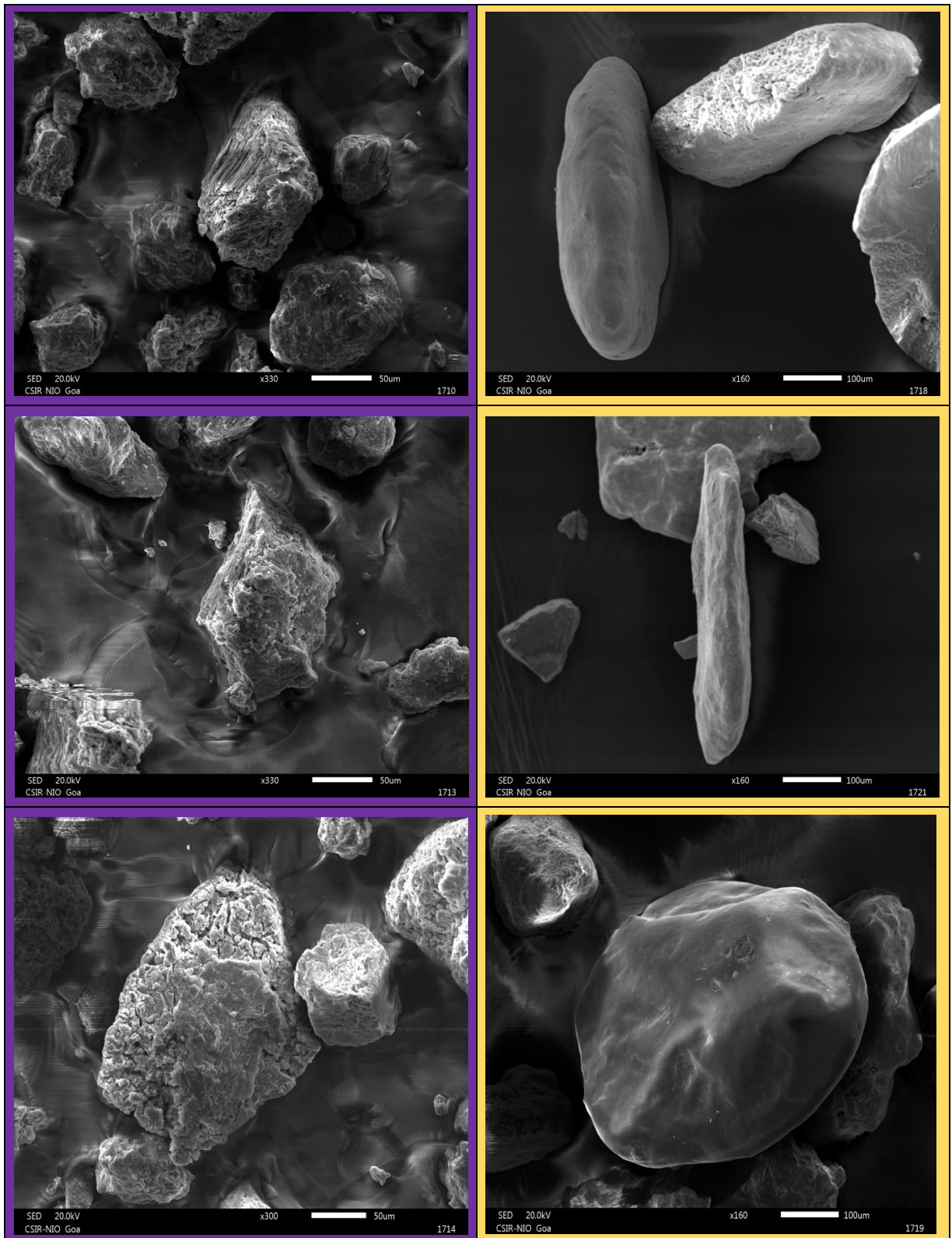
SEM images of selective samples of terekhol river ■ TK-04 ■ TK-19



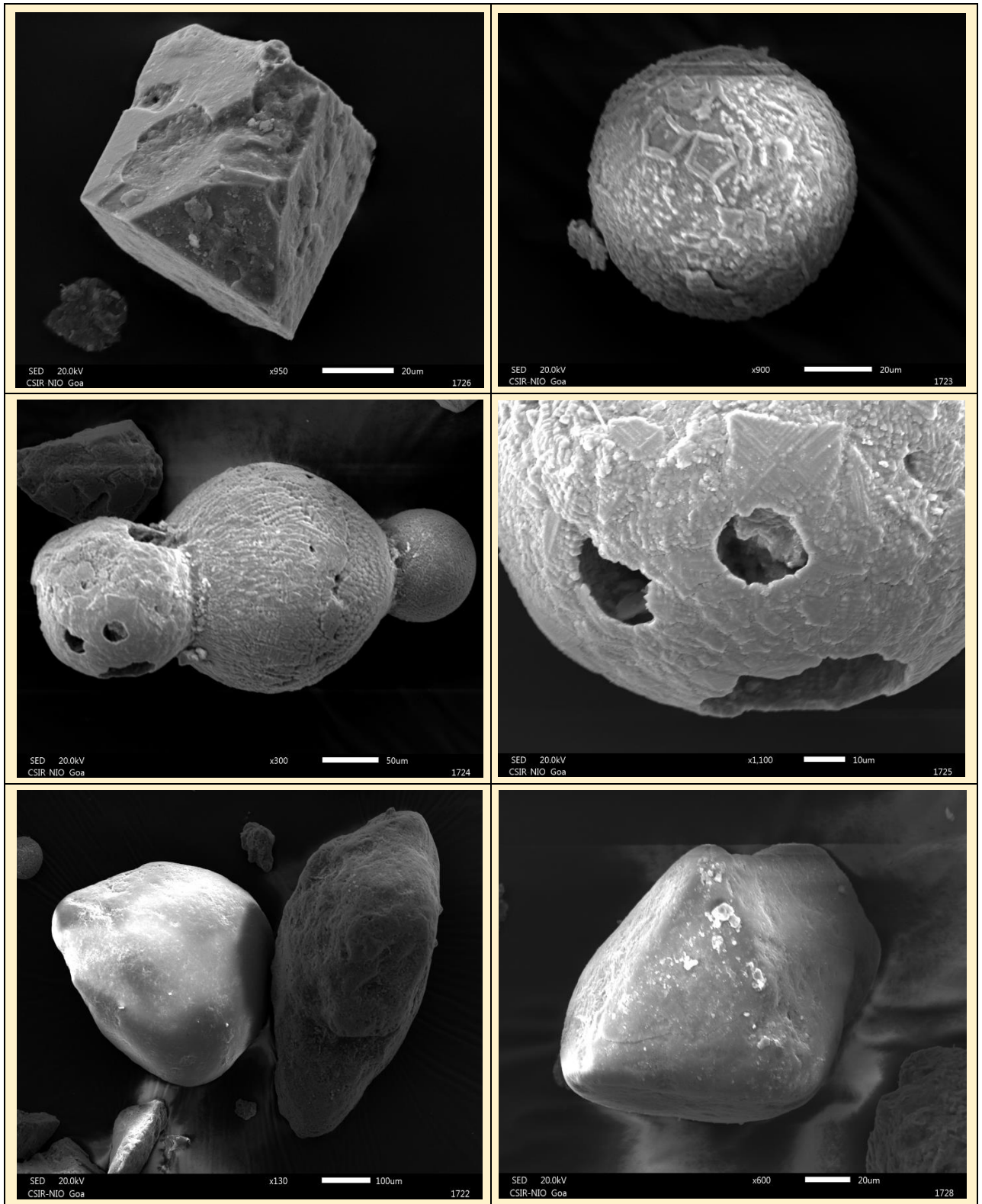
SEM images of selective samples of chapora river ■ CP-01 ■ CP-51



SEM images of selective samples of sal river SL-27



SEM images of selective samples for Talpona river ■ TP-01 ■ TP-16



SEM images of selective samples for Galgibag river GB-13

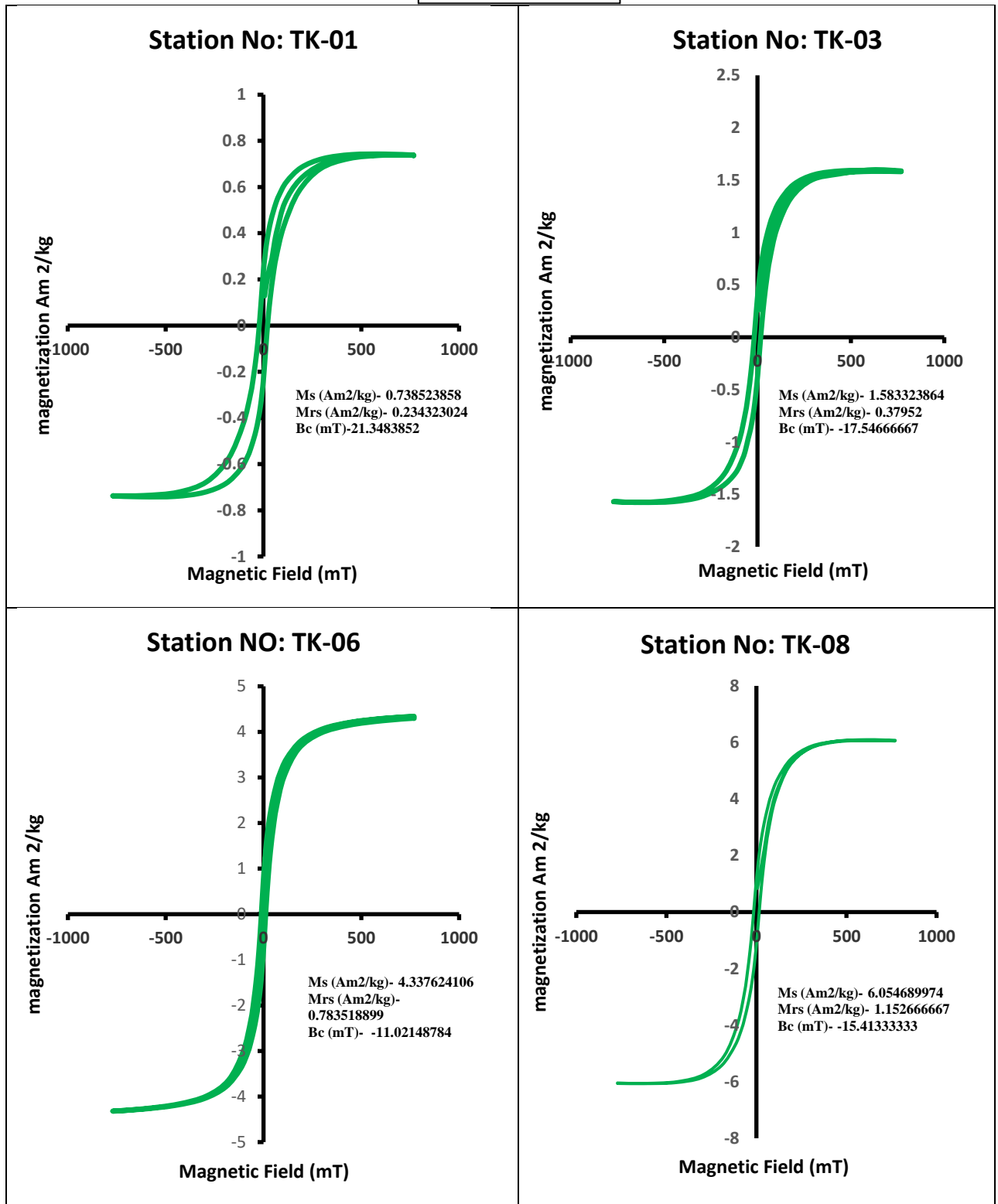
Magnetic mineral extraction and scanning electron microscopy analyses

Magnetic particles extracted from representative bulk sediment samples from Terekhol, Chapora, Sal, Talpona, and Galgibagh Rivers were analyzed for electron microscopy. We noticed large variations in morphology, shape, and size of magnetic particles through the different parts of each river system. Majority of the magnetic particles were mainly coarse size and primarily of detrital origin. Most of the particles displayed diverse morphologies sharp edges, sub rounded to rounded, euhedral type.

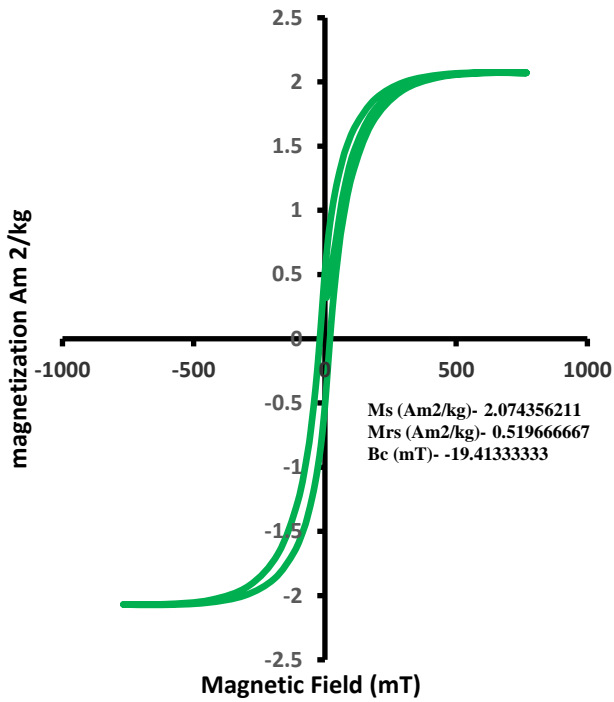
Samples analyzed for terekhol river in SEM showed most samples were sub angular to sub rounded. Chapora, sal and talpona river samples exhibit well rounded and well sorted samples with smooth edges which indicates have experienced long-range transport during their transit from source-to-sink. We did not observe any signature of diagenetic/authigenic minerals (pyrite, greigite) in the analyzed samples. This can be explained by the fact that riverine sediments are well-ventilated and post-depositional geochemical processes had minimal influence on the detrital magnetic mineral assemblages as bulk sediment magnetic signal.

4.6. Hysteresis Loops for selective river sediments samples

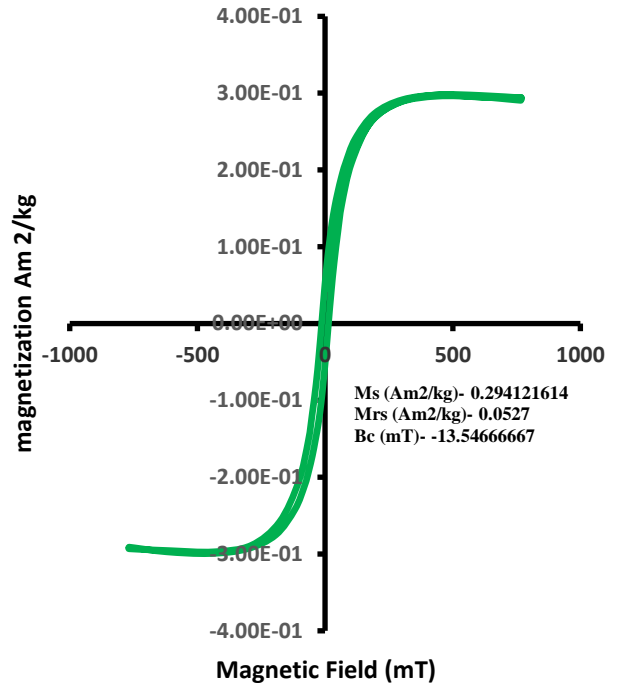
TEREKHOL RIVER



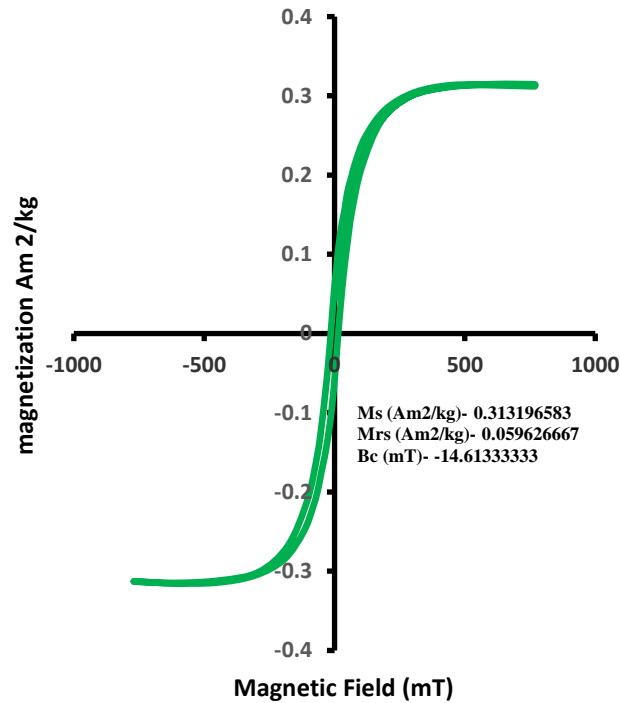
Station No: TK-11



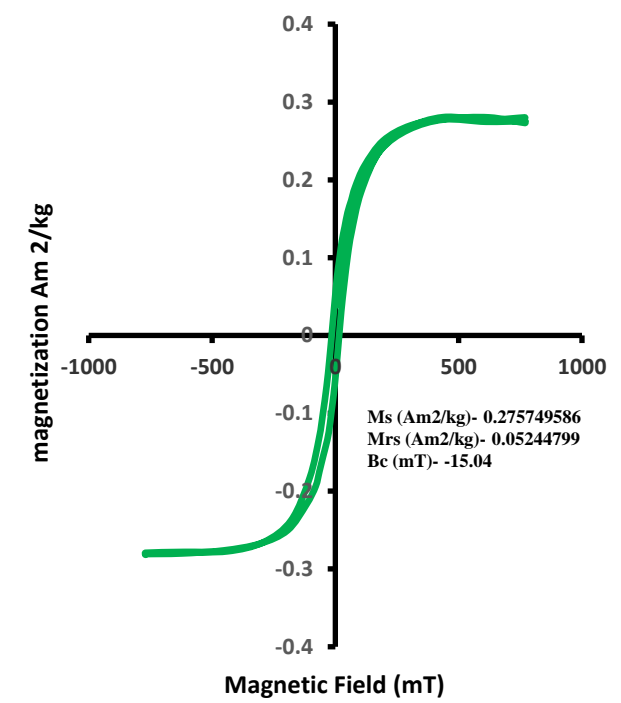
Station No: TK-13



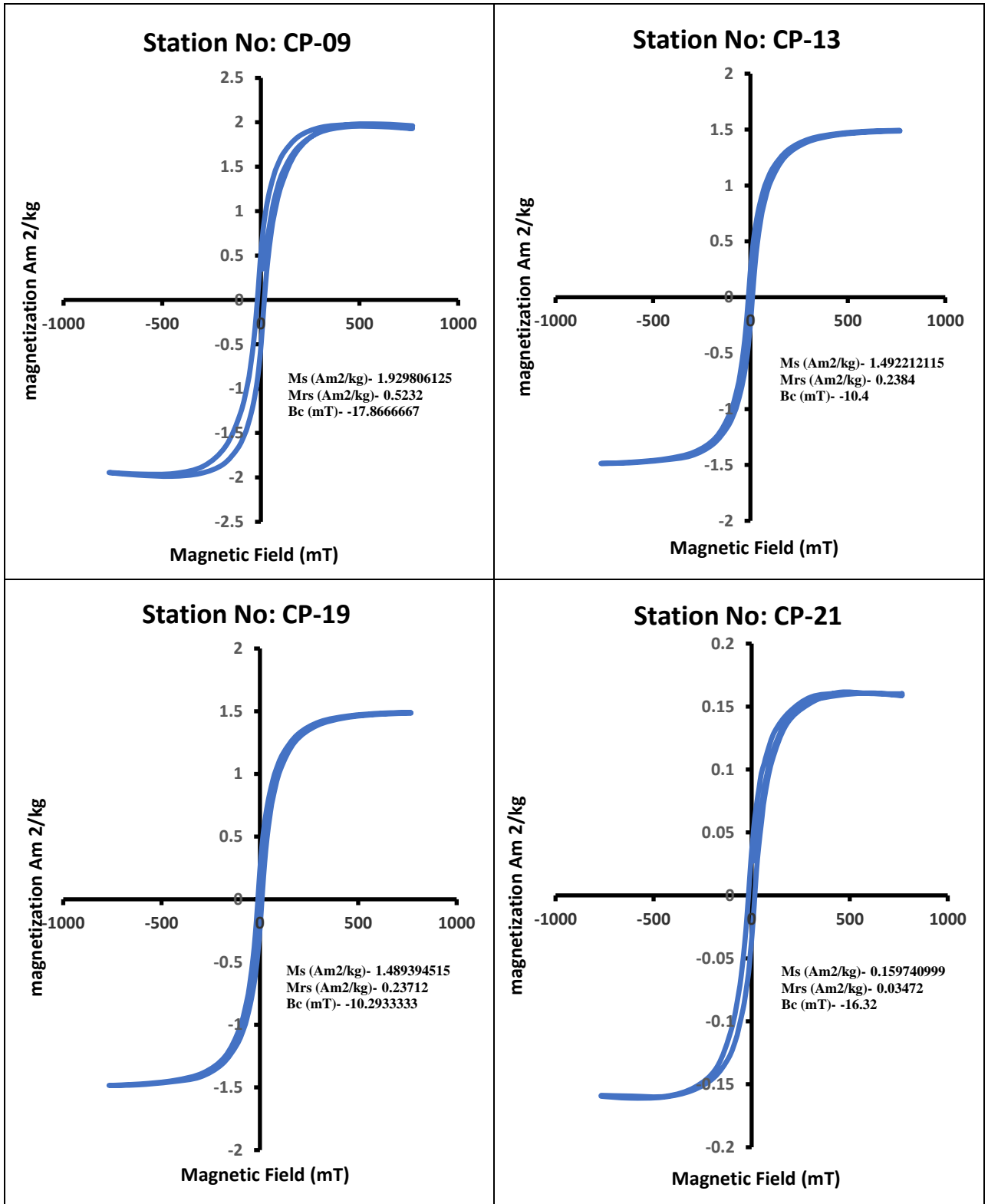
Station No: TK-18

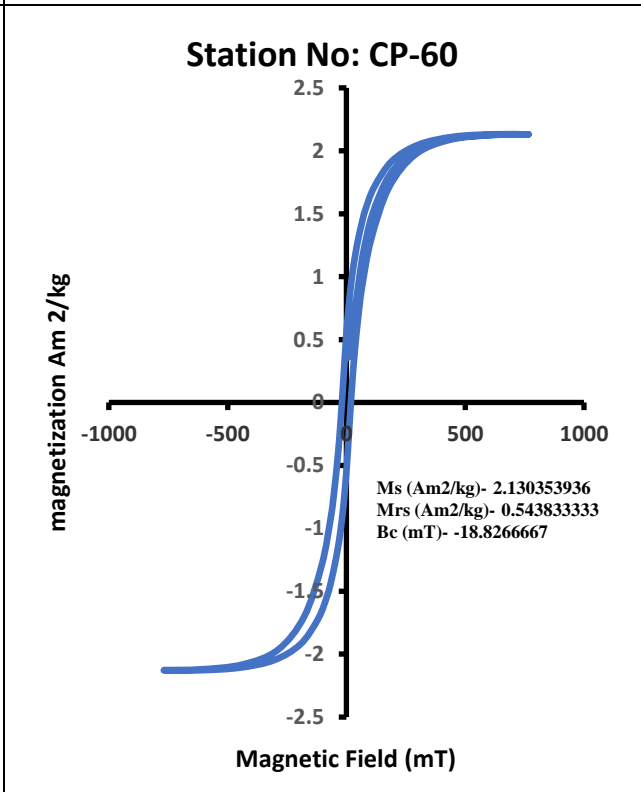
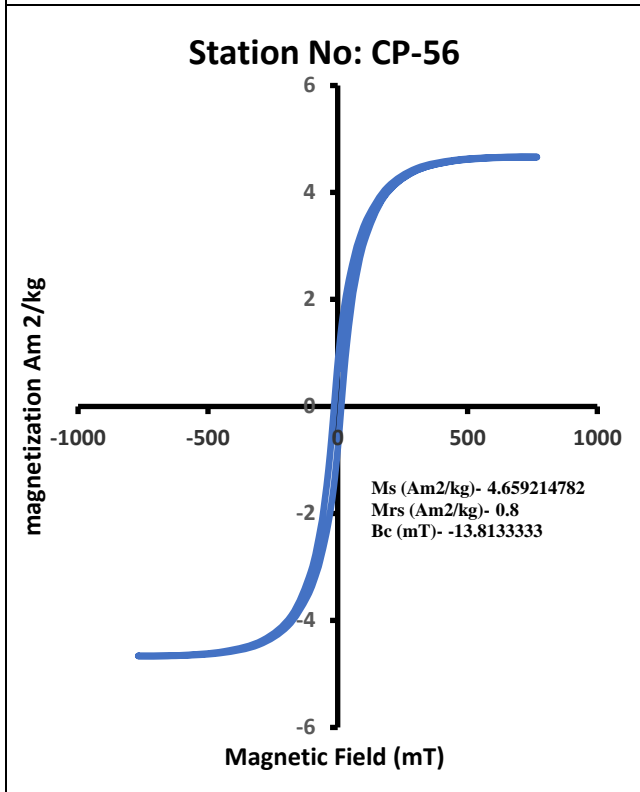
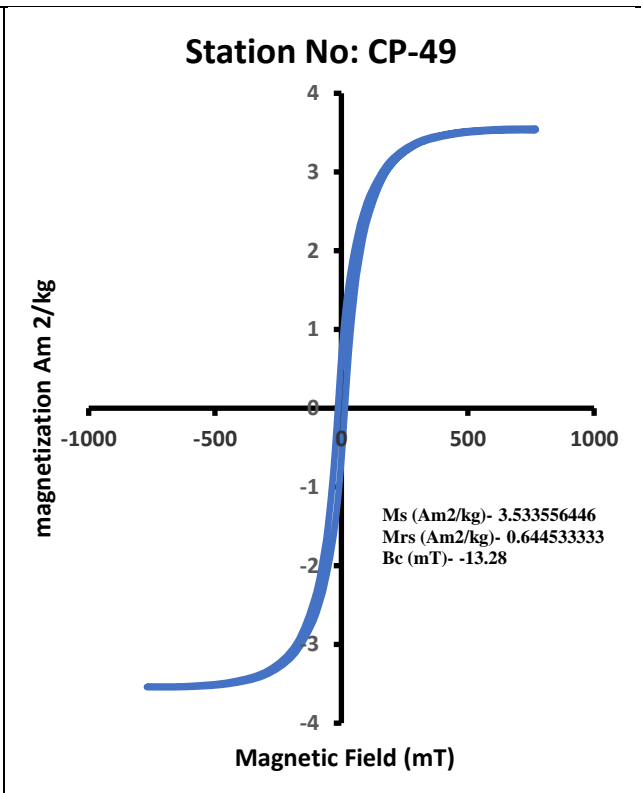
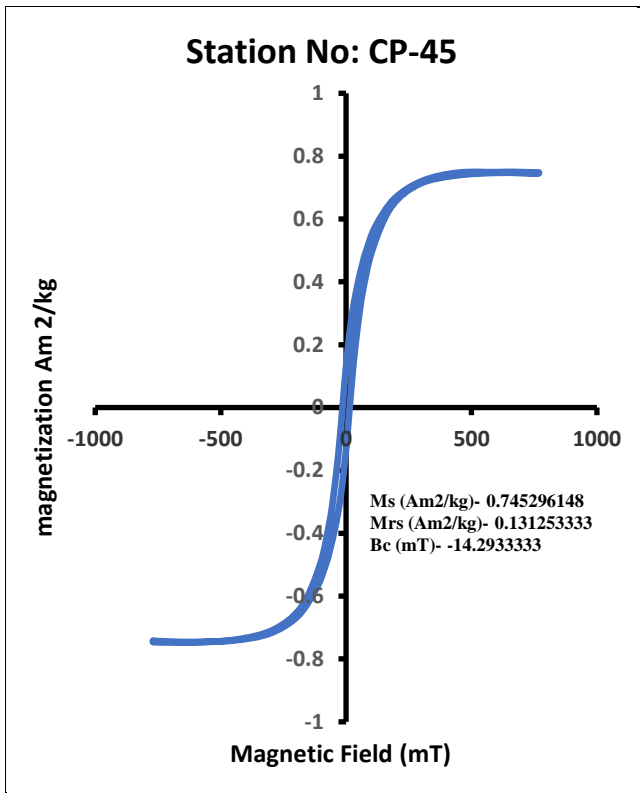


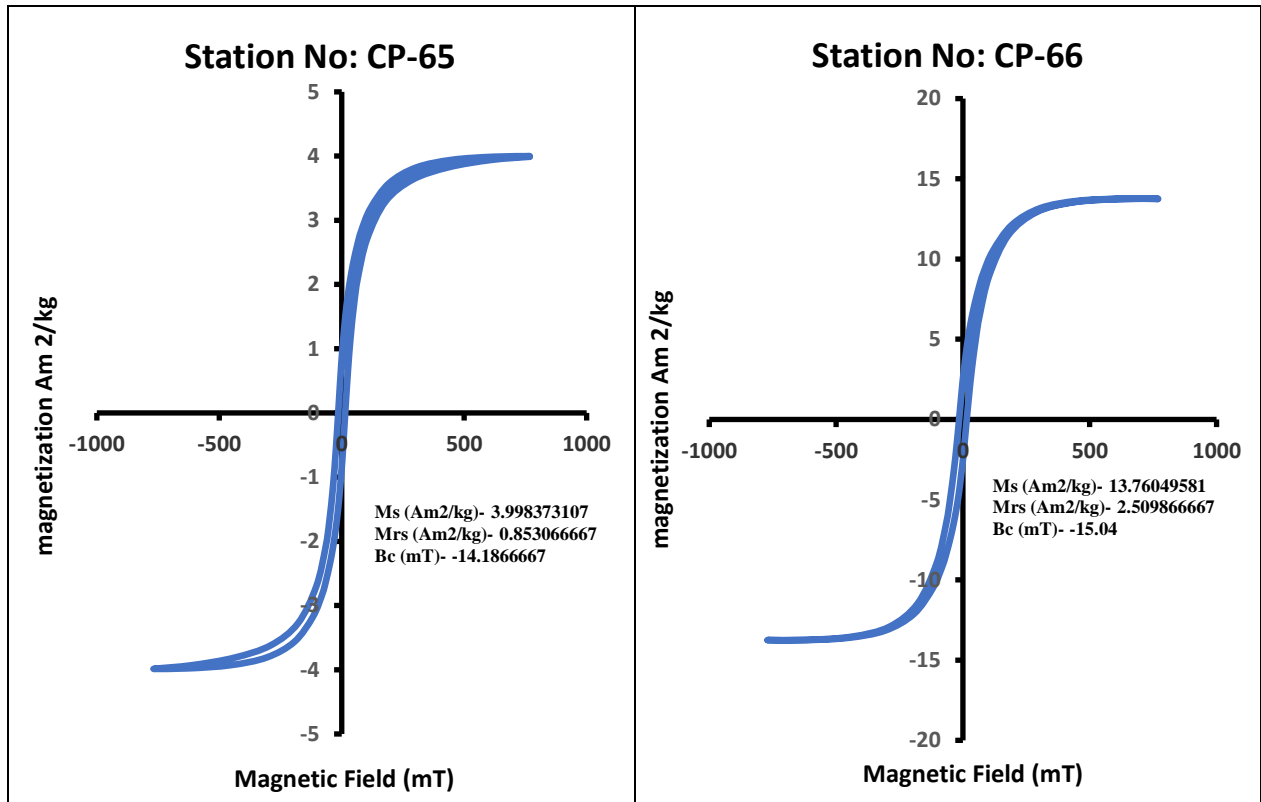
Station No: TK-19



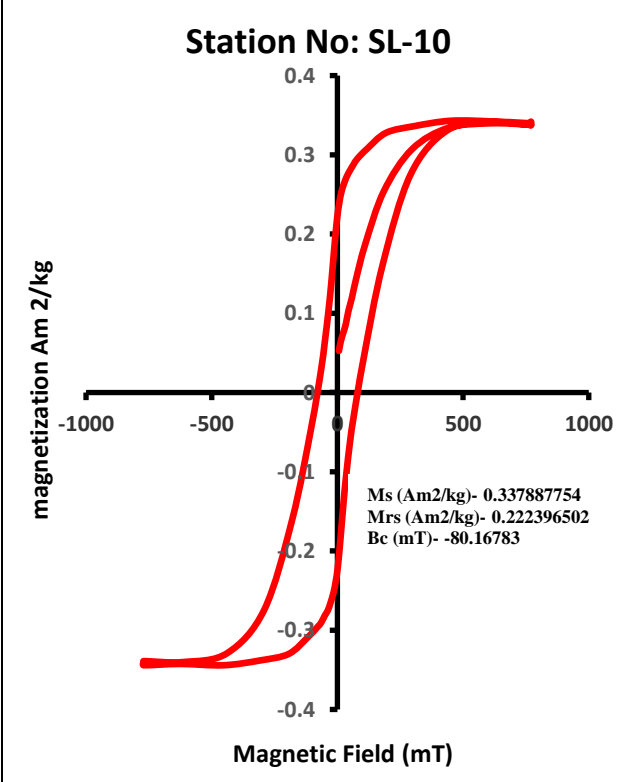
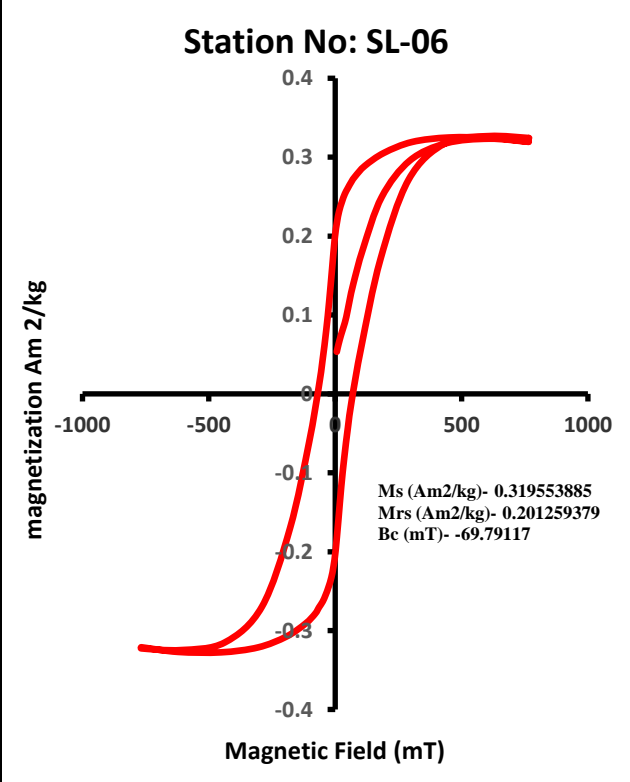
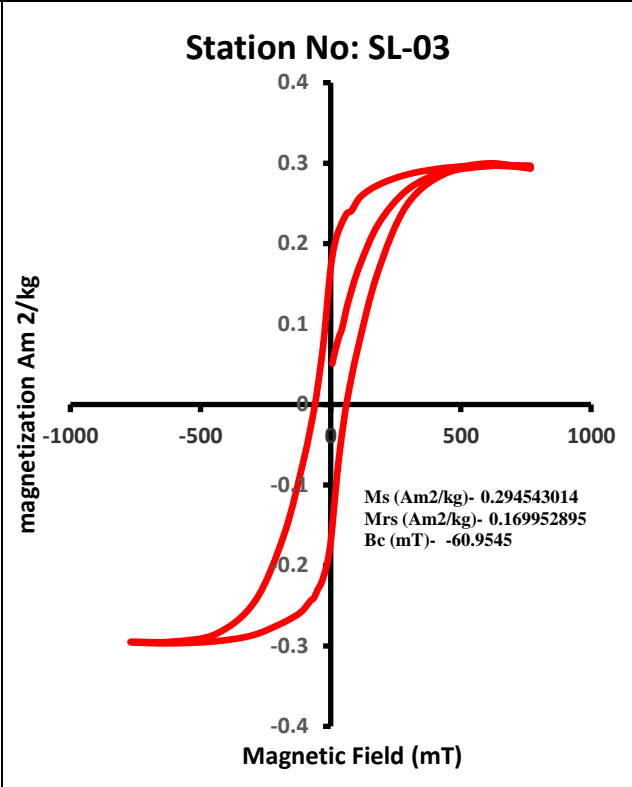
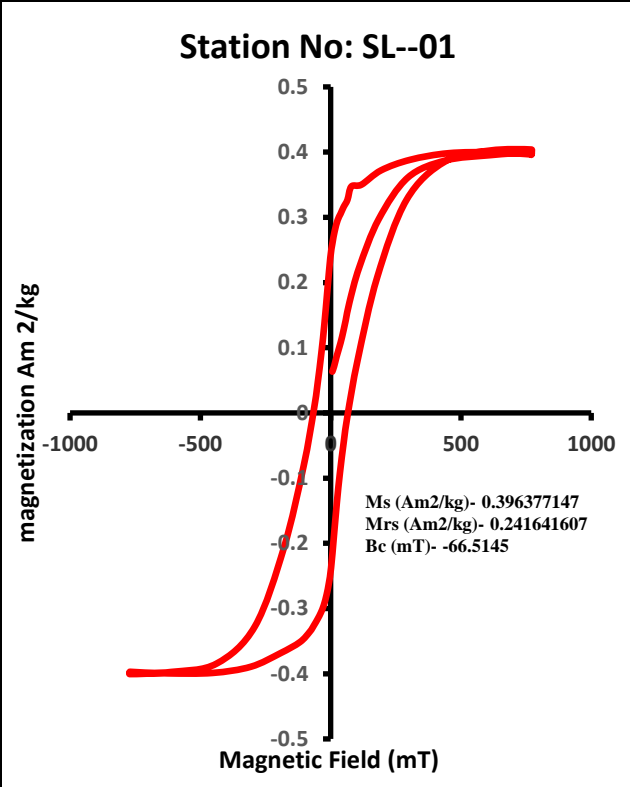
CHAPORA RIVER

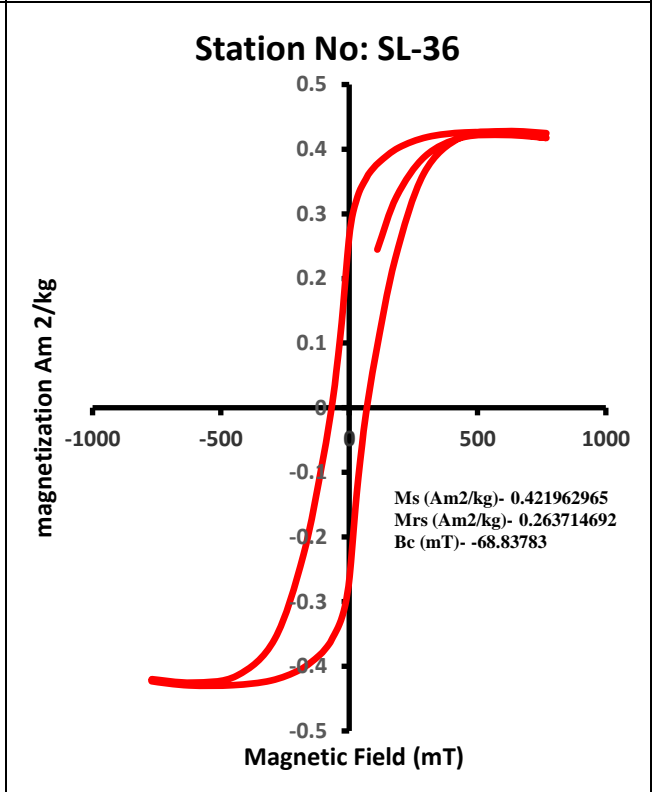
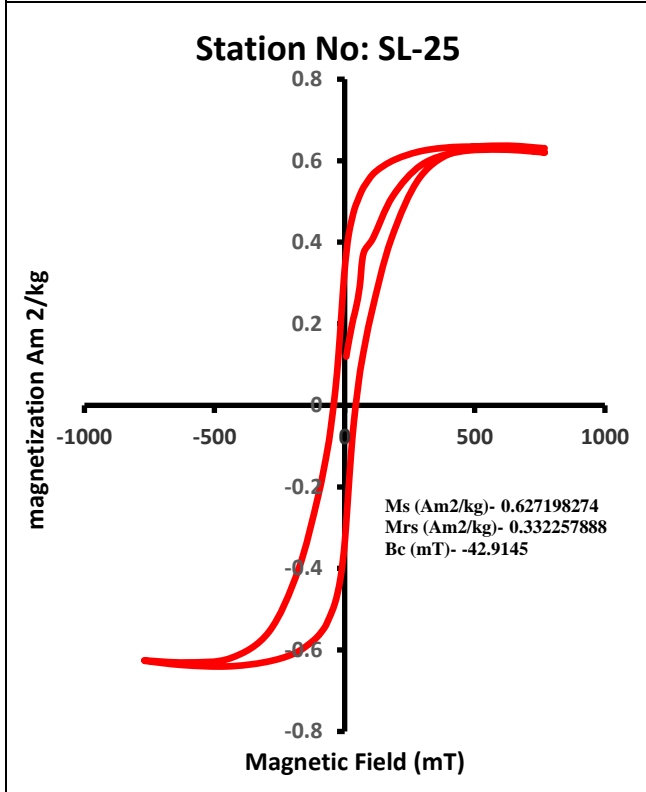
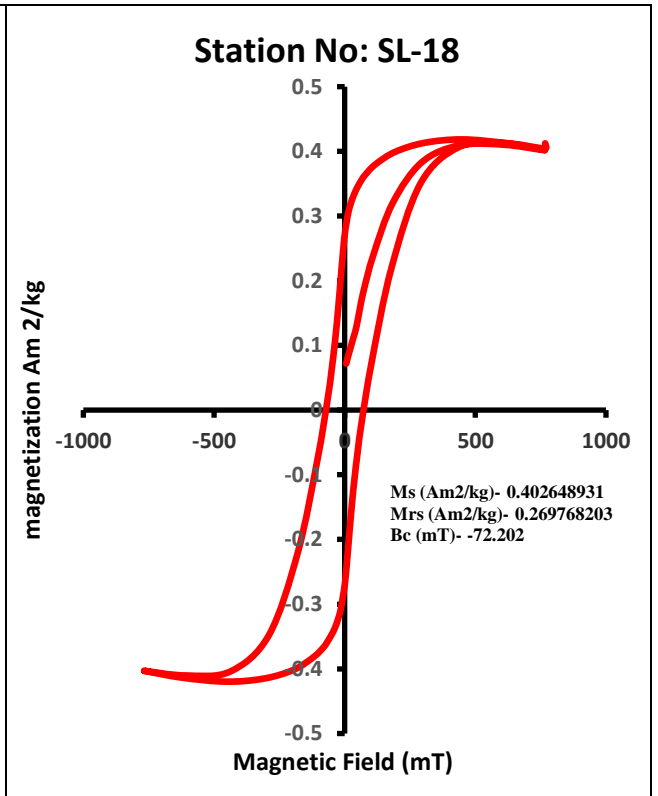
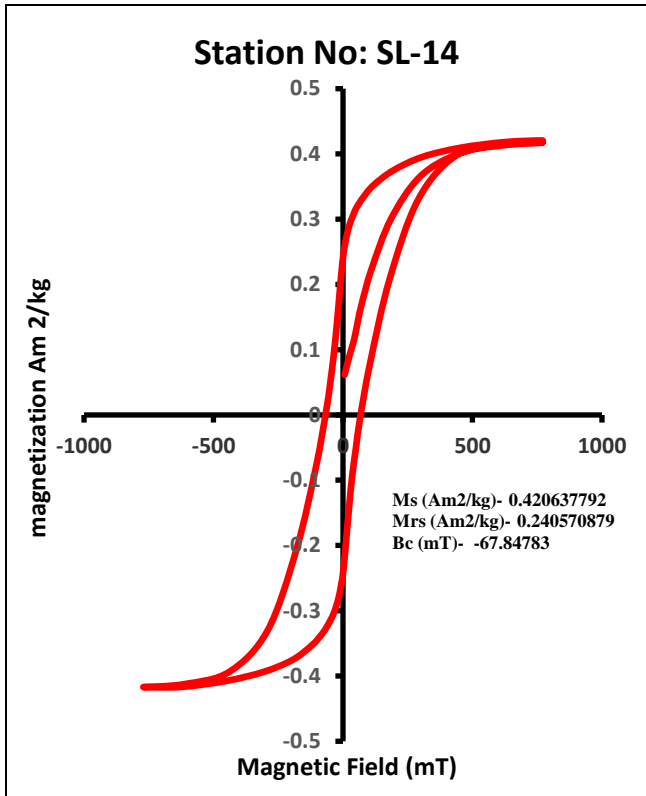




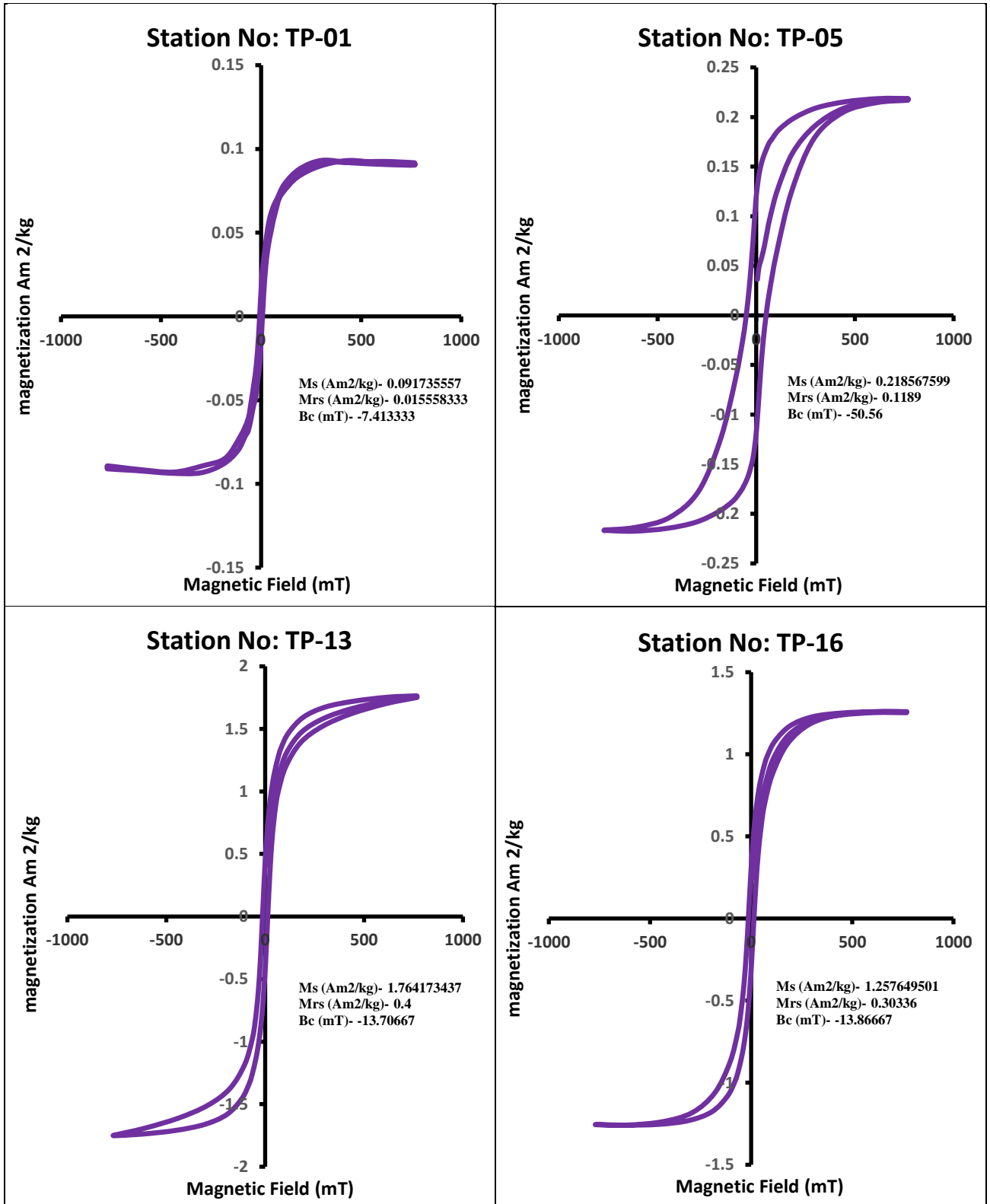


SAL RIVER

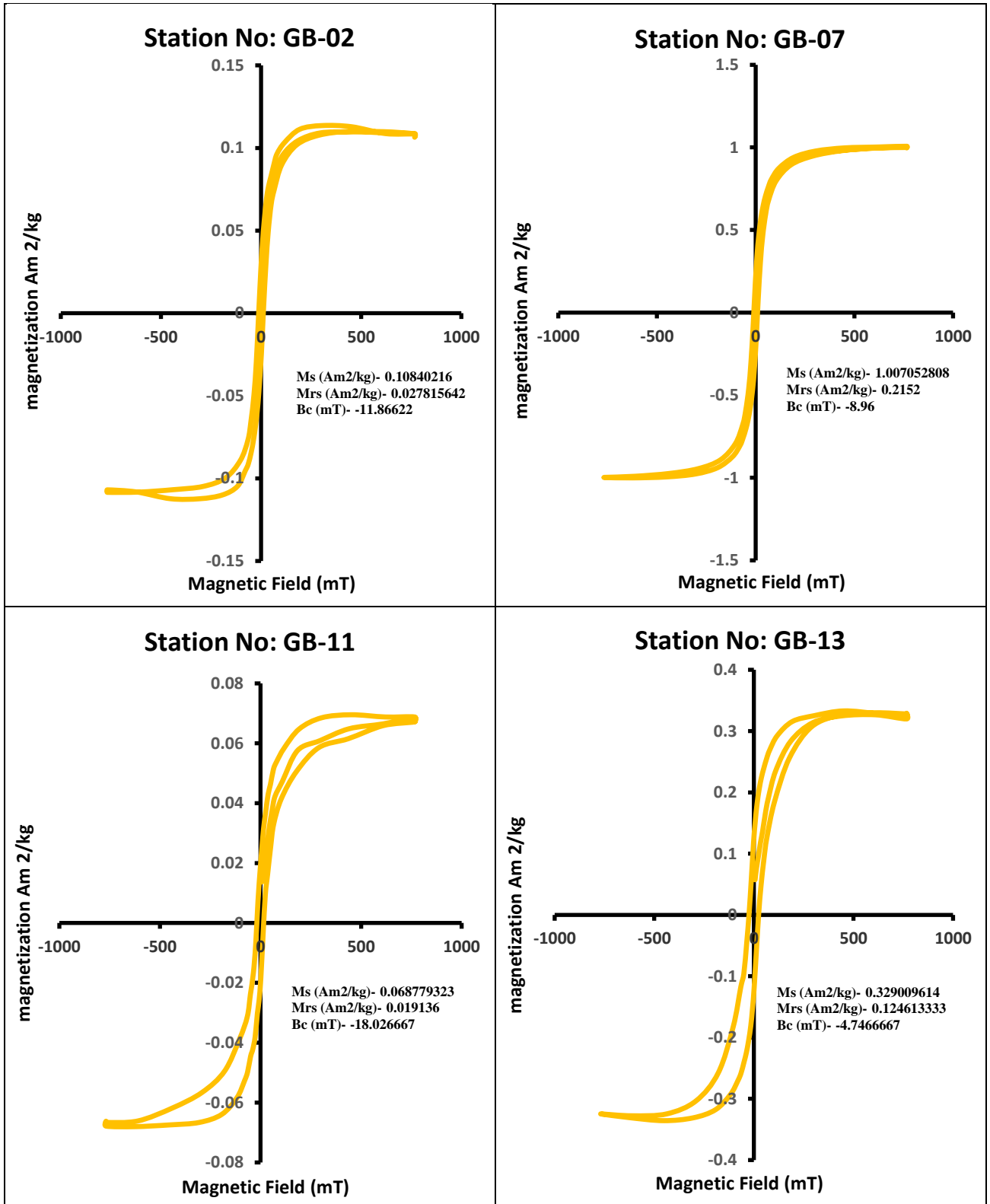




TALPONA RIVER



GALGIBAG RIVER



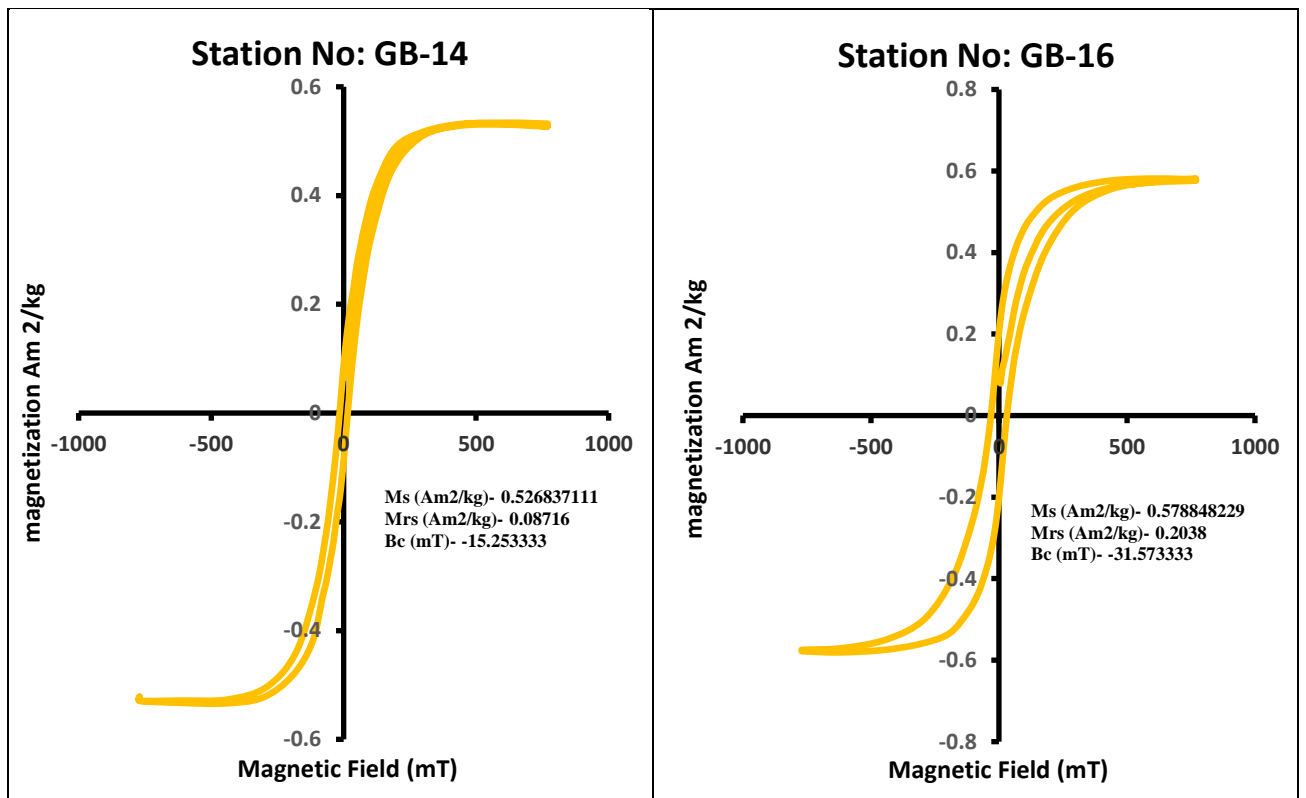


Fig 25: The hysteresis loops for selected representative samples from the five river estuaries, Goa, west coast of India.

Hysteresis loops conclusion

Magnetic hysteresis is a bulk response of magnetic minerals to the applied field. Magnetization is retained after the complete removal of the field, which is the primary reason for the hysteretic nature of magnetic response of a material.

Terekhol river

The concentration of proportion of magnetic particles varied throughout the river from upstream to nearshore. The magnetic mineral content is highest in the upper zone of the river indicated by saturation magnetization values ranges from 6.054 to 0.7385 Am²/kg, and least 0.2757 Am²/kg in the lower zone, whereas saturation remanence value ranges from 0.05244 to 1.1526 Am²/kg. magnetic coercivity values from ranges from -11.021 to -21.3483 mT. values of coercivity of remanence fall between -32.91 to -51.74 mT respectively. The saturation magnetization values ranges on order of 8 that suggest diverse variability in magnetic concentration in between sediment samples from upstream to downstream part. The magnetic coercivity values suggest that the magnetic mineralogy is dominated by ferrimagnetic minerals such as magnetite or titanomagnetite. The magnetic remanence ratio (Mrs/Ms) ranges from 0.1791 to 0.3172. The coercivity ratio (Bcr/Bc) ranges from 1.6905 to 3.9885.

The nature of hysteresis loops for all analysed samples from TK-01 to TK-19 exhibits the same closed loop (pot bellied) type curve which closes at around 200 - 300 mT, this indicates the values of coercivities are lower for analysed samples. The mineralogy could be probably of ferrimagnetic minerals (e.g. magnetite).

Chapora river

Along chapora river throughout, there were considerable variations in the sediments' magnetic particle concentration. saturation magnetization values ranges from 0.0501 to highest 3.5335

Am²/kg nearshore, whereas saturation remanence value ranges from 0.0120 to 0.6445 Am²/kg. magnetic coercivity values from ranges from -10.4 to -18.13 mT. values of coercivity of remanence fall between -31.96 to -44.77 mT respectively. The saturation magnetization values ranges on order of 70 that suggest strong variability in magnetic concentration in between sediment samples from upstream to downstream part. The magnetic coercivity values suggest that the magnetic mineralogy is dominated by ferrimagnetic minerals such as magnetite or titanomagnetite. The magnetic remanence ratio (Mrs/Ms) ranges from 0.1592 to 0.2395. The coercivity ratio (Bcr/Bc) ranges from 2.0431 to 4.349.

The pattern of hysteresis loops from upper zone to nearshore is constant and shows closed loop / pot bellied / narrow loop. Almost all samples are getting closed at around 200-250 mT indicates the sediment grain possesses lower coercivity values. the pot-bellied curves suggest the presence of single domain (SD), pseudo single domain (PSD), and multi-domain (MD) type magnetic grains.

Sal river

The saturation magnetization values ranges from 0.2945 to 0.6271 Am²/kg, whereas saturation remanence value ranges from 0.1699 to 0.3322 Am²/kg. Magnetic coercivity values ranges from -42.91 to -80.16 mT. The saturation magnetization values ranges on order of 2 that suggest negligible variability in magnetic concentration in between sediment samples from upstream to downstream part. The magnetic coercivity values suggest that the magnetic mineralogy is dominated by ferrimagnetic minerals such as magnetite or titanomagnetite. The magnetic remanence ratio (Mrs/Ms) ranges from 0.529 to 0.669. The coercivity ratio (Bcr/Bc) ranges from 1.002 to 1.091.

The hysteresis loops are very typical and shows broadness. The saturation magnetization is almost double than saturation remanence. The loop closes at 500 mT. The values of coercivity

are higher than rest of the river sediment samples. The loops suggest dominant presence of single domain (SD) ferrimagnetic minerals. The magnetic minerals produced by magnetotactic bacteria (magnetofossils) typically shows these kinds of hysteresis loops. The sediment color and physical grain size also suggests an environment suitable for their habitat.

Talpona river

The amount of magnetic particles in the sediments changed dramatically throughout the river. saturation magnetization values ranges from 0.0917 to 1.7641 Am²/kg, whereas saturation remanence value ranges from 0.015 to 0.4 Am²/kg. magnetic coercivity values from ranges from -7.413 to -13.866 mT. values of coercivity of remanence fall between -20.22 to -67.28 mT respectively. The saturation magnetization values ranges on order of 8 that suggest diverse variability in magnetic concentration in between sediment samples from upstream to downstream part. The magnetic coercivity values suggest that the magnetic mineralogy is dominated by ferrimagnetic minerals such as magnetite or titanomagnetite. The magnetic remanence ratio (Mrs/Ms) ranges from 0.1696 to 0.5439. The coercivity ratio (Bcr/Bc) ranges from 1.038 to 9.075.

Among all 4 hysteresis loops except for TP-05, rest TP-01, TP-13 and TP-16 represents narrow loops which closes at 350-400 mT, which suggests dominant mineralogy present are ferrimagnetic minerals such as magnetite. Whereas TP-05 represents broad loop indicating sediment has high coercivity minera, the loop closes at 500 mT. The loops suggest dominant presence of single domain (SD) ferrimagnetic minerals.

Galgibag river

The saturation magnetization values ranges from 0.069 to 1.007 Am²/kg, whereas saturation remanence value ranges from 0.019 to 0.215 Am²/kg. Magnetic coercivity values ranges from -4.75 to -31.57 mT. The maximum, minimum, and average values of coercivity of remanence

are -29.73 mT, -49.26 mT, and -37.36 mT respectively. The saturation magnetization values ranges on order of 14 that suggest strong variability in magnetic concentration in between sediment samples from upstream to downstream part. The magnetic coercivity values suggest that the magnetic mineralogy is dominated by ferrimagnetic minerals such as magnetite or titanomagnetite. The magnetic remanence ratio (M_{rs}/M_s) ranges from 0.16544 to 0.37875. The coercivity ratio (B_{cr}/B_c) ranges from 1.055 to 8.31742.

The hysteresis loop for a sediment sample at station GB-02 is very narrow in shape and shows an opening in between 150 to 400 mT. The loop closes at 500 mT. This suggest that sediment sample is consist mainly of ferrimagnetic minerals (e.g. magnetite). The hysteresis loop for a sediment sample at station GB-07 and GB-14 is similar type to that of GB-02, it is very narrow in shape and closes at very low magnetic field. This suggest that sediment sample is consist mainly of ferrimagnetic minerals. GB-119, GB-121, & GB-124 exhibits a typical wasp waisted loop indicates the values of coercivity are higher than rest of the river sediment samples. The loops suggest dominant presence of single domain (SD), super paramagnetic (SP) and antiferromagnetic minerals.

4.7. DAY PLOT

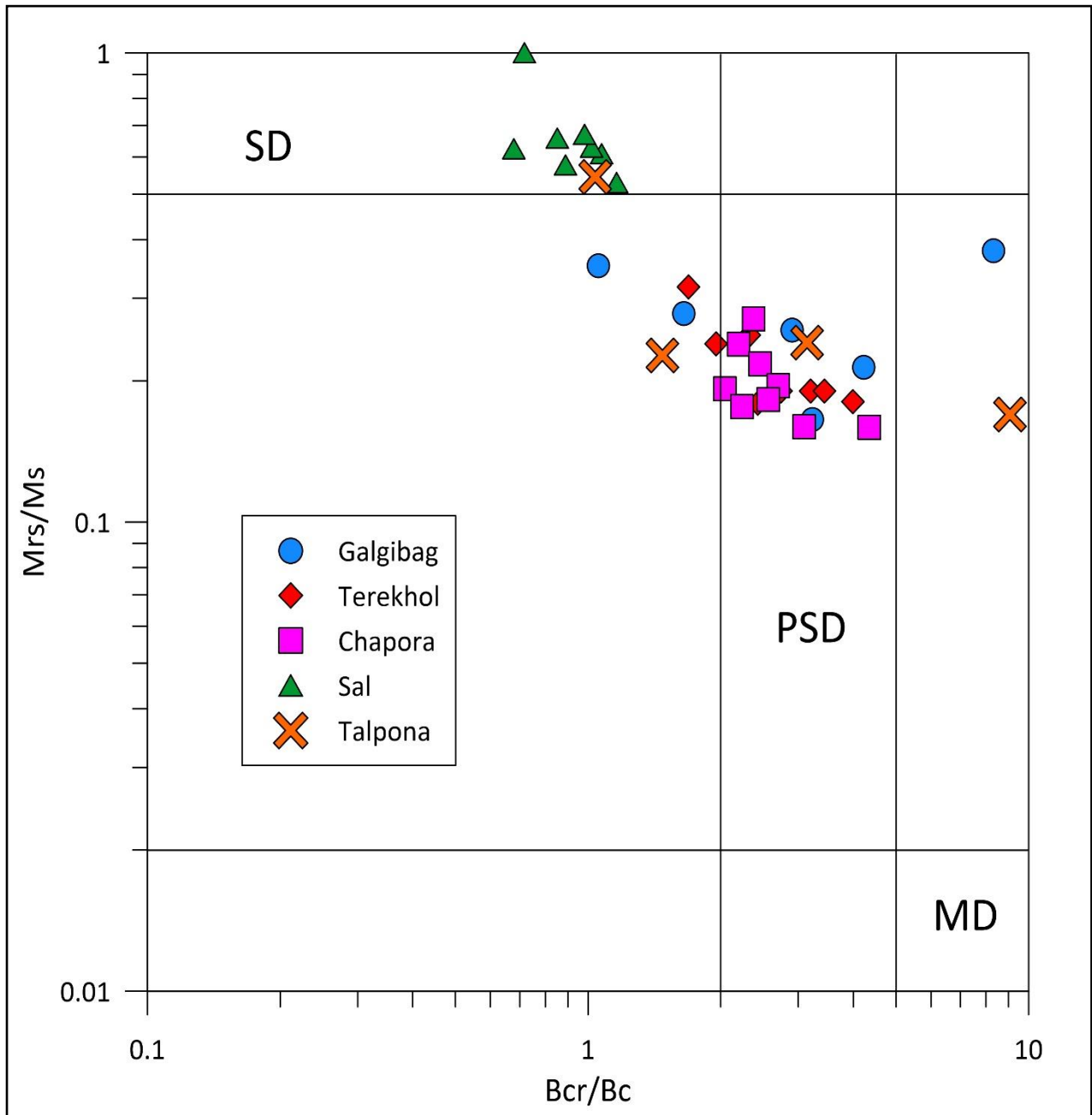


Fig 26: Day plot representing magnetic domain size for various analysed sediment of five river systems.

Day plot conclusion

Mrs/Ms vs. Bcr/Bc are the two ratios that can be used independently at times and are especially helpful when applied simultaneously to a graph which is commonly called a Day plot. Generally speaking, this kind of analysis is only reliable if there is other proof that magnetite is the predominant magnetic material. This is because this mineral is mentioned in the majority of the available experimental data. The plot illustrates the different ways in which mixtures of single-domain (SD), pseudo-single-domain (PSD), multidomain (MD), and superparamagnetic (SP) particles can occasionally be unraveled.

The day plot for terekhol river sediments shows mixed magnetic domain size. Samples TK-01 and TK-03 shows mixture of SD and MD magnetic minerals, whereas the rest samples shows mixture of SD, PSD and MD magnetic minerals.

The plot for chapora river indicated the minerals are exclusively of PSD size, they all fall in the field of PSD.

Sal river plots shows a unique pattern compare to other rivers wherein grains exclusively occupy field of SD magnetic minerals.

Talpona river sediments shows the broad variation with respect to magnetic domains. TP-05 indicates that the grain consist of SD magnetic mineral, whereas TP-13 and TP-16 shows a mixture of SD, PSD and MD magnetic minerals. Sediment sample at station TP-01 shows a mixture of SP and SD magnetic minerals.

The Day plot for the sediment samples of Galgibag River shows mixed magnetic domain sizes. The sediment samples at station GB-124 and GB-119 shows a mixture of SD and MD magnetic minerals. The sediment samples at station GB-115, GB-117 and GB-122 shows a mixture of SD, PSD and MD magnetic minerals. Sediment sample at station GB 121 shows a mixture of SP and SD magnetic minerals.

Preliminary interpretation

While MD and PSD particle enrichment is linked to an input of coarser clastic sedimentary particles and eolian dusts, PSD and SP magnetic mineral particles are susceptible to hydrodynamic sorting and lithology.

CHAPTER 5

CONCLUSION

CONCLUSION

A comprehensive set of rock magnetic data of surficial riverine sediments coupled with electron microscopy of magnetic particles provided valuable insights on the factors controlling the spatial distribution and composition of magnetic minerals in each river system of Goa.

Magnetic susceptibility distribution map helped to identify the magnetite-rich zones in different areas of the river system. Higher magnetite content in these sediments were found to be associated with coarse grained magnetic particles and can be easily linked with erosional processes. Higher density of magnetic particles facilitates better sorting and deposition, while lighter and large grain size sediment fractions gets easily entrained and transported further.

Observed changes in the magnetic mineral concentration, grain size, and mineralogy of surficial sediments can be very well linked with the changing sediment provenance and hydrodynamic conditions in each river system.

We noticed contrasting changes in magnetite content and mineralogies in the studied river sediments. Higher magnetite content in Tiracol and Chapora rivers can be attributed to the increased detrital magnetite rich flux derived from quartz sericite schist, metabasalt, laterite and phyllite with BIF.

While, Granite gneiss, and metasediments rock types appears to be predominant source of magnetic minerals to the south goa river systems and possesses lower magnetite content.

In addition to the change in sediment provenance, we propose that the factors such as river length and regional hydrodynamics within each river system also played a dominant role in the distribution of magnetic particles.

Temperature-dependent magnetization experiments confirmed the presence of mixed type magnetic mineralogies dominated by magnetite, titanomagnetite and titanohematite particles.

Hysteresis loops along with day plot provided vital information about presence of mixed type of magnetic domains dominated by ferrimagnetic content and mixture of SD, PSD and MD type of magnetic domains.

Furthermore, additional information on the mineralogy and elemental data of the suspended and bedload sediment fluxes is required for precise tracking of sediment provenance and will be undertaken as an independent study in future.

REFERENCES

1. A. G. Dessai (2011). The geology of Goa Group: Revisited., 78(3), 233–242. doi:10.1007/s12594-011-0083-7
2. Ahn, H. S., Lim, J., & Kim, S. W. (2021). Magnetic properties of a Holocene sediment core from the Yeongsan Estuary, Southwest Korea: Implications for diagenetic effects and availability as paleoenvironmental proxies. *Frontiers in Earth Science*, 9, 593332.
3. Alagarsamy, R. (2009). Environmental magnetism and application in the continental shelf sediments of India. *Marine Environmental Research*, 68(2), 49-58.
4. Badesab, F., Dewangan, P., & Gaikwad, V. (2020). Magnetic mineral diagenesis in a newly discovered active cold seep site in the Bay of Bengal. *Frontiers in Earth Science*, 8, 592557.
5. Badesab, F., Gaikwad, V., Gireeshkumar, T. R., Naikgaonkar, O., Deenadayalan, K., Samiksha, S. V., ... & Sardar, A. (2018). Magnetic tracing of sediment dynamics of mudbanks off southwest coast of India. *Environmental Earth Sciences*, 77, 1-16.
6. Badesab, F., Gaikwad, V., Nath, B. N., Venkateshwarlu, M., Aiswarya, P. V., Tyagi, A., ... & Prabhu, G. (2021). Controls of contrasting provenance and fractionation on the sediment magnetic records from the Bay of Bengal. *Marine Geology*, 437, 106515.
7. Badesab, F., Iyer, S. D., Gujar, A. R., Naik, D. K., Gaonkar, S. S., Luis, R. A. A., ... & Naik, S. (2017). Understanding heavy mineral dynamics using magnetic fingerprinting technique: a case study of North Maharashtra Coast, India. *Environmental Earth Sciences*, 76, 1-13.
- Badesab, F., Kadam, N., Gullapalli, S., Dewangan, P., Gaikwad, V., Satelkar, N., ... & Banerjee, D. (2023). Control of Source-To-Sink Processes on the Dispersal, Fractionation, and Deposition of Magnetic Minerals in a Tropical Mesotidal Estuarine System. *Geochemistry, Geophysics, Geosystems*, 24(11), e2023GC011178

8. Badesab, F., Mascarenhas-Periera, M. B. L., Gaikwad, V., Dewangan, P., Panda, P. P., Deenadayalan, K., ... & Lakshmi, B. V. (2021). Rock magnetic evidence of tectonic control on the sedimentation and diagenesis in the Andaman Sea over~ 1 million years. *Marine and Petroleum Geology*, 130, 105150.
9. Biggin, A. J., Steinberger, B., Aubert, J., Suttie, N., Holme, R., Torsvik, T. H., ... & Van Hinsbergen, D. J. J. (2012). Possible links between long-term geomagnetic variations and whole-mantle convection processes. *Nature Geoscience*, 5(8), 526-533.
10. Butler, R. F. (1992). Ferromagnetic minerals:[chapter 2]. In *Paleomagnetism* (p. 16).
11. Chaparro, M. A., Sinito, A. M., Ramasamy, V., Marinelli, C., Chaparro, M. A., Mullainathan, S., & Murugesan, S. (2008). Magnetic measurements and pollutants of sediments from Cauvery and Palaru River, India. *Environmental Geology*, 56, 425-437.
12. Dekkers, M. J. (2004). *Environmental Magnetism—Principles and Applications of Enviromagnetics* ME Evans & F. Heller, Academic Press, 2003, ISBN 0-12-243851-5, Hardback, xii+ 299 pp,£ 45 (Vol. 158, No. 3, pp. 1177-1178). Oxford, UK: Blackwell Publishing Ltd.
13. Dong, C., Zhang, W., He, Q., Dong, Y., & Yu, L. (2014). Magnetic fingerprinting of hydrodynamic variations and channel erosion across the turbidity maximum zone of the Yangtze Estuary, China. *Geomorphology*, 226, 300-311.
14. Dunlop, D. J. (2002). Theory and application of the Day plot (Mrs/Ms versus Hcr/Hc) 1. Theoretical curves and tests using titanomagnetite data. *Journal of Geophysical Research: Solid Earth*, 107(B3), EPM-4.
15. Dunlop, D. J., Özdemir, Ö., & Schubert, G. (2015). Magnetizations in rocks and minerals. *Treatise on geophysics*, 5, 277-336.

16. Fernandes, L. L., Kessarkar, P. M., Suja, S., Ray, D., & Bhat, M. (2018). Seasonal variations in the water quality of six tropical micro-and mesotidal estuaries along the central west coast of India. *Marine and Freshwater Research*, 69(9), 1418-1431.
- Fernandes, L. L., Purnachandra Rao, V., Kessarkar, P. M., and Suresh, S. (2018). Estuarine turbidity maximum in six tropical minor rivers, central west coast of India. *Hydrology Research*, 49(4), 1234-1254.
17. Gaillardet, J., Viers, J., & Dupré, B. (2003). Trace elements in river waters. *Treatise on geochemistry*, 5, 605.
18. Gallaway, E., Trenhaile, A. S., Cioppa, M. T., & Hatfield, R. G. (2012). Magnetic mineral transport and sorting in the swash-zone: northern Lake Erie, Canada. *Sedimentology*, 59(6), 1718-1734.
19. Halgedahl, S. L. (2020). Magnetic domains. *Encyclopedia of Solid Earth Geophysics*, 1-12.
20. Hatfield, R. G. (2014). Particle size-specific magnetic measurements as a tool for enhancing our understanding of the bulk magnetic properties of sediments. *Minerals*, 4(4), 758-787.
21. Hatfield, R. G., Cioppa, M. T., & Trenhaile, A. S. (2010). Sediment sorting and beach erosion along a coastal foreland: Magnetic measurements in Point Pelee National Park, Ontario, Canada. *Sedimentary Geology*, 231(3-4), 63-73.
22. <https://doi.org/10.1016/B978-0-12-804830-6.00015-6>
23. João, H. M., Badesab, F., Gaikwad, V., Kocherla, M., & Deenadayalan, K. (2021). Controls of mass transport deposit and magnetic mineral diagenesis on the sediment magnetic record from the Bay of Bengal. *Marine and Petroleum Geology*, 128, 104994.
24. Karbassi, A. R., & Shankar, R. (1994). Magnetic susceptibility of bottom sediments and suspended particulates from Mulki-Pavanje River, estuary, and adjoining shelf, west coast of India. *Journal of Geophysical Research: Oceans*, 99(C5), 10207-10220.

25. Kletetschka, G., & Wasilewski, P. J. (2002). Grain size limit for SD hematite. *Physics of the Earth and Planetary Interiors*, 129(1-2), 173-179.
26. Kletetschka, G., Wasilewski, P. J., & Taylor, P. T. (2000). Hematite vs. magnetite as the signature for planetary magnetic anomalies?. *Physics of the Earth and Planetary Interiors*, 119(3-4), 259-267.
27. Kulgemeyer, T., Bryan, K. R., & von Dobeneck, T. (2018). Formation of coast-parallel heavy mineral enrichments investigated by exploratory numerical modelling. *GSA Bulletin*, 130(11-12), 1875-1888.
28. Lecoanet, H., Leveque, F., & Ambrosi, J. P. (2003). Combination of magnetic parameters: an efficient way to discriminate soil-contamination sources (south France). *Environmental Pollution*, 122(2), 229-234.
29. Li, M., Zhu, S., Ouyang, T., Tang, J., & Tang, Z. (2021). Magnetic properties of the surface sediments in the Yellow River Estuary and Laizhou Bay, Bohai Sea, China: Implications for monitoring heavy metals. *Journal of Hazardous Materials*, 410, 124579.
30. Liu, Q., Roberts, A. P., Larrasoana, J. C., Banerjee, S. K., Guyodo, Y., Tauxe, L., and Oldfield, F. (2012). *Environmental magnetism: principles and applications*. *Reviews of Geophysics*, 50(4).
31. Mascarenhas, A. N. T. O. N. I. O. (1999). Some observations on the state of coastal environment of Goa, west coast of India.
32. Oldfield, F. (2007). Sources of fine-grained magnetic minerals in sediments: a problem revisited. *The Holocene*, 17(8), 1265-1271.
33. Ouyang, T., Li, M., Appel, E., Fu, S., Jia, G., Li, W., & Zhu, Z. (2017). Magnetic properties of surface sediments from the Pearl River Estuary and its adjacent waters: Implication for provenance. *Marine Geology*, 390, 80-88.

34. Piper, J. D. A. (1998). DUNLOP, DJ & ÖZDEMİR, Ö. 1997. Rock Magnetism. Fundamentals and Frontiers. Cambridge Studies in Magnetism Series. xxi+ 573 pp. Cambridge, New York, Port Chester, Melbourne, Sydney: Cambridge University Press. Price£ 80.00, US \$125.00 (hard covers). ISBN 0 521 32514 5. Geological Magazine, 135(2), 287-300.
35. Prajith, A., Rao, V. P., & Kessarkar, P. M. (2015). Magnetic properties of sediments in cores from the Mandovi estuary, western India: inferences on provenance and pollution. Marine pollution bulletin, 99(1-2), 338-345.
36. Praseetha, B. S., Tiju, V. I., Prakash, T. N., Sreenivasulu, G., & Nagendra, R. (2022). Environmental Magnetism, Geochemical and Textural Characteristics of the Sediments of Beypore Estuary, Northern Kerala, India: Implication on Environmental Processes.
37. Rao, K. L. (1979). India's water wealth. Orient Blackswan.
38. Stevenson, D. J. (2003). Planetary magnetic fields. Earth and planetary science letters, 208(1-2), 1-11.
39. Walling, D. E. (2006). Human impact on land–ocean sediment transfer by the world's rivers. Geomorphology, 79(3-4), 192-216.
40. Xue, P., Chang, L., Wang, S., Liu, S., Li, J., Shi, X., ... & Kornkanitnan, N. (2019). Magnetic mineral tracing of sediment provenance in the central Bengal Fan. Marine Geology, 415, 105955.
41. Yang, D., Wang, M., Lu, H., Ding, Z., Liu, J., & Yan, C. (2019). Magnetic properties and correlation with heavy metals in mangrove sediments, the case study on the coast of Fujian, China. Marine Pollution Bulletin, 146, 865-873.
42. Zhang, C., Vali, H., Romanek, C. S., Phelps, T. J., & Liu, S. V. (1998). Formation of single-domain magnetite by a thermophilic bacterium. American mineralogist, 83(

APPENDIX I

ROCK MAGNETIC DATA USED IN STUDY

TRREKHOL RIVER					
LF	fd%	ARM	SIRM (10-5Am2kg-1)	ARM / SIRM	S-ratio
10-8m3kg-1					
33.93966667	0.84856461	17.11067232	1.076194253	0.010828063	0.732119867
46.27033333	0.281677965	23.32273459	1.59327596	0.006902259	0.719084917
76.06133333	0.375135855	38.24028605	2.124177236	0.006594748	0.864914125
100.9766667	0.419238768	50.95551243	3.447398406	0.006261966	0.935419862
450.5766667	0.934358193	227.297445	14.93101902	0.007584924	0.947414878
337.2966667	4.018223325	169.4859861	8.741442728	0.009519582	0.948831444
88.10333333	1.675305512	44.4814243	2.73108871	0.008333725	0.763347163
297.0666667	0.85951526	149.8682608	9.845973193	0.006474893	0.964476266
422.37	2.669855024	212.089704	12.54015147	0.011356046	0.955433476
449.6866667	1.809408032	225.8173882	18.19351667	0.007329267	0.954950985
112.4166667	1.948109711	56.58323275	3.450785459	0.008925523	0.927203183
273.4066667	0.749798834	137.4658681	9.122047904	0.006567377	0.941465109
384.4633333	1.525069578	192.3873102	12.53843347	0.00770675	1.000474262
503.2866667	0.311287139	252.0132376	14.17581427	0.00563778	1.035540981
217.1733333	0.739808448	109.8043946	6.619514323	0.00677659	1.003912831
7.973866667	2.435455822	4.379691973	0.129832758	0.012225623	0.961926194
246.5466667	0.785517279	123.713482	6.653504253	0.008084566	1.134703682
372.98	0.880297424	186.6575998	11.62299698	0.007190121	0.957560472
271.48	0.335199646	136.0115372	8.013889063	0.006971045	0.946205894
188.4333333	0.543074474	96.73558279	5.818667149	0.002856471	0.348711754
257.7166667	5.037832245	128.8583333	5.947324742	0.021691867	0.94503723

CHAPORA RIVER

LF	fd%	Mean ARM	SIRM (10-5Am2kg-1)	ARM / SIRM	S-ratio
10-8m3kg-1					
273.4033333	1.014374368	0.2981342	8.225586437	0.004465684	0.867546219
592.08	0.922172679	0.5417426	15.16097977	0.004908964	1.123651322
130.4066667	1.623127652	0.1772995	3.99265776	0.005887383	0.833332046
112.55	1.418628758	0.1398548	3.144359504	0.007903114	0.992120659
94.097	1.787871381	0.1783549	2.56448125	0.011214638	0.945360782
101.2166667	1.505351556	0.1825859	2.684813397	0.010493891	0.932867128
137.6333333	3.027367401	0.1465836	3.441419729	0.010627886	0.908022869
156.7433333	2.079833273	0.3040477	4.527387707	0.010240317	0.957470295
89.59933333	1.835207107	0.1207593	2.301690799	0.010208215	0.925869303
250.99	1.268310822	0.3700122	7.348301075	0.007760565	0.938932235
358.4666667	5.804351869	0.0941481	2.050776521	0.008376518	0.408007109
115.1366667	1.415708868	0.2144155	2.696913411	0.010830011	1.073100893
119.7533333	1.600512164	0.2140374	3.675616788	0.009138551	0.90477921
266.98	1.584388344	0.3843774	6.828228836	0.009605449	0.940494651
179.4933333	0.922968355	0.2430411	5.39953719	0.007997906	0.949820972
410.61	0.765527711	0.7081193	13.19291886	0.007296071	0.964289366
304.8166667	1.53316201	0.6021237	8.919095918	0.008886455	0.961029385
330.6333333	0.577679202	0.5725731	11.02546193	0.006801233	0.96252698
91.978	1.933070952	0.1149684	1.766914005	0.010311655	0.91312537
178.0133333	0.962474721	0.2790717	5.299708383	0.008019922	0.975406858
243.7366667	1.01202117	0.4180885	7.963478579	0.007076902	0.966222235
277.53	1.02811708	0.4972615	8.99521748	0.007247159	0.969570325
155.9566667	1.831705388	0.3001883	4.621663774	0.009087705	0.968201721
90.097	1.572379399	0.1789526	2.620736842	0.01053654	0.936218584
188.16	0.754676871	0.270137	5.542317746	0.007539045	0.922465755
406.27	0.507051961	0.4851196	13.09633159	0.006238212	0.978777466
732.91	0.579880204	0.9263984	12.50384901	0.011828575	1.928921886
170.3266667	0.935457356	0.263247	26.17858081	0.0017046	0.196430662
568.4766667	0.585776021	0.7881986	4.644993236	0.024678381	4.002634396
435.9133333	0.49551134	0.464112	14.69006995	0.006479448	0.979277827
751.8633333	0.32098032	1.093006	26.24068182	0.005550879	0.969777938
652.49	0.443940392	0.8423141	22.62617225	0.005744423	0.976788852
504.6833333	0.463657079	0.5975065	17.28657025	0.006141676	0.972266246
116.4666667	1.030337722	0.1732867	3.541223776	0.008828675	0.954771275
159.7133333	0.818132487	0.218133	5.267668038	0.007327657	0.961458857
213.44	0.802723638	0.2460325	7.198936482	0.007180348	0.963742382
214.0966667	0.557380622	0.2930853	7.749516605	0.00600093	0.961995646
124.5633333	0.781396345	0.1844337	4.234192649	0.007121679	0.949909572
395.9966667	0.482327292	0.4871848	13.84175066	0.006021727	0.962824385
310.9333333	0.823327616	0.4276201	10.90735085	0.006645748	0.963292667
224.9066667	0.650640266	0.337387	7.654107184	0.006483715	0.958286382

111.05	0.756416029	0.1685639	3.667546174	0.00782185	0.950648201	
184.9833333	0.490134246	0.2133472	6.374041787	0.006221603	0.95475118	
220.6233333	1.155816097	0.3997161	7.28797032	0.008076639	0.837314321	
195.0866667	1.823121348	0.432613	5.995479167	0.009234318	0.975204035	
103.69	1.5591346	0.1188056	2.429250364	0.009183275	0.869565191	
419.7166667	1.928284954	0.6431648	11.37062944	0.009259792	0.945388846	
215.2733333	5.561921278	0.2980419	2.520337572	0.01763568	0.914491682	
176.73	2.238820046	0.3433788	5.8121772	0.009443888	0.64073676	
138.5966667	4.09100748	0.3251123	3.297988462	0.016303445	0.780287984	

SAL RIVER					
LF	fd%	Mean ARM	SIRM (10-5Am2kg-1)	ARM / SIRM	S-ratio
10-8m3kg-1					
2.7029	12.01795602	0.0093774	0.069006359	0.020994066	0.7262477
3.7189	9.768121398	0.0153895	0.078364917	0.030087108	0.701084
4.3102	11.0884259	0.0221029	0.0917001	0.038721629	0.6564719
2.8834	13.16270144	0.0124017	0.063893263	0.029285305	0.6785004
1.435233333	1.848712172	0.0055525	0.041708303	0.024086086	0.7729015
4.438833333	9.20737431	0.015691	0.107355648	0.021822359	0.8061448
3.311733333	8.105523794	0.0076099	0.06861533	0.016021237	0.822085
2.657066667	2.076224408	0.0076337	0.082787559	0.014887197	0.8707017
3.0565	10.15758765	0.0122144	0.075730438	0.022205052	0.8218695
1.574833333	0.114297809	0.0090127	0.047160586	0.028901235	0.7743078
0.71794	-11.89375157	0.0063935	0.028985863	0.032970941	0.930659
2.662766667	11.02487388	0.0104435	0.062560079	0.024443454	0.8891561
0.305453333	16.70413375	0.0054206	0.018139335	0.044981599	0.8538231
1.118	7.528324389	0.0071743	0.029395668	0.031141158	0.4353377
2.246766667	8.958058247	0.0080505	0.055830812	0.020418331	0.885784
1.1622	18.09585269	0.0067308	0.039397941	0.027008018	0.870891
1.723166667	13.58738756	0.008033	0.046715708	0.022774329	0.8653692
2.969266667	4.67118705	0.0147871	0.075642647	0.026489213	0.7622183
2.595666667	3.347887505	0.0109505	0.074607657	0.021638752	0.9091378
2.466633333	1.740564062	0.010616	0.069839393	0.025869078	0.921664
5.533	4.064100247	0.0147597	0.140993439	0.016408486	0.8436625
6.2206	2.875392513	0.0277024	0.15956407	0.026041953	0.8449103
4.1872	7.618456248	0.0127628	0.132640848	0.015045424	0.8624036
13.81633333	2.152042269	0.0393288	0.331797297	0.020663117	0.8515509
21.92766667	4.628855479	0.0589859	0.465504988	0.020381644	0.8622508
46.64766667	5.66587825	0.1614935	0.788783989	0.035835972	0.8332681
56.80333333	5.486767208	0.1138417	0.698310584	0.025584129	0.9190058
4.666233333	6.96207505	0.0134004	0.123810147	0.01866593	0.8443855
3.9395	4.304268731	0.0108017	0.117238712	0.015618025	0.8592763
3.970566667	2.569742354	0.0109401	0.106648041	0.01683587	0.8589966
3.512166667	5.377497271	0.0115987	0.104425075	0.017955245	0.8491385
4.2093	6.377940909	0.0114229	0.1277471	0.015779661	0.8463959
3.105033333	0.344601776	0.0119068	0.105584709	0.014829098	0.8177661
5.168433333	8.779578596	0.0141933	0.148102872	0.016139157	0.8276566
6.914166667	6.823189104	0.0153712	0.189418315	0.010252972	0.7161618
2.489666667	3.877359754	0.0074284	0.073795355	0.017383426	0.8959061
2.387366667	2.263302663	0.0094995	0.108627111	0.013413936	0.5509929
4.065366667	6.060953911	0.0091091	0.083312428	0.018413088	1.2470878
1.555566667	3.567831658	0.0049664	0.128415884	0.006003598	0.2384626
9.719666667	-0.225659316	0.0226038	0.192731289	0.04335044	0.8058101

TALPONA RIVER					
LF	fd%	Mean ARM	SIRM (10-5Am2kg-1)	ARM / SIRM	S-ratio
10-8m3kg-1					
244.4466667	6.538576922	0.4220024	3.114070175	0.025557604	0.890535036
76.32133333	5.278559075	0.0278196	1.045659406	0.033980438	0.831479591
465.9466667	0.839151834	0.6249167	11.70050505	0.005799503	0.63839434
141.6033333	9.630187613	0.04714	1.578837975	0.048754492	0.87180846
293.5166667	1.225370507	0.3678057	8.506497674	0.005188585	0.567407678
41.76466667	3.449486807	0.0770491	5.44558672	0.001808929	0.171575277
161.34	2.028841783	0.2380147	8.629872247	0.00391835	0.069851481
285.2133333	1.486606517	0.5294988	10.08349583	0.008073867	0.693632534
132.15	8.124605877	0.1013447	1.982976364	0.039956668	0.780510839
145.5933333	7.413343102	0.066547	1.73072	0.055112342	0.888492779
248.18	1.301474736	0.5917855	14.33017834	0.006786296	0.622357254
129.9333333	7.732170344	0.3664928	1.72025	0.041390008	0.717862615
134.41	3.863799816	0.2156316	3.673361233	0.011119656	0.201622628
76.77933333	6.496539867	0.1801209	1.202072984	0.038970978	0.87495895
35.04633333	2.668847906	0.048719	0.689611794	0.011195899	0.898163158
64.47266667	1.541738618	0.0792718	1.294336272	0.009950406	0.876985082

GALGIBAG RIVER					
LF	fd%	Mean ARM	SIRM (10-5Am2kg-1)	ARM / SIRM	S-ratio
10-8m3kg-1					
65.159	8.74885536	0.0652341	0.777500662	0.071678131	0.750169928
162.9033333	2.63346361	0.3635423	6.006261845	0.009735674	0.632435766
94.934	6.89426338	0.0624354	1.420798347	0.046849266	0.797815918
174.22	1.79466575	0.2005517	5.133104651	0.008372197	0.460639669
49.921	4.9678492	0.0659335	3.215463281	0.010332664	0.501138663
68.05366667	7.89230068	0.101498	0.883945872	0.067946178	0.742587709
112.1633333	7.45341615	0.361162	1.716137057	0.048134968	0.764114791
111.81	6.65116418	0.3032309	3.815647059	0.016298376	0.038416444
253.3266667	1.62767441	0.5470457	9.395482653	0.007664223	0.613629129
89.337	8.80374313	0.3553956	0.924962684	0.081121568	0.86285482
249.23	1.41235004	0.2108293	3.963506039	0.008287257	0.480098776
71.65033333	2.00324725	0.1214178	2.083726918	0.009774734	0.660446359
18.943	2.83833958	0.037609	0.479139033	0.012547188	0.638062334
27.61933333	0.99326559	0.0290028	0.454074178	0.012894425	0.799443329
46.43633333	0.29718109	0.033703	1.038382183	0.005253427	0.52638696
24.248	0.75882547	0.0212424	0.690996683	0.004871839	0.349827805